

University Of Szeged
Faculty of Science and Informatics
Doctoral School of Geosciences
Department of Geoinformatics, Physical and Environmental Geography

Mapping and Evaluating the Condition of Artificial Levees

PhD Dissertation

Diaa Elsayed Hamed Abdallah Hamed Sheishah

Supervisor:

Dr. György Sipos

2023

Szeged

List of abbreviations

GPR	Ground Penetrating Radar
ERT	Electrical Resistivity Tomography
lkm	Levee kilometer
VLLH	Very low level of levee health
LLH	Low level of levee health
MLLH	Medium level of levee health
HLLH	High level of levee health
VHLLH	Very high level of levee health
W	Water content
d	Depth
D50	Mean grain size
ϕ	Porosity
ρ	Bulk density
K	Saturated hydraulic conductivity
R	Resistivity based on ERT profiles
N/BH	Number of samples/borehole
M	Material type
BH	Borehole

Contents

1.	Introduction	4
1.1	Importance of artificial levees	4
1.2	Assessment of levee health	7
2.	Study area	11
3.	Data and methods.....	15
3.1	GPS measurements	15
3.2	ERT measurements	16
3.2.1	<i>Wenner array</i>	18
3.3	GPR measurements.....	20
3.3.1.	GPR data collection	22
3.3.2.	Checking the levee by two different antennas	24
3.3.3.	GPR data processing.....	25
3.4	Sedimentological data.....	26
3.5	Methodology of evaluating levee health	30
3.6	Inventory of historical flood phenomena	31
4.	Results	33
4.1	ERT data evaluation	33
4.1.1	Comparison of different resolution of ERT data	33
4.1.2	Integrating ERT and sedimentological data to identify structural units at Tisza and Maros levees	37
4.2	Drillings.....	45
4.2.1	Sedimentological analysis	45
4.2.2	Relationship among resistivity, grain-size and water content of levee materials 51	
4.2.3	Relationship of resistivity and other physical parameters.....	56
4.3	Mapping the materials along the investigated levees	59
4.4	Elevation change of levees.....	63
4.5	GPR.....	66
4.5.1.	Identification of GPR anomalies.....	66
4.5.2.	Spatial distribution of penetration depth and GPR anomalies	70
4.5.3.	Comparison of applying two different antennas on the Tisza levee section.....	71
4.5.4.	Justification of GPR results using recordings of flood phenomena	72
5.	Evaluation of levee health.....	75
5.1	Evaluation of levee materials.....	75
5.2	Evaluation of levee defects	79

5.3	Structural assessment by comparing different geophysical data	79
5.4	Overall analysis of levee health	82
6.	Conclusion	85
7.	Acknowledgements.....	88
8.	References.....	89
9.	Abstract	99
10.	Supplements	102
10.1	Supplement section 1: Rest of the interpreted ERT data measured on Tisza levee.	102
10.2	Supplement section 2: Rest of the interpreted ERT data measured on Maros levee 106	
10.3	Supplement section 3: Rest of relationships among physical properties for the other boreholes	117

1. Introduction

1.1 Importance of artificial levees

Floods are among the most widespread types of natural hazards, as confirmed by almost half of the catastrophes 2018 were related to floods. A flood occurs when the water exceeds the river banks, leaves its channel and temporarily inundates otherwise dry areas with water, and this overflow is not regular. One of the most dangerous results of floods is the loss of human lives, but Floods also harm economic and social infrastructure (Mezősi, 2022).

Artificial levees that is, linear manmade earthworks along rivers, are ultimately important earthworks for preventing flooding. Thus, knowing their conditions for successful flood protection is essential. Artificial levees have been built to inhibit the inundation of floodplains since historical times. However, large-scale construction works started at the turn of the 19th and 20th centuries (Szűcs et al., 2019; Knox et al., 2022). These mixed-age structures were built using different techniques and materials (Tobin, 1995 & Sheishah et al., 2023a).

As revealed by many authors that there are three basic elements related to the modern flood management system; Hazard, Vulnerability, and Risk (Chakraborty & Mukhopadhyay, 2019). Therefore, *flood risk* can be defined as a function of vulnerability and hazard (Chen, 2022). Flood risk has been reviewed from various perspectives by authors with diverse scientific backgrounds, and the conceptual frameworks of risk assessment have been established: the gathering of hazard and vulnerability and integrating the possibility of the hazardous event with the expected damage (de Brito et al., 2017). Flood risk is expected to increase because of socioeconomic development and climatic change (Willner et al., 2018).

Many researchers explained four main types of urban flood risk assessment methods; index system assessment, historical disaster assessment, scenario simulation assessment, and remote sensing impact assessment (Xu et al., 2020). The index system method chooses suitable urban flood impact factors, including many other factors within the evaluation system, to calculate a single assessment. This way is generally easy to follow and widely used, but choosing the factors and weights is subjective (Chen et al., 2015; Lyu et al., 2018). The historical disaster assessment depends mainly on the history of flood data affecting a certain study area. This method is easy to assess but needs more data, and the model's accuracy could be higher. The simulation scenario method to build

a hydrodynamic model to simulate the flood occurrence and predict flooding processes under different scenarios (Yu et al., 2018). Remote sensing impact assessment is to study the land affected by flood disasters by satellite remote sensing images, and the accuracy is a function of time, but it is hard to explain some important information, such as inundation depth and flood flow (Tellman et al., 2021).

In lowland areas, a key protection element is water drainage and the construction of dams and levees. The latter is often the key to flood protection. In the Carpathian Basin, a system of flood protection levees provides safety for millions of inhabitants and hundreds of thousands of houses and thousands of km of roads and railways. In Hungary, more than one-third of the country is protected by an over 2940-km-long levee system, with some sections older than 150 years. Levees were mostly composed of nearby floodplain sediments; their core was preferably clay, above which silty layers were compacted. It is also frequent that the protected side is covered by sand to enable the draining of the levee core during floods. However, the precise structure and composition of the levee are only known along newly constructed sections, as works in the 19th century were scarcely documented. Moreover, due to the application of nearby materials, their composition can be highly heterogeneous in vertical and horizontal terms. Consequently, mapping structural and compositional changes is crucial from the aspect of future flood management (Sheishah et al., 2023a).

Most of the levees along the Tisza were originally constructed in a relatively short period. The first levees needed to be higher and recurring floods overtopped them regularly. Consequently, their height and size continuously increased over time, usually after significant and destructive flood events. This resulted in the development of an onion-like complex earth structure with spatially variable composition (Galli, 1976; Schweitzer, 2002; Amissah et al., 2018). Moreover, levees were then affected by various post-constructional processes, such as compaction, subsidence or water seepage during floods (Galli, 1976; Kovács, 1979; Tímár, 2010). Due to the reasons above, there is a lack of information concerning their structure and composition, making flood risk assessment and preparedness difficult (sheishah et al., 2022).

The height of the levees is variable. These levees are in different conditions. The levees have been raised several times, but flood risk is affected not only by their height but also by their composition, structure, and the various defects in and on them. Because of their age, we have limited information on their condition and changes through time (Ihrig, 1973; Szűcs et al., 2019; Kiss et al., 2021). They were designed by considering

many factors, such as the estimated flood stage, material type, types of land use and structures on the protected side, foundation, and the availability of land for construction (Lászlóffy, 1982; Kiss et al., 2019b; Sheishah et al., 2023a).

It is no coincidence that inspecting the condition of the levees and raising them in case of floods or increasing flood levels due to their confinement makes the regular raising of the barriers an important technical task. The expected deterioration of levees built using old traditional technology, the sliding of the levee material, the seepage through the dam and the loss of stability all require intervention. There are thousands of such precarious levee sections on the Hungarian levee failure of the Tisza, the weakness of which was brought to the surface by the floods, causing the dam in the Tivadar area (Upper Tisza, Hungary), which slipped in 2001, to have to be rebuilt. Work is still ongoing to raise some sections of the flood protection barriers.

The continuous rise in water levels requires the regular raising of dams along the Tisza and its tributaries in Europe. Rising flood levels increase the water pressure that the artificial levee has to withstand and the occurrence of seepage under dams, which poses a significant threat to the stability of the dams. At the same time, the cost of raising the levees increases exponentially. It is more of a practical question that in this logical sequence, after each of the major floods on the Tisza (1876, 1895, 1930, 1970, 2001 and 2006), a decision was taken to raise the levees. Still, a new raising was necessary at some localities by the time it was completed. This reason led to the construction of emergency reservoirs in several places (e.g. Tiszaroff and Tisza-Túr emergency reservoirs in Hungary).

If we had a quick look at the artificial levees of other countries, we could notice that these structures are also very important in terms of flood protection measures. For example, in the United States, the construction of artificial levees started in the early 1700s alongside the lower part of the Mississippi River (Wohl, 2005). Then, most of the basin was protected by levees with confusion instructed by communities and individuals in the 1800s (Hudson et al., 2008). After that, levee construction increased in the lower Mississippi River Basin in the twentieth century (Wohl et al., 2017). The levee construction increased even more in the Mississippi basin after the flood events occurred in 1927 and 1937 and in California after flood events in 1907 and 1909 (ASCE, 2017). Consequently, the government focused on artificial levee construction, resulting in thousands of kilometres of levee (Tobin, 1995).

In China, artificial levees have been constructed on the tidal marshes in the yellow river delta since 1960, as this delta is the main production of the Shengli oilfield, which is counted as one of the biggest oilfields in China. The Chinese levee history started much earlier. The yellow river has one of the longest levee systems in the world. Most levees and diversion canals were undertaken to introduce freshwater or seawater in 2002 and 2006 (Li et al., 2016). The biggest loss of human life on Earth was due to the flood events that occurred in many rivers in China in 1931, and the total loss was around three million people (Floods, 2019), regarding the flood events in the Yellow River occurred in 1887 and 1938, around two million loss of human lives. These are also regarded as the largest flood events in Asia (Mezősi, 2022).

1.2 Assessment of levee health

The height of artificial levees, a key indicator for risk assessment, is widely monitored using various methods (Tanajewski & Bakula, 2016; Kiss et al., 2021), but their internal structures remain hidden. As levees are critical and spatially extended infrastructure, using invasive and time-consuming techniques, usually providing only local information, is not a viable option for assessment. Geophysical methods generally can provide useful physical information on large areas with high accuracy. Such investigations depend on the contrast in physical properties between the layers of different physical properties and anomalies. Shallow and nondestructive geophysical methods have widely been utilized recently in levee investigations (e.g., Perri et al., 2014; Busato et al., 2016; Sentenac et al., 2017; Borgatti et al., 2017; Rahimi et al., 2018; Dezert et al., 2019; Jodry et al., 2019; Tresoldi et al., 2019; Lee et al., 2020; Sheishah et al., 2023a).

Electrical Resistivity Tomography (ERT) and Ground penetrating radar (GPR) are the most widespread among these. The two methods offer advantages in different applications, and their combination with geotechnical assessment can provide a robust picture of levee conditions (Asch et al., 2008; Di Prinzio et al., 2010; Hibert et al., 2012; Morelli & Francese, 2013; Chlaib et al., 2014; Busato et al., 2016; Borgatti et al., 2017; Bakula et al., 2017; Crawford & Bryson, 2018; Sheishah et al., 2022; Sheishah et al., 2023b).

Many authors have used ERT to investigate the health of various levee sections along rivers and check their flood protection abilities. For instance, two-dimensional (2D) and three-dimensional (3D) ERT were utilized to locate fissures in levees (Sentenac et al., 2012; Jones et al., 2014). Meanwhile, a 3D extended normalization approach of ERT

was used in the levee investigation (Fargier et al., 2014). Tresoldi et al., 2019 introduced a valuable study to monitor earth levees and control seepage water saturation and evolution in pseudo-real time by utilizing the ERT technique. The authors analyzed the effect of external variables like temperature, the water level in the canal and rainfall events on resistivity data at different depths of the levee body and in different year periods. ERT is not only adequate for structural assessments but also can enable the identification of seepage zones and sections affected by intensive water saturation through long-term monitoring, as demonstrated by Lee et al. (2020). Sentenac et al. (2017) focused on mapping the structural integrity of historical earth reservoir levees, susceptible to natural decay with time. The authors used four geophysical techniques to assess the post-flood damage, which is fast scanning technique using a dipole electromagnetic profile apparatus (GEM2), ERT to obtain a high-resolution image of the damaged/seepage zone, Self-Potential surveys to relate the detected seepage evolution and change of the water displacement inside the levee, and the washed zone in the areas with piping was characterized by microgravimetry. Active thermal sensing is used along with other geophysical techniques to detect leaks and erosion zones in levees (Radzicki et al., 2021). Using ERT enabled authors to assess the function between water content and resistivity values, which allowed the transformation of resistivity profiles into water content maps. Geotechnical investigations were also applied to validate geophysical surveys (Perri et al., 2014; Dezert et al., 2019). 2D DC ERT and seasonal temperature profiles were applied by Jodry et al. (2019) to monitor the seasonal change in soil moisture in an earthen levee to produce seasonal resistivity change models. Meanwhile, near-surface structures were mapped through the combined use of capacitively coupled resistivity and multichannel analysis of surface waves (Rahimi et al., 2018), and information on potential problem areas along the levee could be provided (Sheishah et al., 2023a).

Although ERT can reveal subsurface configurations and is commonly used for levee investigations, it still has some drawbacks. Different parameters such as rainfall, temperature, sheet piling, and 3D effects can disturb ERT measurements (Fargier, 2011; François et al., 2016). Furthermore, ERT requires high contrast in resistivity to provide promising results. Seismic surveys can also be used in levee investigations. However, if the contrast in acoustic impedance is not high enough, the levee structure cannot be resolved (Karl et al., 2008). Also, if a heterogeneous material within the levee core is located below the resolution level, it cannot be easily detected. However, ground-

penetrating radar (GPR) provides the best solution for surveys on long sections, especially when fast, high-resolution data are necessary (e.g., Di Prinzio et al., 2010; Chlaib et al., 2014; Antoine et al., 2015). GPR has been used in many applications in the last decades as it is a nondestructive and high-resolution shallow geophysical technique that can resolve various defects and structural and compositional changes. It is widely used for detecting animal burrows, which can be considered one of the main reasons for levee failures by piping phenomena (Di Prinzio et al., 2010). In this sense, animal burrows can be a major issue and an important factor behind increased flood risk (Sheishah et al., 2023a).

Consequently, GPR was utilized by (Chlaib et al., 2014) to detect small-scale animal burrows during levee assessment and found a good agreement between the observed features and the interpreted anomalies. The affordability of GPR was also considered in discriminating voids from water-filled cavities or metallic objects (Chlaib et al., 2014; Samyn et al., 2014). A good matching was clear between the observed features and the interpreted anomalies. However, validation of results by field evidence, geotechnical data, or other geophysical techniques is crucial, as underlined by Borgatti et al. (2017) and Sentenac et al. (2017). Nevertheless, not only compositional but at-a-point defects can also reduce the flood retention capacity of earthen structures. Therefore, another major issue affecting levee health is the occurrence of sections with more porous compositions or complex structures where seepage can develop, and GPR can also be applied in identifying these risky sections (Antoine et al., 2015; Busato et al., 2016). Antoine et al. (2015) used GPR and permeability logging to detect leakage areas in the levee. They managed to detect seepage zones from the interpretations of GPR sections (Sheishah et al., 2023a).

Combining geophysical techniques provides excellent results, especially when applied to the same area and integrated to confirm the outcomes. Busato et al. (2016) implemented three effective geophysical techniques, which are Multichannel analysis of surface waves, ERT, and GPR, to describe a reconstructed levee. The results of the geophysical methods can be compared and integrated with geotechnical data to characterize structures of river levees effectively. The utilization of electrical resistivity imaging became state of the art in studying the characterization of levees (Cho & Yeom, 2007; Sjö Dahl et al., 2009), together with ground-penetrating radar (Di Prinzio et al., 2010). Nevertheless, integrating two or more different geophysical techniques can provide more reliable outcomes (e.g. Inazaki and Sakamoto, 2005; Cardarelli et al., 2014).

Not only GPR but resistivity surveys and multichannel analysis of surface waves (MASW) were used by (Rahimi et al., 2018) to detect cavities responsible for piping and the formation of sand boils on the protected side of levees. The cause and path of leakage in a damaged levee were interpreted by (Lee et al. 2020) by using an integrated method of 3-D resistivity inversion (Sheishah et al., 2022).

Sometimes authors agree that GPR has a limited investigation depth in the levee applications because of the usually high clay content of these earth structures, and they turn to ERT, providing a higher penetration depth and more information on the sedimentary composition of the levee structure (Perri et al., 2014; Busato et al., 2016). However, using ERT, a serious compromise must be made regarding spatial resolution and measurement time. Besides, the need for more geotechnical control, in many cases, turns off the validation of the quality of results (Dezert et al., 2019; Lee et al., 2020; Radzicki et al., 2021).

In the present study, we aimed to combine the strength of the geophysical techniques GPR and ERT as well as Levelling data, real-time kinematic GPS (RTK-GPS), and Persistent Scatterer Synthetic Aperture Radar (PSI) on levee sections along the Tisza and Maros River in order to test the potential of an integrated approach in levee health assessment and to determine the limitations of the applied methods.

Based on the above, the following objectives were set forth during the research for the studied levee sections:

1. The structural analysis includes identifying the units forming the levee body and mapping the changes along the levee.
2. The compositional analysis includes investigating the materials forming the levee and detecting the anomalies.
3. Investigation of relationships between parameters.
4. Evaluation of levee health by integrating different methods and verifying the outcomes by the records of previous flood events.
5. Create a measuring plan that can be applied for more extensive surveys along different levee sections.

2. Study area

Artificial levees were built more than 150 years ago as a part of flood risk protection measures in most floodplains in the Carpathian Basin. Flood hazard maps in Hungary are available and can be accessed online (ÁKK, 2015), and they provide information about the protected areas from floods where artificial levees failure might cause serious problems. Although the levee failures are limited, people have created a false sense of security. During the twentieth to twenty-first centuries, peak flow levels had increased, particularly in the dynamic fluvial system of the Tisza River (Kiss et al., 2019b).

The Tisza River drains the eastern half of the Pannonian Basin, where river systems have a long evolution history. The oldest fluvial deposits date back to the Late Miocene (Gábris & Nádor, 2007). The courses of the rivers, including the Tisza, are influenced by several sinking grabens. One of the most active ones is the South Tisza Graben, where approximately 700-m-deep fluvial sediments have accumulated (Rónai, 1985). Until the Late Pleistocene, the graben subsidence was continuous but fluctuating (Kiss et al., 2014); during the Holocene, it terminated as Early Holocene floodplain forms were not buried by younger sediments (Kiss et al., 2012). However, in historical times, the subsidence became active again, mainly driven by natural gas, oil, and water extraction (Sheishah et al., 2023a).

Tisza River is the largest tributary of the Danube River: its current length is 962 km, its catchment area is 157 000 km², and it has a mean discharge of about 865 m³/s at Szeged. Before the massive regulation works that happened in the 19th century, the lowland part of this river (at that time approximately 800-900 km) was characterised by large-scale floodplains (38 500 km²) inundated almost every year; therefore, it represented a challenge for the agricultural activities. Consequently, the main target of river training was to expand the flood wave velocity by making 112 cut-offs to decrease the river length and widen the floodplains by building artificial levees system along the Tisza River and its tributaries (Sheishah et al., 2022).

The Maros is considered one of the essential rivers flowing in the Transylvanian Basin. It enters the Great Hungarian Plain through the southern boundary of the depression of Körös. Due to tectonic movements, the river formed its current location at the end of the Pleistocene. The Maros (Mures) River has the largest tributary (catchment area=30 332 km²) of the Tisza. The sediment discharge and slope of the lowland part are greatly affected by the alluvial fan of the river. The alluvial fan has a radius of

approximately 80–100 km, and its anterior part is only 20 km from the outlet, which shortens the lowland part of the river (15 km). The fan apex at Lippa (Lipova) represents the top (130 m asl) of the Great Plain Hungarian rivers, which results in steep slopes in the lowland area (0.0013) and on the alluvial fan (0.0028) (Laczay, 1975).

Regarding the flood events on the Tisza River, many occurred in 1919, 1925, 1940, 1948, 1970, 1974, 1998, 1999, 2000, 2006, and 2010 and the high water exceeded the crown of the levees. The levees were built for the possibility of the highest floods occurrence once in 50 years; because of the silting up of the floodplain, they were raised several times (Schweitzer, 2009).

Regarding flood events on the Maros River, they usually occur in the spring and the early summer. Flood events on the Maros normally exceed those on the Tisza, but, in some cases, floods can be coincident. In these cases, the Maros is confined by the Tisza, resulting in long-lasting overbank floods that record higher levels of water. Examples of this case occurred in 1941, 1970, 1975, 2000, and 2006). Altogether, 725 overbank flood days were documented at the gauge station of Makó in the 20th century (average six d/y). Short floods of approximately 1 to 2 days are the most frequent; the large-scale overbank flood (which lasted for 47 days) took place in 1970 because of impounding. The maximum and average documented discharges were 2440 m³/s and 161 m³/s in 1970, respectively, while the discharges interval of overbank floods lasting for one year and 30 years were 710 m³/s and 1500 m³/s, respectively (Boga & Nováky, 1986).

To decrease the area of flood inundation in Hungary, artificial levees were constructed with a length of 2940 km, which restrict the width of the floodplain to 0.4–5 km (Kiss et al., 2008). The active confined floodplain width is irregular, and the flood risk increases in narrow sections (Lóczy et al., 2009). The active floodplain on the right side along the lower Tisza (western side) is narrow with an average width of 270 m, and in several places, the artificial levee has a length of 25 m of the main channel, while the active floodplain on the left side (eastern side) is 2.5 times wider (with an average 635 m); so, artificial cut-offs are located in the area on the active floodplain. The height of the artificial levee was raised to provide flood safety, especially after the recorded flood event in 1970. Therefore, the Lower Tisza Water Directorate conducted a levelling survey in 1976–77 to measure the height conditions of the artificial levee system.

Because of the repeated flood events mentioned above, the height increase of artificial levees with time is shown in **Fig. 1**. The levee height ranges from 5 to 7 meters. The earth's structure's material is primarily clayey and silty.

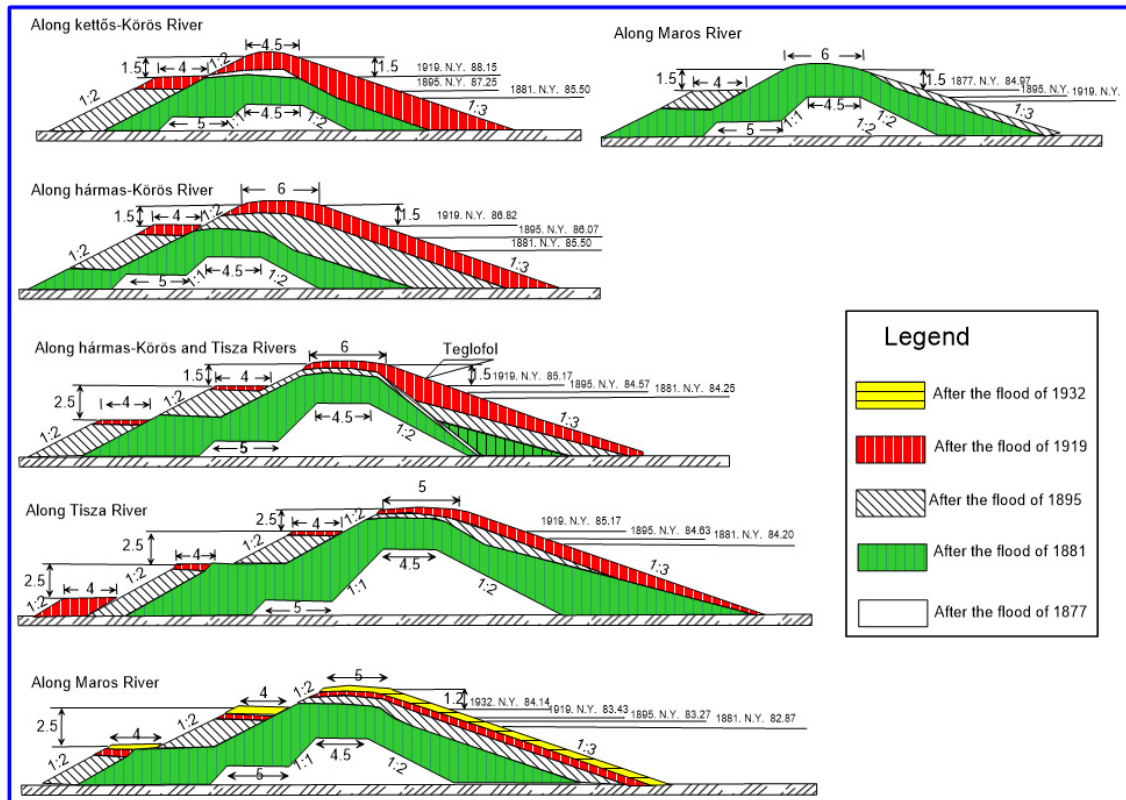


Figure 1 Typical cross sections from levees of three rivers in Hungary, which show the change of heights through time (Nagy & Tóth, 2001)

The height of artificial levees might be decreased for many reasons. Traffic from the roads on the crown can cause compaction of the sandy-clayey material of the levee. The height decrease of the levees could also be because of surface deformation based on subsidence or uplift. These parameters should be combined and integrated for estimating the flood risk because serious situations might happen during peak flows in the Tisza and Maros rivers and the height decrease of the artificial levees. Therefore, the changes in the height should be mapped for flood protection measures.

The study area is situated on the left bank of River Tisza and the left bank of River Maros in the southern part of Hungary. A 48 km levee section was chosen for geophysical surveys and drillings (Fig. 2). 1km stands for levee kilometre. The investigated levee was last reinforced in the 1970s, but only little is known of its internal structure and the composition of layers. The precise structure and composition of the levees are only known along newly constructed sections, as works in the 19th century were scarcely documented. Moreover, because of the application of nearby materials, such compositions can be highly heterogeneous in vertical and horizontal terms. Consequently, mapping structural

and compositional changes is crucial from a future flood management perspective (Sheishah et al., 2023a).

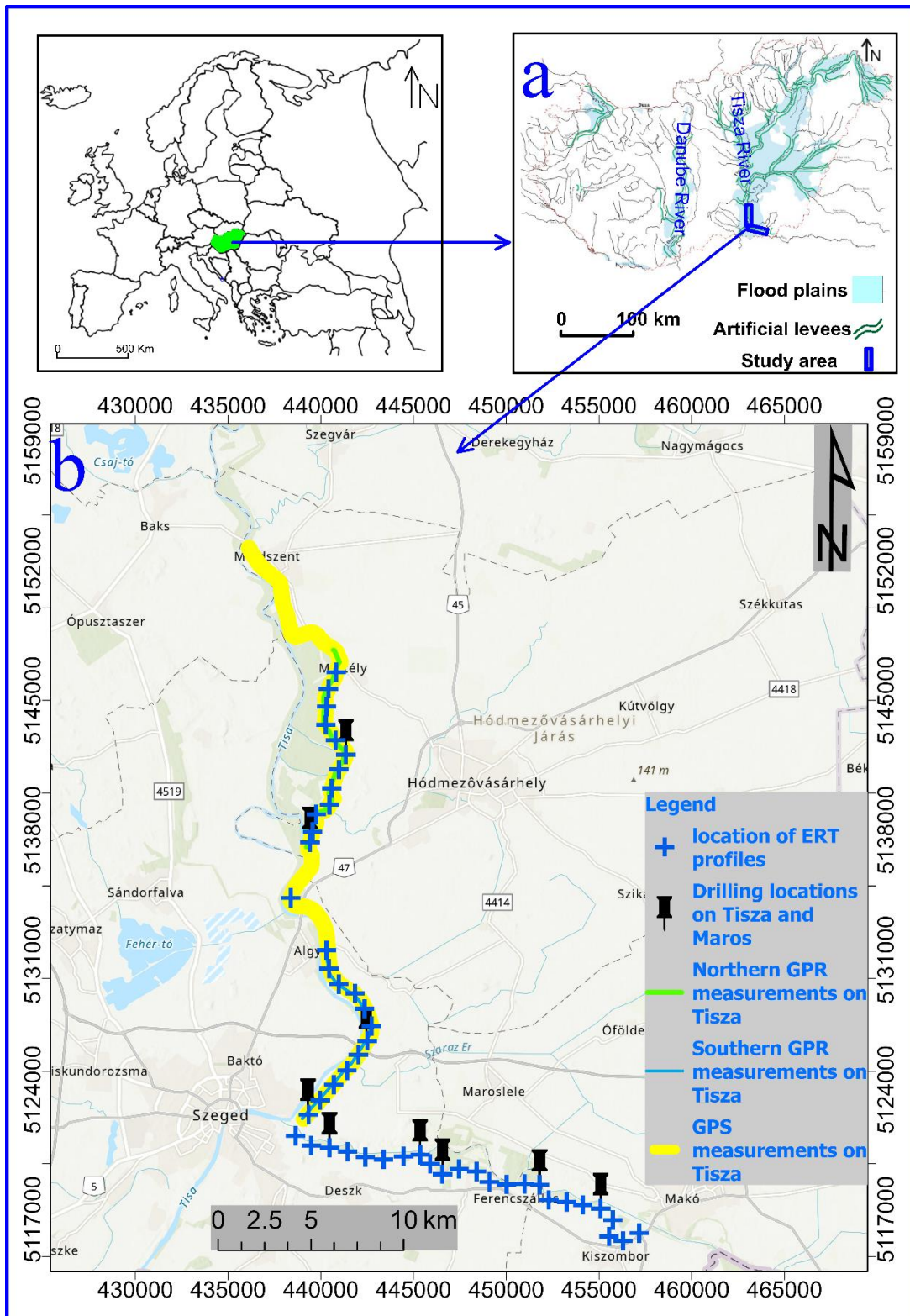


Figure 2 A) Location map with potential floodplains and artificial levees in Hungary (modified after OVF 2014), and B) the study area showing the places of RTK-GPS measurements as a yellow line and levee sections surveyed by GPR and ERT and drilling locations

3. Data and methods

3.1 GPS measurements

GPS measurements were performed on the levee crown and levee foot at every 200 m between 12.5 and 42.0 lkm, using a TopCon Hyper Pro device in 2017 and 2018 (**Fig. 3**). The 3D accuracy of the instrument was measured to be 2-3 cm. Concerning the levee crown, the baseline elevation data was derived from differential levelling made by the Lower Tisza Water Directorate in 1976. Levelling data were referenced to the national benchmark system at the time, which was later renewed and incorporated into the National GPS Network. Still, there is a spatially variable height difference between the two systems, and at the study site, this difference is estimated to be 6 to 7 cm. Consequently, we corrected the levelling data by -7 cm to obtain more realistic height change values (Sheishah et al. 2023a).

The long-term height change of the investigated levee section was assessed by comparing archive levelling data to recent real time kinematic GPS (RTK-GPS) measurements. GPS-based height changes, however, are hard to evaluate in terms of surface deformation, as there can be several other factors in the mm to cm range affecting levee height besides geologically driven subsidence or uplift. Therefore, subsidence velocity was also estimated using Persistent Scatterer Synthetic Aperture Radar (PSI) data (Sheishah et al. 2023a).

Along the levee foot, our GPS measurements were compared to the data of an earlier GPS survey, made again by the Water Directorate in 2003. The points of the 2003 survey were staked out at least with a 5 cm horizontal precision and then height was measured again. In this case, no additional corrections were made, as both surveys used the same reference system (Sheishah et al. 2023a).

Acknowledging the above-mentioned uncertainties, and in order to verify the height change derived from geodetic data, measurements were complemented by space-based PSI data. PSI analysis was based on 70 ERS-1, ERS-2 and Envisat Single Look Complex data of the European Space Agency (ESA) acquired between 1992 and 2010. For every 500 m section between 12.5 and 39.0 lkm average vertical velocity values were calculated from those PSI point targets which were located on and around the levee within a 1500 m buffer zone. The width of the buffer zone was decreased to 300 m near the city of Szeged due to greater point density (Sheishah et al. 2023a).



Figure 3 Location of GPS points measured on levee crown and levee foot

3.2 ERT measurements

The variations in the subsurface resistivity can be determined by carrying out surveys on the ground surface. From these measurements, the true subsurface resistivity can be calculated. Electrical resistivity techniques have been used for decades in many applications, such as geotechnical, mining, hydrogeological, and environmental investigations (Loke, 2004).

Ohm's Law is the fundamental physical Law used in resistivity investigations and controls the current flow in the ground. The equation for the flow of the current in a continuous medium is given by

$$J = \sigma E \dots \dots \dots \text{Eq. 1}$$

where J is the current density, E is the intensity of the electric field, and σ is the conductivity of the medium.

instruments that measure resistivity usually give a resistance value, $R = \Delta\phi/I$, therefore practically the value of apparent resistivity (ρ_a) is calculated by the following equation

$$\rho_a = k.R \dots \dots \dots \text{Eq. 2}$$

k is a geometric factor that relies on the arrangement of the current and potential electrodes used in the measurement and the electrode spacing.

The calculated resistivity value does not represent the true subsurface resistivity but an “apparent” value. There is a complex relationship between the apparent and the true resistivity. Therefore, inversion is used to calculate the true subsurface resistivity from the apparent resistivity values (Loke, 2004).

ERT can issue high-resolution and significant images of the electrical resistivity of the levee body. The unconsolidated sediments have a wide range of resistivity values from 10 to 10000 Ωm (Loke, 2004).

The resistivity of sedimentary layers and earthen structures depends primarily on the deposit's water content and grain size (in close relation to porosity). In general, by increasing grain size, resistivity values increase (see, e.g. Samouelian et al., 2005; Cosenza et al., 2006; Sudha et al., 2009; Osman, 2012; Perri et al., 2014; Oludayo, 2021; Siddiqui), whereas increasing water content has a reverse effect (McCarter, 1984; Abu-Hassanein et al., 1996; Fukue et al., 1999; Michot et al., 2000; Yoon & Park, 2001; Pozdnyakova, 2002; Loke, 2004). Gupta & Hanks (1972) and Goyal et al. (1996) proposed an empirical linear relationship between resistivity and water content. Consequently, we also investigated the effect of these parameters on the measured resistivity to see to what extent structural units can be separated. Specific resistivity values used for the analysis were obtained from the ERT profiles at the boreholes and the sampling depths. The high resolution that characterizes ERT makes it a recommended tool for such investigation.

There is a variation in the shape of the contours in the ERT pseudo section resulting from using different arrays on the same structure. Therefore some factors should be put into consideration when selecting the best survey; (1) the sensitivity of the resistivity meter used in the survey, 2) the sensitivity of the array to vertical and horizontal changes in the subsurface resistivity, 3) the type of structure to be mapped, 4) the background noise level, 5) investigation depth, 6) the signal strength and 7) the horizontal coverage of the data (Loke, 2004). In practice, five types of arrays are common for 2-D imaging surveys; 1) Wenner, 2) dipole-dipole, 3) Wenner- Schlumberger, 4) pole-pole, and 5) pole-dipole.

ERT profiles were collected along the investigated levee sections using a Wenner array with different electrode spacing at some locations. The following section explains the features of the applied array in our study.

3.2.1 Wenner array

The Wenner array has an advantage in mapping vertical variations (i.e., horizontal structures) but is poor in resolving horizontal variations (i.e., vertical structures). The Wenner array has a higher sensitivity to the vertical changes below the centre of the array because its sensitivity plot has almost horizontal contours below the centre of the array. The investigation depth for the Wenner Alpha array is approximately 0.5 times the "a" spacing used. The Wenner Alpha array has a medium investigation depth compared to other array types. The strength of the signal has an inverse relation with the geometric factor used in calculating the apparent resistivity of the Wenner array. Wenner array has a geometric factor of $2\pi a$ which is considered small compared to the geometric factor of other arrays (**Fig 4**). One advantage of the Wenner array is that it has the strongest signal strength among other array types, which is useful if the investigation is carried out in high background noise areas. One drawback of this array for 2-D data collection is the relatively poor horizontal coverage because of the increase in the electrode spacing (Loke, 2004).

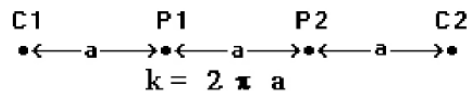


Figure 4 Electrode configuration of Wenner array used in the ERT data collection along the investigated levee sections

ERT data was collected using a GeoTom MK8E100 apparatus with a multi-electrode system (50 electrodes) (Fig. 5a and b). A total of 109 ERT profiles were collected at two levee sections: the first section was at the left bank of River Tisza from 13-1km to 42-1km, and the second section was at the left bank of River Maros from 1-1km to 24-1km. Because the levee core might show a difference in the composition compared to both sides and even the core itself might show variation in its structure; therefore, the data collection plan of the ERT survey was to measure two profiles at each 1km for all the investigated sections. At each levee km, the first profile was measured longitudinally on the levee crown (**Fig. 5a**) and the second profile was measured transversely covering the levee crown and both sides of the levee which are river and protected sides (**Fig. 5b**). Elevation data were collected at each odd number electrode along the survey line by a TopCon Hyper Pro RTK GPS to apply a topographic correction for the transverse profile (**Fig. 5c and d**).

Regarding the investigated section of Tisza levee, 61 ERT profiles were measured at levee km from 13 to 24 and 31.4 to 42. The section from 25 lkm to 30 lkm was not investigated because the levee crown was paved. Only one longitudinal ERT profile was measured at 28 lkm, while the transverse profile was not measured because of the car traffic on the levee crown. Data collection was done in May, June, and July 2020. In the case of the preliminary ERT measurements carried out in May and June, one cable was connected to the control unit with 25 electrodes. For the longitudinal profiles, the electrode spacing was 2.5 m, the total number of datum points was 92, the total number of data levels was 8, and the profile lengths were 60 m. The electrode spacing was reduced to 2 m for the transverse profiles because the profile length was enough at some sections to cover the levee width, including the crown and its sides. The total number of data levels was 8, the total number of data points was 92, and the profile lengths were 48 m. In the case of ERT measurements carried out in July, the longitudinal profiles were collected as the same strategy as May and June measurements, whereas, in the case of transverse profiles, the levee showed a variation in its width and became even wider than the preliminary investigated section, on the other hand, the resolution had to put into consideration. Therefore, they were collected by two cables with 50 electrodes and 1.5 m electrode spacing. The total number of data points was 392, the total number of data levels was 16, and the total length was 73.5 m.

Regarding the investigated section of Maros levee, 48 ERT profiles were successively measured in June 2020 at each lkm from 1 lkm to 24 lkm. ERT data collection in this section, including profile lengths, the total number of data points, the total number of data levels, electrode numbers, and electrode spacing for longitudinal and transverse profiles, were the same as the ERT data collection strategy on the Tisza levee.





Figure 5 Data acquisition by A and B) GEOTOM MK8E100 multi-electrode ERT system on the crown and crossing the levee, C, and D) TopCon Hyper Pro RTK GPS

In order to obtain the true resistivity values for the building materials of the levees, apparent resistivity values obtained during ERT profiling were processed in RES2DINV 3.4 was used (Loke, 2004). Before initiating the inversion process, noisy outlying data points were taken out. The inversion scheme was based on the least-squares smoothness-constrained iterative optimization algorithm (Constable et al., 1987; De Groot-Hedlin, Constable, 1990). Since transverse profiles show elevation changes, a topographic adjustment was also carried out before initiating the inversion. After obtaining low and satisfactory RMS values, the inverted ERT profiles were exported and drawn in Surfer v20 for evaluation.

3.3 GPR measurements

GPR transmits high-frequency electromagnetic pulses that are partially attenuated but reflected off the interface of layers or objects with various dielectric characteristics. It is a quick, high-resolution, non-invasive electromagnetic technology. Higher reflectance is felt when the dielectric permittivity contrast increases. The frequency and wavelength of the transmitted electromagnetic pulses directly impact the depth of penetration of GPR. According to Daniels (2004), the maximum penetration depth is equivalent to 20 wavelengths; however, in most circumstances, this depth will be much lower due to the electromagnetic characteristics of the sediments (Utsi, 2017).

Electromagnetic pulses are carried throughout the survey medium, the upper layers of the earth's crust, such as a levee (**Fig. 6**). Parts of the signal are reflected in the receiver as they pass through this substance. Each of these reflections is brought on by the changing properties of the subsurface buried substance. The returned signals convey information to the controller via the receiver in **Fig. 6**. This information needs to be visual, and radar does not, at least not in the usual sense of the word, provide a picture of what is under the surface.

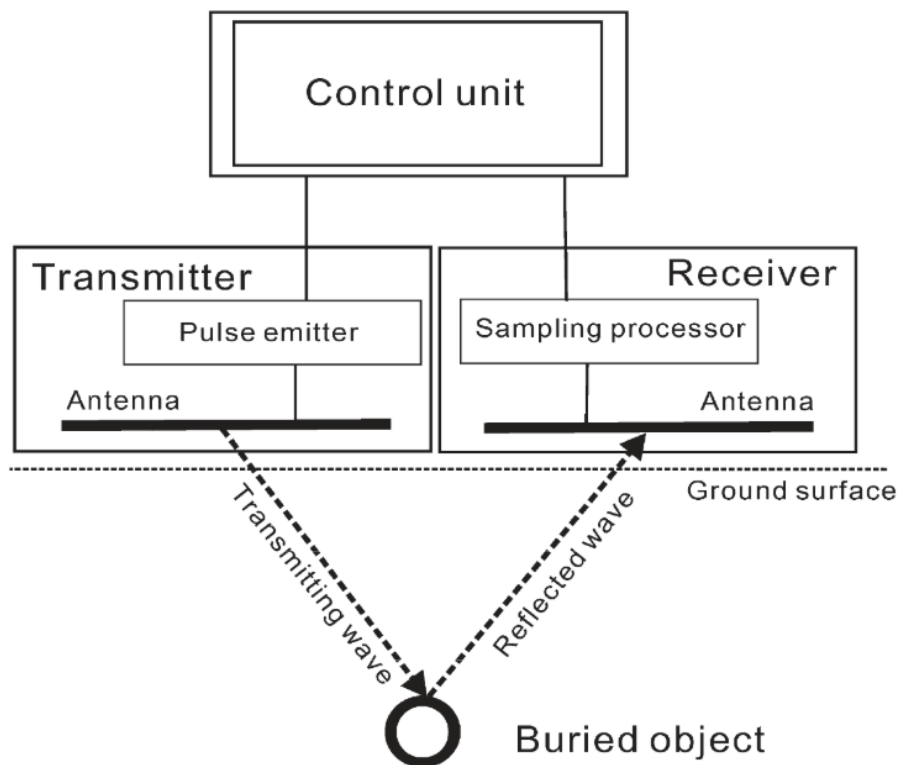


Figure 6 Basic set up of GPR.

GPR data quality is influenced by the environment being studied. Open soil or man-made materials like asphalt and concrete are the two types of surfaces used for GPR most frequently. It can also refer to ice, building floors, ceilings, walls, and any other material containing potential targets for investigation. The difference in electromagnetic characteristics between each material determines whether signal portions are returned. This means that any substance may be detected by the radar as long as its magnetic and electrical reactions differ from those of the materials around it. The characteristics of the EM signal, such as its velocity, energy, waveform, and absorption, are controlled by the medium's electromagnetic properties. An essential characteristic that governs the signal's

velocity is the dielectric constant (ϵ_r), which compares the medium's (ϵ) dielectric permittivity to a vacuum. ($\epsilon_0 = 8.89 \times 10^{-12}$ F/m) (Jol, 2009):

$$\epsilon_r = \frac{\epsilon}{\epsilon_0} \dots\dots\dots \text{Eq.3}$$

There are many factors affecting dielectric constant values of materials such as porosity, density, texture, chemical composition and water content. The EM wave velocity (v (m/ns)) in a medium can be expressed as:

$$v = \frac{c}{\sqrt{\epsilon_r}} \dots\dots\dots \text{Eq. 4}$$

where c is the speed of light in vacuum (0.3 m/ns).

EM wave velocity can be calculated if the target depth (D) and the travel time of the signal (t) are known:

$$v = \frac{2 \cdot D}{t} \dots\dots\dots \text{Eq. 5}$$

t is the two-way travel time, which represents the pulse duration from the transmitter, reaching the target, reflecting back to the receiving antenna. t is measured from the GPR profile. It is also possible to calculate the target's depth, D , if the dielectric constant is known:

$$D = \frac{c \cdot t}{2 \sqrt{\epsilon_r}} \dots\dots\dots \text{Eq. 6}$$

The antenna frequency is a significant component that affects the GPR penetration depth (Jol, 2009; Olhoeft, 1998). While the reflecting coefficient (R) for the interface between them may be written as follows, when an electromagnetic wave reaches the interface between two different types of electric materials, its reflection quantity relies on the difference in dielectric constant between them.

$$R = \frac{1 - \sqrt{\epsilon_2 / \epsilon_1}}{1 + \sqrt{\epsilon_2 / \epsilon_1}} \dots\dots\dots \text{Eq. 7}$$

where ϵ_1 and ϵ_2 refer respectively to the dielectric constants of the two materials.

3.3.1. GPR data collection

The GPR survey was conducted using SIR 3000 control unit (Geophysical Survey Systems Inc.) attached to a 200 MHz centre frequency antenna in the survey wheel mode (**Fig. 7b**). In order to achieve a high vertical resolution, we recorded 1024 samples per scan (16 bits per sample) and applied no stacking. The scanning rate was set to 64 scans per second, and data was acquired at a 60-scan-per-meter horizontal resolution. The time range window was set to 170 ns, the gain and the position of the first positive peak

were set automatically, and the dielectric constant was kept at 16 throughout the measurements (Sheishah et al., 2023a).

The wavelength of the signal can determine the penetration depth. In ideal conditions, the maximum penetration depth before the transmissions' full energy is lost is about 20 wavelengths (Daniels, 2004). In practice, there are only so many environments with so little signal loss capacity that a depth near the 20 wavelengths will be able to be achieved. In most site conditions, but depending on the ground's electromagnetic properties, the penetration depth will be considerably less than 20 wavelengths. Water in the investigated soil reduces the depth to which the radio waves can effectively penetrate (Utsi, 2017). In the current study, the successive GPR profiles' dissipation depth was approximately detected using RADAN software 7 (GSSI, 2018).

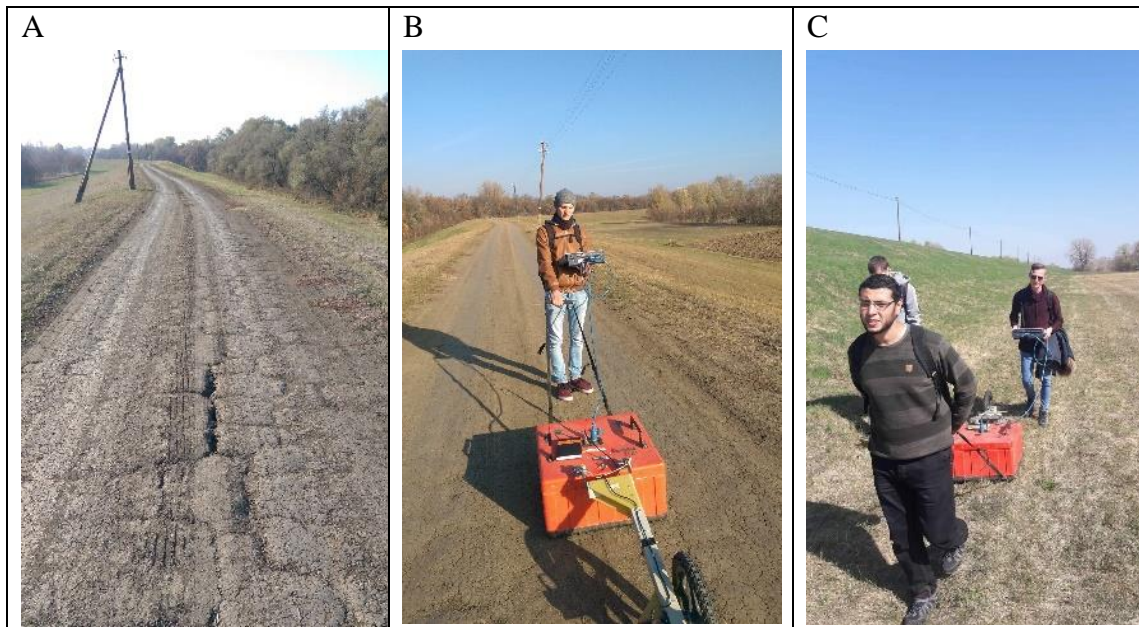


Figure 7 A) Tensile cracks on the levee crown, B) GPR survey by using SIR3000 attached to 200 MHz shielded antenna on the levee crown, C) GPR survey on the levee foot

The GPR survey was conducted on the left bank of the Tisza River. It is subdivided into two zones termed as Southern levee zone (12.6 lkm - 23.9 lkm) and the Northern levee zone (31.2 lkm- 43.10 lkm) as these zones are separated by a 7 km long asphalted levee section **Fig. 7C**. Measurements were performed on the levee crown and at some places at the levee foot as well.

A total of 282 GPR cross-sections were measured on the Tisza levee (southern and northern zones) by a 200 MHz centre frequency antenna. In more detail, 162 GPR Profiles were measured in the southern zone, as shown in (**Fig. 2**). 114 GPR profiles were conducted on the levee crown. 48 GPR profiles were conducted on the levee foot.

Regarding the northern zone, 120 GPR profiles were measured on the levee crown. All the GPR profiles were successive, which means that the endpoint of one profile is the starting point of another profile. Each GPR profile has a 100 m length, as shown in **Table 1**.

Table 1 GPR survey on Tisza levee by 200 MHz centre frequency antenna

	From lkm	To lkm	Location on the levee	Number of GPR profiles
Southern zone	12.6	24.3	crown	114
	12.6	17.4	foot	48
Northern zone	31.2	43.2	crown	120

3.3.2. Checking the levee by two different antennas

To study the application of different centre frequency antennas and their applicability for the levee studies, GPR surveys were also carried out by applying two systems (GSSI SIR 3000 and IDS) with different centre frequencies (200 MHz **Fig 8a** and 80 MHz **Fig. 8b**) at a specified section on the crown of Tisza levee between 13 lkm and 16.5 lkm. The survey track was divided into 100 m pieces for both systems, and the survey wheel mode was used for measurements. Each 100 m section's beginning and ending locations were identical for both polls to improve comparison. Data was gathered using a scanning frequency of 64 scans per second and a temporal range of 170 ns (200 MHz) and 300 ns (80 MHz). There were 1024 samples for each scan and 60 scans for every unit (metre). The depth of the strata discovered by drilling served as the basis for the dielectric permittivity value 16 that was used (Sheishah et al., 2022).



Figure 8 Data acquisition by A) GSSI SIR3000 GPR system with a 200 MHz antenna, B) IDS GPR system with an 80 MHz antenna

3.3.3. GPR data processing

Since no filters were applied during data acquisition, the signals contained a variety of unwanted signals that had to be removed, including low-frequency noise, high-frequency monochromatic unwanted signals, spurious noise, and flat-lying noise, which originated from antenna ringing and any other reflections arriving from above the ground (such as reflections from nearby vehicles, buildings, fences, power lines, and trees). To increase the signal-to-noise ratio, we employed the programmes RADAN 7 (GSSI, 2018) and REFLEXW 8 (Sandmeier, 2016). Time zero (Tz) removal was the first processing step to make up for the delay in the first arrivals. Each trace is treated individually by the filter. The filter parameter move time determines the time value for each trace that has to be moved. The move time parameter in the data was set to -14 ns. The backdrop reduction filter was the second stage, employed to eliminate horizontal banding brought on by the GPR and other reflections over the ground. These undesirable reflections are minimised by using the shielded antenna. Additionally, horizontally coherent energy is suppressed. This filter is used after time zero correction because it eliminates the direct coupling pulse. This filter applies to the specified quantity of traces.

The filter subtracts an averaged trace (trace range), constructed from the real section's selected time/distance range. The timestamps for the start and finish were both set to 0 ns. In order to stop traces from drifting over time and remove the low-frequency component (dewow) from the received signal, the third stage used a 1D filter to subtract the mean (Sandmeier, 2016). A running mean value is computed for each trace's value due to the filter's actions on each trace. The centre point is then removed from this running mean. In the fourth phase, a 1D bandpass frequency filter was used to remove any leftover low-frequency noise and extra high-frequency monochromatic signals that did not fall within the GPR's operating frequency range (Sandmeier, 2016). Each trace is treated individually by the filter. It is used on every trace. The lower cut-off is set at 10, a lower plateau at 85, a higher plateau at 185, and the upper cut-off at 300. The bandpass filter suppresses noise with a different frequency content from the signal. The fifth step was a 2D filter running average. This filter emphasizes horizontally coherent energy to clarify targets and reduce spurious noise (Utsi, 2017). To suppress trace-dependent noise, the running average is performed over several traces. The average number of traces used here was 7, the start time was set to 0 ns, and the end time was set to 156 ns. The mean value is calculated and assigned to the current sample as a new value from these seven samples.

The remaining traces up until the conclusion of the profile were examined once the first seven had been completed. The strength was manually adjusted in the y-direction for each signal in the sixth step because, as each signal descended deeper into the earth, some components were lost (attenuated), and others were reflected into the receiver (Utsi, 2017). It makes up for changes in the input signal's intensity over time. Each trace is treated individually by the filter. It enables us to interactively create and apply a digitised gain curve to the data in the y-direction (often the time axis). We did not perform the topographical correction because no elevation changes could be seen in the 100 m-long GPR cross-sections measured along the examined levees.

After processing, the GPR profiles were carefully examined to spot interfaces and document irregularities. Then, anomalies were categorised and assessed for flood danger. Regarding other criteria for the health of the levees, the geographical distribution of the various categories was examined. Changes in levee composition were also evaluated in addition to mapping structural variations and flaws, mostly by examining the attenuation of signals. Effective penetration depths at a given dielectric constant ($\epsilon=16$) were used to calculate differences in attenuation. Using RADAN's automatic Max Depth tool, which examines noise and signal loss from trace to trace, penetration depth was estimated. We presumed that there is a direct correlation between penetration depth and the grain size/porosity of the sediments making up the levee body because measurements along the examined levee sections were conducted on consecutive days, which rendered environmental conditions, particularly moisture content.

3.4 Sedimentological data

In order to correctly interpret and validate ERT surveys, 19 boreholes were drilled at definite locations on Tisza and Maros levees. Borehole locations in Tisza levee were at 13 lkm, 18 lkm, 31.4 lkm, and 37 lkm, while in Maros levee were at 3 lkm, 8 lkm, 10 lkm, 16 lkm and 20 lkm. Two boreholes were made at each mentioned site: the first one was on the riverside edge of the levee crown with a depth ranging from 6 to 7 m, and the second one was on the protected side slope of the levee with a depth ranging from 3 to 4 m. One borehole was drilled on the levee foot of 16 lkm with a 2 m depth. Drilling was carried out using an Eijkelkamp drilling system with a 5 cm diameter drilling head (**Fig. 9**). TopCon Hyper Pro RTK GPS was used to measure the accurate coordinates and elevation data at the drilling location. On-site, macroscopic description of sediments extract was recorded.



Figure 9 Drilling using an Eijkelkamp drilling system

Simultaneously, at every 20 cm, samples were collected for grain-size analysis. Measurements were performed with a Fritsch Analysette 22 laser analyzer, having a measurement range of 0.08-2000 μm (**Fig. 10a**). A total of 457 samples were collected. Two hundred-two samples were taken from the levee of River Tisza, and 255 samples were taken from the levee of River Maros. The samples were dried at 105°C in a drying oven to ensure total dryness. Samples underwent ultrasonic homogenization, and all measurements were repeated three times to check for further disintegration. Sample D50 values were applied for control geophysical results. The dominant grain-size fraction of samples was given using the Udden-Wentworth scale.

In the current study, bigger drilling samples (220 samples) were collected to determine in situ water content during the drilling procedure at every 40 cm and stored in

special plastic bags. The wet samples' weight was measured and dried in a 100°C oven in the laboratory. After that, the weight of the dried samples was measured. The difference between the two weights gives the percentage of the water content in the samples.

Aquitard materials are a Poorly permeable underground layer that limits water flow from the riverside to the protected side. This layer is very important in the levee structure from flood risk mitigation issues. As there is not much information about the nature of this layer and other physical parameters of the levee composition like density, porosity and saturated hydraulic conductivity, 49 samples were collected during borehole drillings in soil sample rings. The samples were collected at depths where there were stratigraphical changes. Penetrometer was used to measure saturated hydraulic conductivity (K) through the collected samples **Fig. 10b**. After measuring K, the samples were placed in the drying oven to be dried, and a laboratory-measured their weight.



Figure 10: A) a Fritsch Analysette 22 laser analyzer, and B) Penetrometer.

Darcy studied the movement of water through beds of sand used for water filtration. He found that the rate of water flow through materials of a given nature is proportional to the difference in the height of the water between the two ends of the filter bed sand inversely proportional to the length of the flow path. He determined also that the quantity of flow is proportional to a coefficient K, which is dependent upon the nature of the porous medium. Darcy found experimentally that the discharge Q is proportional to the difference in the height of the water, h (hydraulic head), between the ends and inversely proportional to the flow length

$$Q \propto hA - hB \quad \text{and} \quad Q \propto -1/L \dots \dots \dots \text{Eq. 8}$$

The flow is also obviously proportional to the cross sectional area of the pipe, A, when combined with the proportionality constant, K, the result is the expression shown as Darcy's law:

$$Q = -KA\left(\frac{h_A - h_B}{L}\right) \dots \dots \dots \text{Eq.9}$$

In more general terms

$$Q = -KA (dh/dl) \dots \dots \dots \text{Eq. 10}$$

where dh/dl is the hydraulic gradient.

dh: the change in head between two points that are very close together.

dl: the small distance between these points.

the negative sign indicates the flow is in the direction of decreasing hydraulic head.

The bulk density was obtained from the weight of the dry samples divided by the volume of the soil sampling cylinder. The total porosity can be calculated from the relationship

$$n = 100 \left[1 - \frac{\rho_b}{\rho_d}\right] \dots \dots \dots \text{Eq11}$$

Where n: the total porosity (%); ρ_b : the bulk density of the material (g/cm^3); ρ_d : the particle density of the material (g/cm^3). Particle density was 2.65 g/cm^3 (Fetter, 2001). Regarding Fetter 2001, the porosity will be lowered if sediment contains a mixture of grain sizes. The smaller particles can fill the void spaces between the larger ones. The case of artificial levees of River Tisza did not show this big variation in grain size. Therefore, the calculated porosity values are high.

The spatial and temporal change in soil moisture content is challenging in determining saturated hydraulic conductivity (Farzamian et al., 2015). Otherwise, the saturated hydraulic conductivity measurements can be triggered with so-called pedotransfer functions, which estimate the infiltration rate with the help of easier measurable parameters. Pedotransfer functions are used to estimate the soil's electrical resistivity as well. Hadzick et al. (2011) have shown that particle size, bulk density and pH were the most influential soil properties to resistivity. Pedotransfer functions for hydraulic conductivity and electrical resistivity are based on very similar groups of soil properties. It allows us to work out new multivariate pedotransfer functions as a direct connection between electrical resistivity and saturated hydraulic conductivity.

In our study, one of the important tools that help find the correlation between the parameters and their degree of significance is IBM SPSS with the ease-of-use features of statistical analysis for ordinary researchers in mind. SPSS is a powerful and user-friendly

software package for statistical data analysis (Levesque, 2007). The correlation was done by two methods which are Pearson and Spearman.

The linear relationship of the two variables is measured by Pearson's correlation coefficient (r). The correlation coefficient ranges in value from -1 to +1. Positive correlation coefficient values signify a propensity for one variable to rise or fall along with another. Negative correlation coefficient values show a tendency for one variable's increase to be correlated with the other variable's drop and vice versa. Correlation coefficient values near zero show little association between variables, whereas those near -1 or +1 show a significant linear relationship between the two variables. The prerequisites for using Pearson's correlation coefficient are that the variables have a linear relationship. A Spearman rank correlation can measure a monotonic association (Kirch, 2008).

Regarding the 49 samples collected from 10 different boreholes, the correlation between resistivity based on ERT profiles and other parameters like water content, mean grain size, saturated hydraulic conductivity, porosity, and bulk density was correlated.

Regarding the water content percentage, 220 samples were classified into three classes then the correlation was made between the resistivity based on ERT (R) and the grain-size (D_{50}) at every water content class.

3.5 Methodology of evaluating levee health

The risk potential at every km of the investigated levee section was assessed by a methodology of combining the different data we obtained. The analysis was carried out by calculating 1) the mean elevation decrease, 2) the mean penetration depth of GPR signals, 3) the mean number of GPR anomalies and 4) the dominance of fine silty units in the levee core over medium silt per 1 km for the entire investigated area. These values were compared to values calculated for 1 km sections (**Fig. 11**). At each 1 km section, the values of the above four parameters were compared to the mean of the entire section. If the 1 km value was higher than the section means, it received a score of 2, referring to a higher level of levee health (HLLH) than average. On the other hand, if the 1 km value was below the section mean, it received a score of 1, referring to a lower level of levee health (LLLH) than average. Subsequently, scores of levee health levels were added up, and for each 1 km section, a potential level of levee health value was assigned: score 8 meaning very high level of levee health (VHLLH), score 6 meaning medium level of

levee health (MLLH) and score 4, meaning very low level of levee health (VLLLH) potential (**Fig. 11**) (Sheishah et al 2023a).

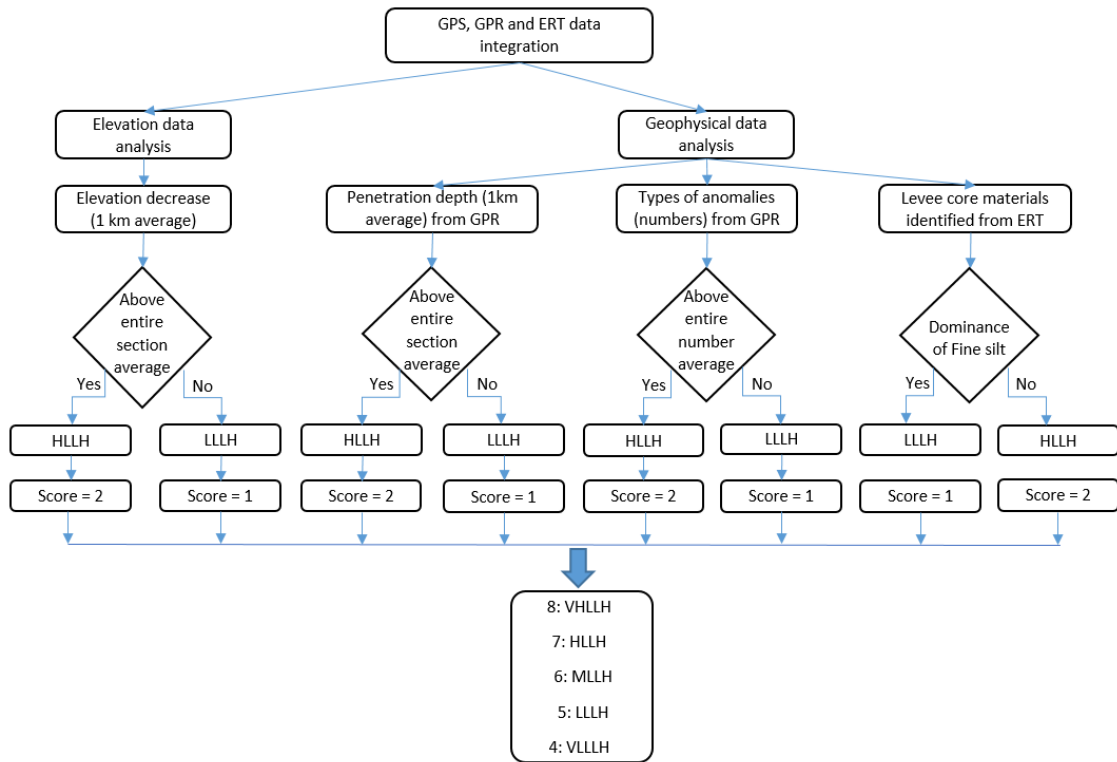


Figure 11: Diagram of calculating health along the investigated levee section.

3.6 Inventory of historical flood phenomena

High flood levels and/or extensive flooding can lead to the gradual soaking of the levee body, which can decrease the flood resistance capacity of the earthwork and, in extreme situations, can lead to the failure of the structure. Therefore, knowing and recording of different flood phenomena during floods is a major tool in the hand of levee guards to assess the condition of the levee and to locate weak zones. Based on the 50-year long record of the Lower Tisza Water Directorate, six categories of flood phenomena have been identified along the studied levee section: soil softening, moderate seepage, concentrated seepage (piping), levee subsoil weakening, levee bottom seepage, and sand boil (**Fig. 12**). These have been recorded since 1970 along the studied levee section. Since then 11 significant floods caused flood phenomena. Based on an overall review of recordings, seepage and piping were identified as the most frequently occurring phenomena in the investigated area. These affect the upper part of the levee body, mostly within the estimated range of penetration depth of GPR (Sheishah et al 2023a). Since following the extreme floods in 1970 and 2000 the investigated levee section was

reinforced at several critical sites, recordings of the subsequent 2006 and 2010 floods were chosen to determine the spatial distribution of flood phenomena and their connection with the geophysical data. Moreover, in the past 20 years, the largest and most damaging flood was in 2010 (Borsos and Sendzimir 2018).

Flood phenomena were recorded on digital blueprints showing their actual position along a scale representing the levee. In case their spatial frequency is high at certain sections they are not marked individually, but intervals of occurrence are recorded. Graphical data were converted into an excel sheet: each 100 m section was evaluated whether it is affected by flood phenomena (score 1) or not (score 0). The scores from both investigated years were summed for each levee km and plotted against the horizontal distance along the investigated levee section. The frequency diagram of seepage and piping phenomena were compared to the spatial frequency of anomalies, identified using GPR profiles (Sheishah et al 2023a).

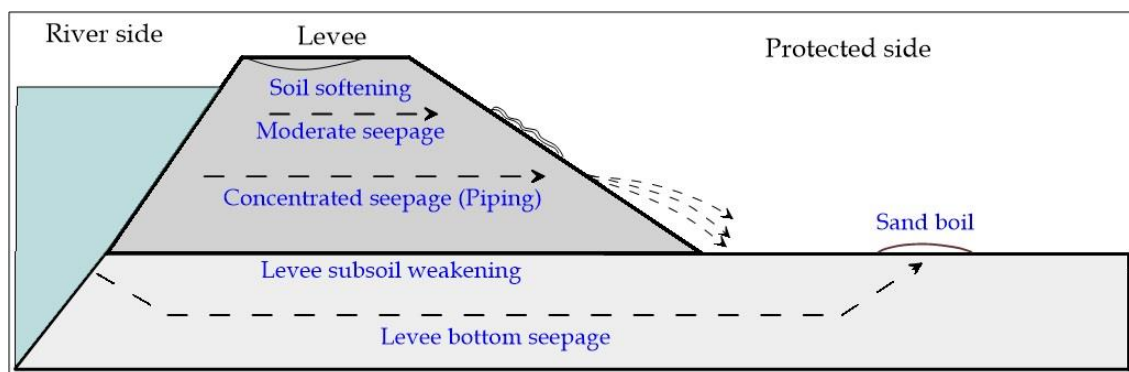


Figure 12: Six types of flood phenomena identified by the Lower Tisza Water Directorate along the investigated levee section.

4. Results

4.1 ERT data evaluation

The drilling information obtained from certain locations on Tisza and Maros levee sections helped correctly interpret the ERT profiles measured at these locations. Because of the limitations of drilling boreholes from every levee km, the borehole information was used to interpret the ERT profiles close to them.

Because of the large number of ERT profiles collected in this study, I will focus my research here on two levee km points at 13 Lkm and 37 Lkm of Tisza levee where repeated ERT surveys were carried out longitudinally and transversely by different electrode spacing to present the effect of spacing on the levee investigations. Then, I will compare the structures and compositions of Tisza and Maros levees using two representative levee km locations, 31.4 Lkm of Tisza levee and 3 Lkm of Maros levee because the drilling information was provided on the levee crown and the protected side for both of them from which the comparison results are verified. Based on the realised relationships, I will map the materials along the two investigated levees of Tisza and Maros by following up the longitudinal ERT profiles from one lkm to another and exhibit the material change from one levee km to another by following up the transverse profiles measured on each levee km. The rest of interpreted ERT profiles show valuable information about the investigated levees, but they were moved to supplement sections 1 and 2.

4.1.1 Comparison of different resolution of ERT data

Since the applied electrode spacing determines the resolution of ERT data, i.e. the shorter the distance is between electrodes, the thinner levee units can be resolved. The topmost layer of the levee body could only be detected using a 1 m electrode spacing (**Fig. 13a**). In turn, at a larger spacing (1.5 and 2 m), it was possible to provide information on the sedimentary layers below the levee body (**Fig. 13b and c**). This way, along the longitudinal profile on the levee crown at a higher vertical resolution (1.0 m), a thin, low resistivity layer could be identified at the top, with resistivity values ranging between 7–20 Ωm . Below, a 1.5–2.0 m thick, slightly higher resistivity (23–32 Ωm) layer was identified, then again, a lower resistivity unit (15–30 Ωm) (**Fig. 13a**). The maximum survey depth at this resolution was 7 m, which is equal to the relative height of the levee.

By comparing the resistivity ranges of the whole ERT profile obtained using three different electrode spacings, it was noticed that the range in the case of 1 m electrode

spacing is higher than that obtained by 2 m electrode spacing because a larger electrode spacing profile could investigate the conductive layer located below the levee body which is characterised by its low resistivity range.

The combination of sedimentological information and ERT profiles also referred to the layered structure of the levee body. BH-1 exposed a 1 m fine silty layer, 1.8 m medium silty layer and a fine silty layer again below 2.8 m. BH-2 exposed two units. The first unit contained fine sand at the top 0.4 m, then alterations of medium and fine silt layers. They are explained in more detail in the sedimentological section.

Low and moderate resistivity values were found and exhibited a range between 7 and 100 Ωm and the average value of specific resistivity was 22 Ωm for the longitudinal ERT profile at 1 m spacing recorded on the riverbank edge of the Tisza levee crown at 13 lkm. A greater specific resistivity (30-40 Ωm) unit could be seen below the levee body at a 1.5 m electrode spacing (**Fig. 13b**), and this effect was much more obvious at a 2 m electrode spacing (35-50 Ωm) (**Fig. 13c**). Values in terms of the transverse profile were much higher and peaked at 640 Ωm . The mean specific resistivity, however, was 120 Ωm (**Fig. 13d**).

Three ERT units were designated for the levee crown in the transversal profile. However, the measured values of specific resistivity varied (**Fig. 13d**). Levels reached 280–420 Ωm at the top 1 m of the levee, which is unusually high compared to the earlier levels. Although the specific resistivity of the following unit, which had a 1.5–2.0 m thickness, was lower (70–240 Ωm), it was still much higher than those identified by the longitudinal profile. Values decreased to 7-30 Ωm from a depth of 3 m, as shown by the longitudinal ERT profiles. The obvious discrepancy in the uppermost strata can be attributed to shallow, air-filled tensile fractures, also seen during the GPR cross-sections (**Fig. 4d**), considerably affecting the observed specific resistivity values. The impact of air-filled spaces was minimal in their instance since the longitudinal measurements were taken along the levee crown. The transverse profile's electrode spacing was only 1.0 m, but it nevertheless allowed for the detection of a greater resistivity unit beneath the structure and the existence of higher resistivity lenses (30–50 Ωm) close to the riverside slope of the levee.

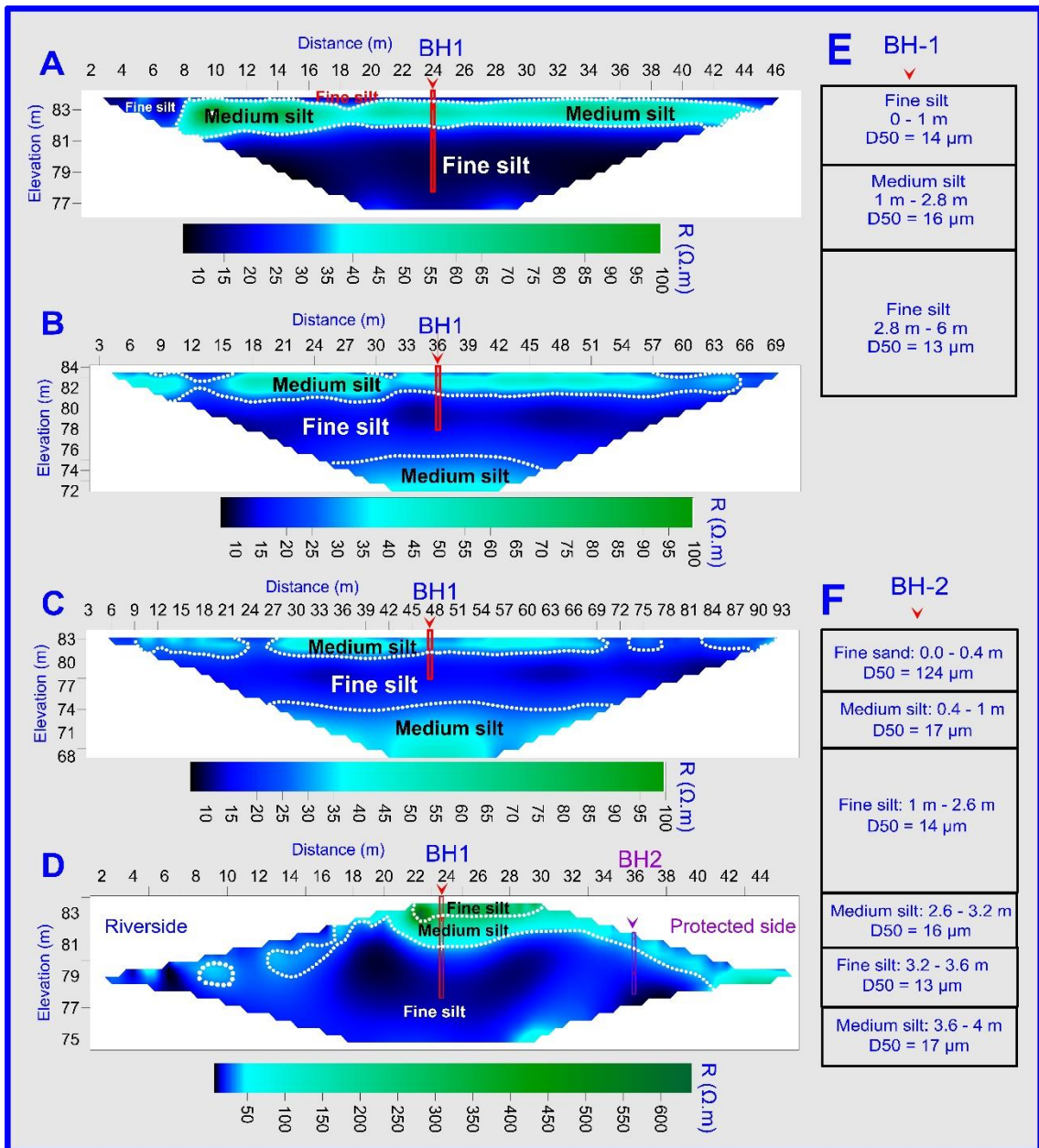


Figure 13: Interpretation of ERT profiles measured longitudinally using A) 1.0 m, B) 1.5 m, and C) 2 m electrode spacing, and D) transversally using 1 m electrode spacing. The profiles had the same centre point at 13.00 lkm of the Tisza levee. E) and F) are boreholes drilled on the levee crown and protected side respectively

Another test was carried out at 37 lkm to check and compare different resolutions of ERT data. In the case of the longitudinal ERT profiles measured on the riverside edge of the Tisza levee crown at 37 lkm, I could receive low and moderate resistivity values with a range between 9 and 53 Ωm at 1 m electrode spacing, and the average value of specific resistivity was 31 Ωm . However, the case of the transverse profile was different. Values were significantly higher and reached a maximum of 312 Ωm , while the mean specific resistivity was 150 Ωm (Fig. 14).

The second test at 37 lkm confirmed that the layered structure of the levee body could be detected by using ERT measurements. Also, the topmost layer of the levee body is more visible by using a 1 m electrode spacing as the lower distance between electrodes enables the thin layers to be easily detected (**Fig. 14a**). In the case of 1.5 m electrode spacing, part of the topmost layer is still visible. By increasing the distance between electrodes (2 m), I can receive more information about the layers below the levee core (**Figs. 14b and c**). This way, three resistivity ranges were received before unifying the colour scale; a resistivity range between 10 and 72, a resistivity range between 7 and 62, and a resistivity range between 3 and 52 for 1, 1.5, and 2 m electrode spacing, respectively. Therefore, increasing the electrode spacing allows more resistivity information to be received laterally and vertically, and a smaller range could be obtained. Along the longitudinal profile on the levee crown at a higher vertical resolution (1 m electrode spacing), a thin, low resistivity layer could be identified at the top (1 m thick) on the left-hand side of the profile, with resistivity values ranging between 36–52 Ωm . Below, a 1 m thick, slightly lower resistivity (20–34 Ωm) layer was found. Then, a much lower resistivity unit (10–18 Ωm) could be identified. The latter is considered the main composition of the levee core (**Fig. 14a**). The maximum survey depth at this resolution was 7 m, equal to the levee's relative height. Using 1.5 m and 2 m electrode spacings, the levee core and the structure below the core can be identified, and the interface between them is more visible (**Figs. 14b and c**).

The sedimentological information exposed fine-grained materials as a main component of the levee core and protected side. BH-7 exposed alteration of layers of fine and medium silt until a depth of 6 m (**Fig. 14e**), while BH-8 exposed only one unit of fine silt until a depth of 4 m (**Fig. 14f**). They are explained in more detail in the sedimentological section as well.

In terms of the transverse profile, the riverside and a part of the levee crown exhibit a succession of three resistivity layers (**Fig. 13d**). Values at the top of the levee were significantly higher than those below it and reached 185 - 311 Ωm in the uppermost, roughly 1 m thick layer. With a thickness of 2.0 m, the next unit had a specific resistivity range of 83–154 Ωm , which was lower than those seen in the longitudinal profile but still substantially higher. Values dropped to 22 - 4 Ωm from a depth of 3 m, as shown by the longitudinal ERT profiles. Similarities between the topmost layer's situation and the previous test site at 13.00 lkm can be explained by shallow, air-filled tensile cracks mapped during the GPR surveys (**Fig. 7a**), significantly increasing the measured specific

resistivity values. The impact of air-filled spaces insignificant in their case since the longitudinal measurements were taken along the levee crown. Asymmetric low resistivity composition between 4 and 30 Ωm was found on the protected side.

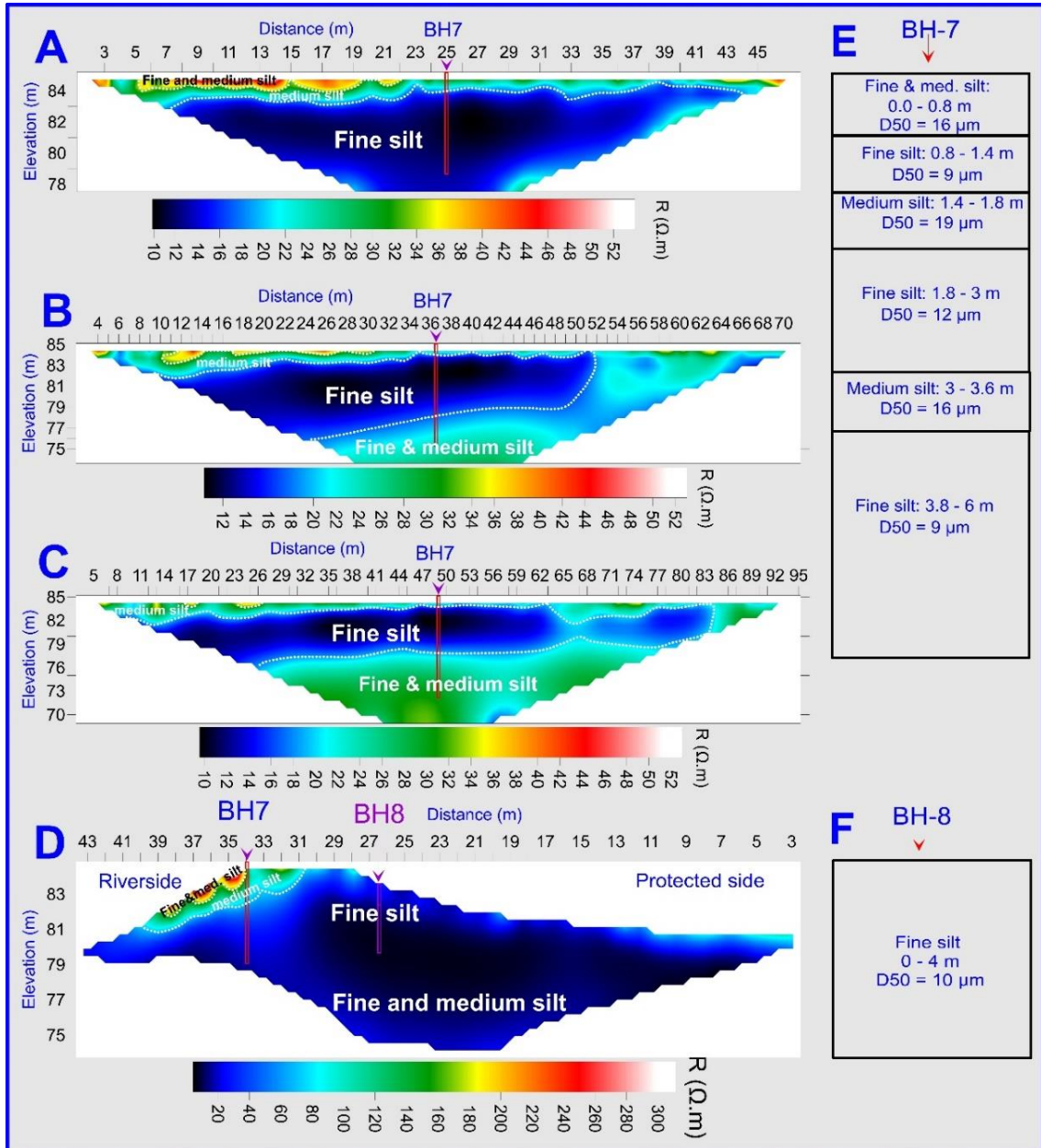


Figure 14: Interpretation of ERT profiles measured longitudinally using A) 1.0 m, B) 1.5 m, and C) 2 m electrode spacing, and D) transversally using 1.5 m electrode spacing. The profiles had the same centre point at 37.00 lkm of the Tisza levee. E) and F) are boreholes drilled on the levee crown and protected side respectively

4.1.2 Integrating ERT and sedimentological data to identify structural units at Tisza and Maros levees

The difference in the composition of the Tisza and Maros levees is visible in the resistivity results at the representative levee sections 31.4 lkm and 3 lkm of Tisza and

Maros levees, respectively, because more drilling information and analysis are provided at the mentioned locations. In general, the inverted ERT profiles exhibited low resistivity values in the Tisza levee and medium and high values in the case of the Maros levee. The longitudinal and transverse profiles measured on the Tisza levee exhibited a range of values from 6 Ωm to 60 Ωm , averaging 17 Ωm . In the case of the longitudinal profile measured on the Maros levee, values ranged between 15 Ωm and 46 Ωm with an average of 30 Ωm . In the Transverse profile measured on the Maros levee, values were considerably higher, reaching a maximum of 2200 Ωm , and the mean specific resistivity was 660 Ωm (**Fig. 15**).

The electrode spacing is an important factor in the resolution of ERT data. 2 m electrode spacing can provide 1 m vertical resolution, which could resolve the levee layers in this range or above. The maximum survey depth of the profiles at this resolution was between 8 m and 13 m, which is more than the relative height of the levee; therefore, the layers below the levee could also be investigated.

The longitudinal profile measured at the investigated site of the Tisza levee exhibited two units; the first unit of fine silt is the dominant component of the levee body, with resistivity values ranging between 6 Ωm and 20 Ωm which extends from 0.8 m until 6 m. Then the second unit of medium silt was noticed below this depth with resistivity value ranging between 21 Ωm and 60 Ωm (**Fig. 15a**). As can be seen in **Fig. 15f** that there are two topmost thin layers of fine and medium silts 0.4 m thick for each. However, they could not be resolved on the ERT profile as the medium silt showed only minor accumulations and did not show a layered structure. The transverse profile measured at this zone exhibited the same unit succession with approximately the same resistivity range. In addition, a third unit of medium silt was noticed at the top 1 to 2 m of both sides of the Tisza levee, with resistivity values ranging between 16-61 Ωm (**Fig. 15b**). The protected side of the Tisza levee shows a main composition of fine silt at the drilling location with a thin layer of medium silt (0.4 m thick) in between (**Fig. 15b and G**), ERT could not resolve the latter.

The materials forming the Maros Levee differ from that in the Tisza Levee. Three successive units were identified in the longitudinal ERT profile measured on the crown of the Maros levee at 0 – 0.8 m, 1 m – 4.4 m, and 4.6 – 7 m with resistivity values ranging between 15 – 26 Ωm , 31 – 46 Ωm , and 15 – 30 Ωm which relate to fine, medium, and fine silts respectively (**Fig. 15c and H**). The variation in Maros levee composition is even more visible, especially on the protected side. Five units could be resolved; the first fine

silty unit with a thickness of ~ 0.2 m has a resistivity range between $15 \Omega\text{m}$ and $260 \Omega\text{m}$, the second medium silty unit with a thickness of ~ 0.2 m has a resistivity range between $260 \Omega\text{m}$ and $700 \Omega\text{m}$, the third very fine sandy unit with ~ 0.2 m thick has a resistivity range between $800 \Omega\text{m}$ and $1630 \Omega\text{m}$, the fourth medium sandy unit (~ 1.6 m thick) is in the form of a lense of very high resistivity that ranges between 1800 and $2200 \Omega\text{m}$, and the fifth fine silty unit (~ 0.6 m thick) is located below the high resistivity lense of medium silt (**Fig. 15d and I**). To see the interface that separates the fine-grained units (alteration units of fine, medium and fine silts) in the riverside, a small scale $5\text{--}60 \Omega\text{m}$ was applied on the transverse ERT profile measured on Maros levee section and the low resistivity range could help in separating the two compositions as shown in (**Fig. 15e**). More analysis about the grain-size analysis related to the mentioned boreholes is found in the supplement.

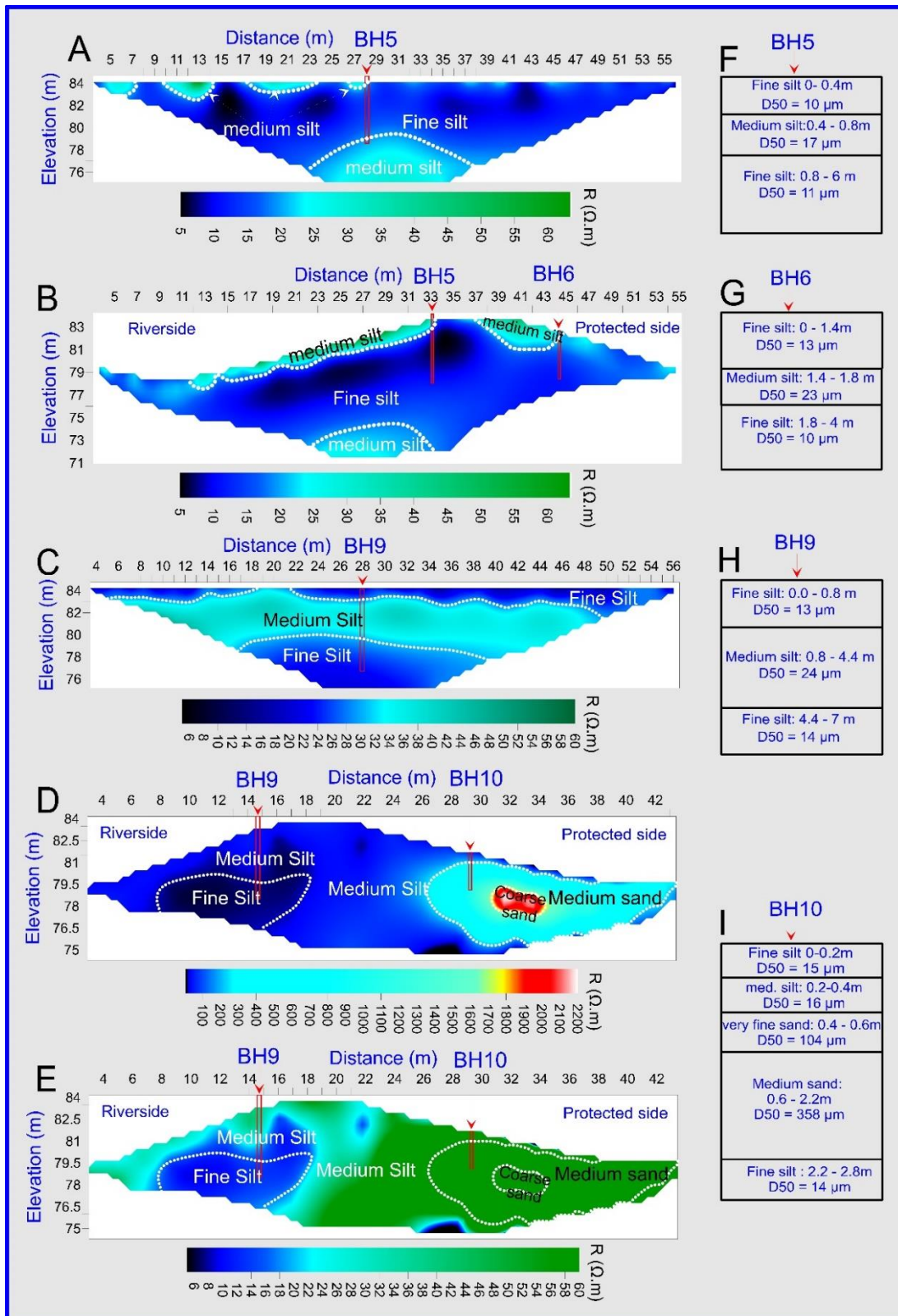


Figure 15: Longitudinal (A) and transversal (B) ERT profiles acquired on the Tisza levee at 31.4 Lkm. Longitudinal (C) and transversal (D) ERT profiles acquired on the Maros levee at 3 Lkm. The same profile as the proceeding one (D) but with applying a small resistivity range between 5 and 60 Ω.m (E), Thickness and mean grainsize values of structural units, identified by drillings (F-I)

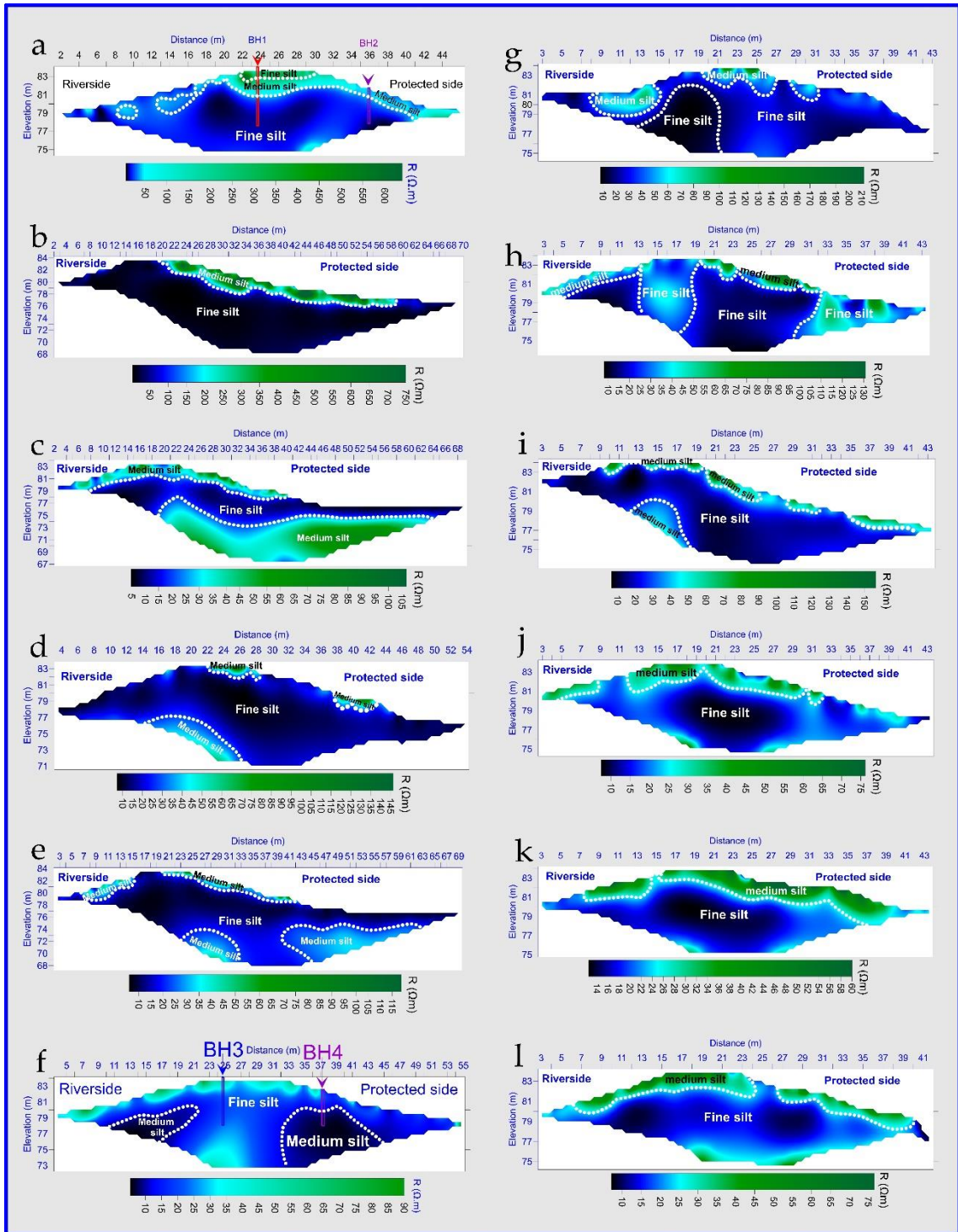


Figure 16 Transverse profiles measured along Tisza levee at a) 13 lkm, b) 14 lkm, c) 15 lkm, d) 16 lkm, e) 17 lkm, f) 18 lkm, g) 19 lkm, h) 20 lkm, i) 21 lkm, j) 22 lkm, k) 23 lkm, l) 24 lkm

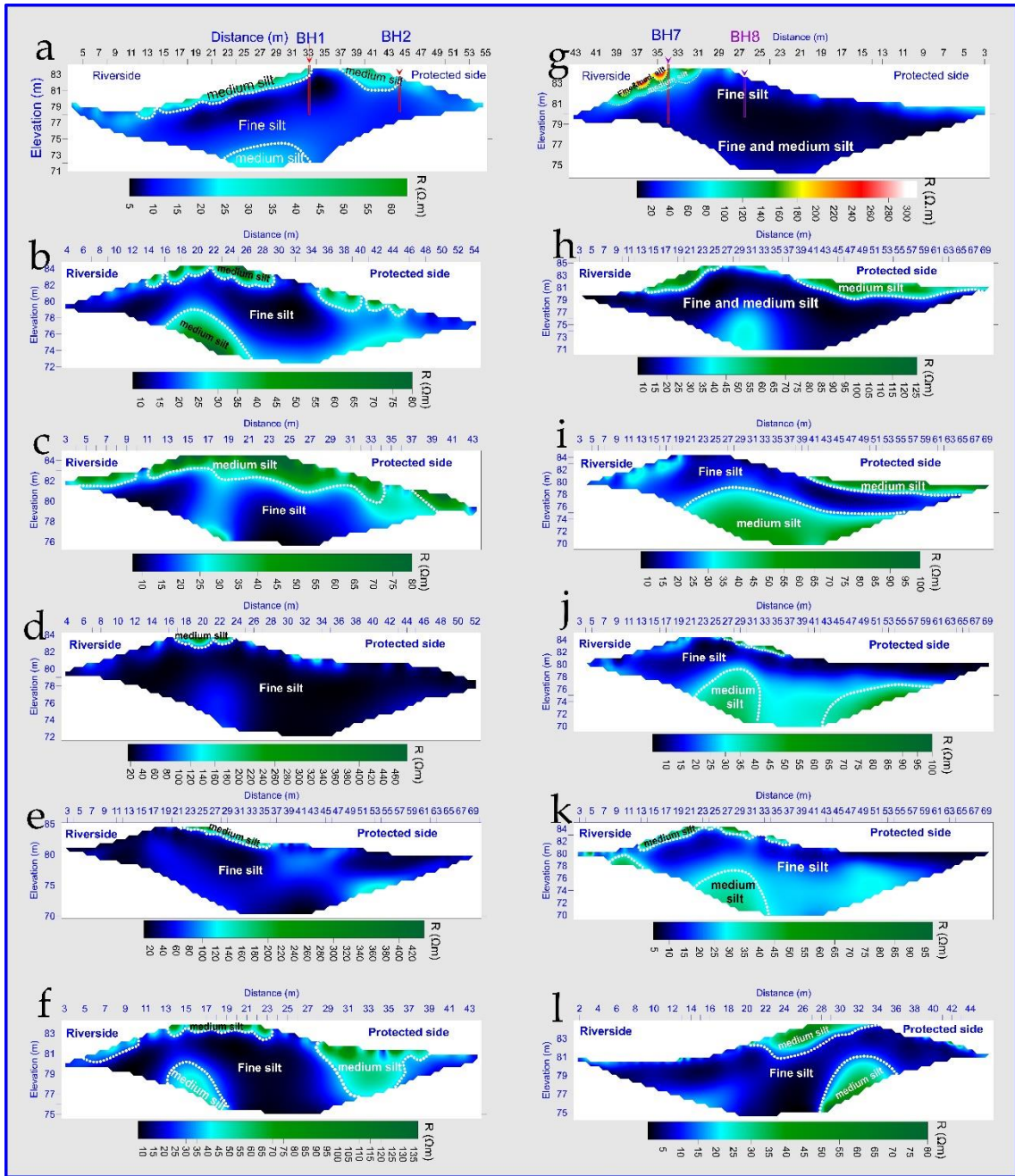


Figure 17 Transverse profiles measured along Tisza levee at a) 31.4 lkm, b) 32 lkm, c) 33 lkm, d) 34 lkm, e) 35 lkm, f) 36 lkm, g) 37 lkm, h) 38 lkm, i) 39 lkm, j) 40 lkm, k) 41 lkm, l) 42 lkm

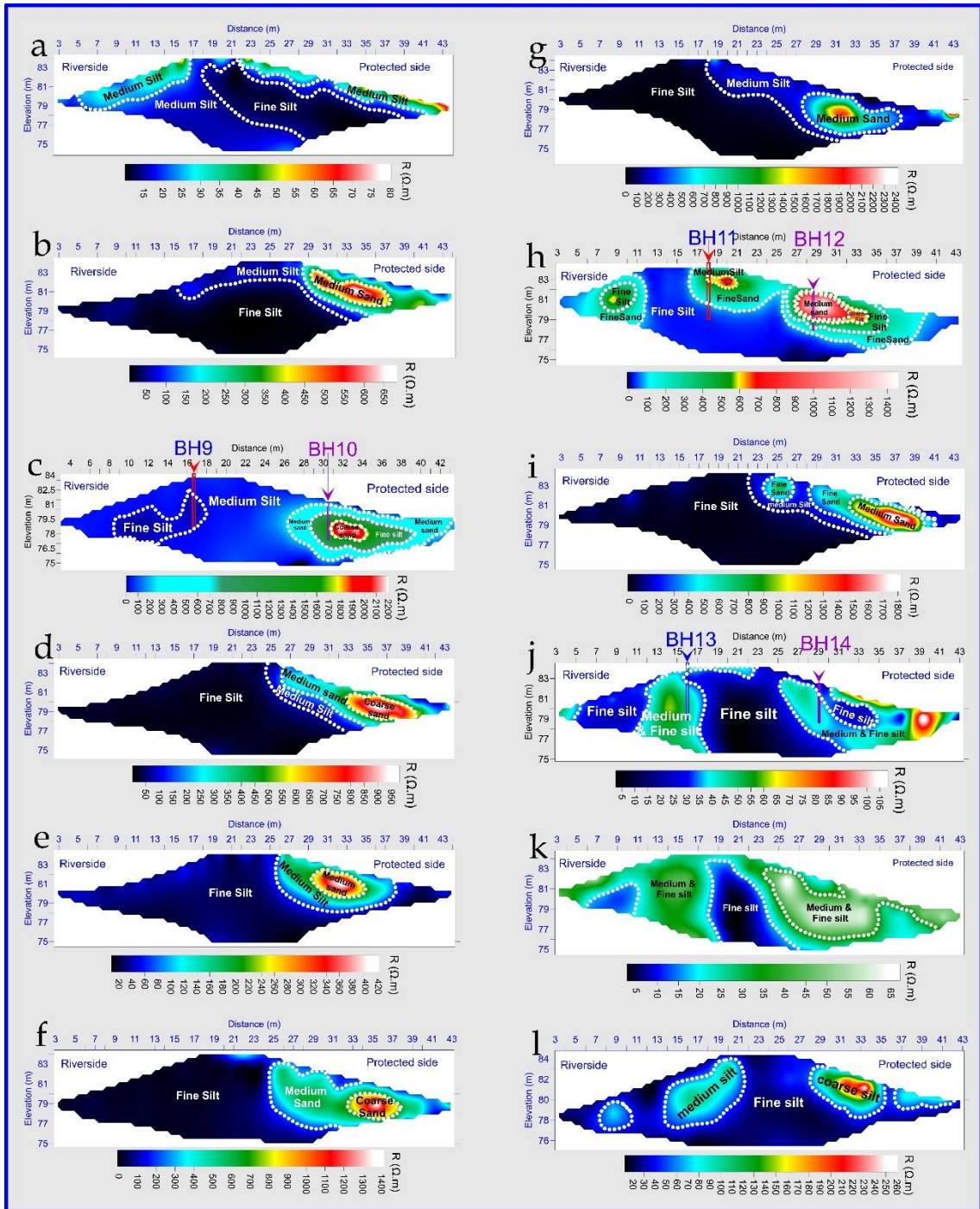


Figure 18 Transverse profiles measured along Maros levee at a) 1 lkm, b) 2 lkm, c) 3 lkm, d) 4 lkm, e) 5 lkm, f) 6 lkm, g) 7 lkm, h) 8 lkm, i) 9 lkm, j) 10 lkm, k) 11 lkm, l) 12 lkm

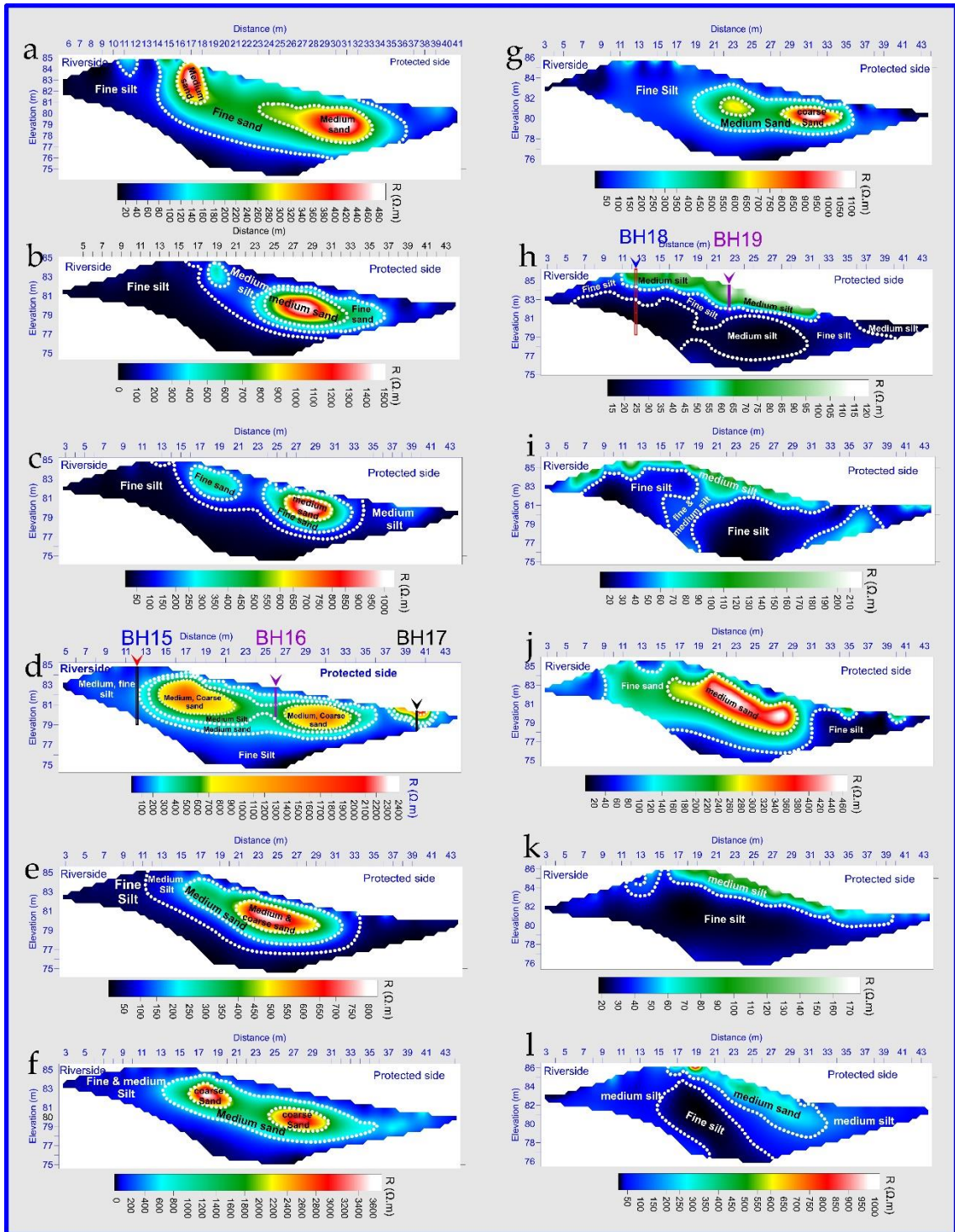


Figure 19 Transverse profiles measured along Maros levee at a) 13 lkm, b) 14 lkm, c) 15 lkm, d) 16 lkm, e) 17 lkm, f) 18 lkm, g) 19 lkm, h) 20 lkm, i) 21 lkm, j) 22 lkm, k) 23 lkm, l) 24 lkm

4.2 Drillings

4.2.1 Sedimentological analysis

In this section, we explain the grain-size then the water content analysis. Three sites were chosen as representative data; the first levee kilometre is at 13.00 of Tisza levee, the second is at 37 lkm of Tisza levee, and the third is at 16.00 lkm of Maros levee. These sites were chosen as they show more variation of the materials with depth. The interpretations of other boreholes are found in the supplements under sections 1 and 2.

The first borehole (BH-1) drilled on the levee crown of Tisza levee at 13.00 lkm, exposed three units (**Fig. 20a**); A fine silty layer existed from the surface to a depth of 1.0 m with a D50 value between 12 and 15 μm , a medium silty layer existed at depths between 1.0 and 2.8 m with a D50 value from 15 to 20 μm , and a fine silty layer once more existed below 2.8 m with a D50 value ranging from 10 to 15 μm (**Fig. 20a**). The grain-size curve has some abrupt changes, particularly in the bottom unit, but they are not large enough to shift the D50 value into another grain-size class. I decided not to separate any further sedimentary units at BH-1. The levee body is often made up of fine and medium silt, despite minor differences in averages, according to the overall mean grain size values for the various units of 14 μm , 16 μm , and 13 μm . A large change in depth could be seen in the water content of BH-1 samples (**Fig. 20b**). The uppermost samples had a rather high 25% water content, which was brought on by the wet weather that had occurred before the measurements and sampling. Moisture dropped to 21% at 0.8 m and stayed there until 1.6 m. Below, there was yet more of a drop; between 2 and 4 metres, an average value of 16% was recorded. From 4.4 m down in the borehole, values increased once again to 25% (**Fig. 20b**).

Two units were revealed by the second borehole (BH-2), which was drilled on a 13.00 lkm protected slope (**Fig. 20c**). The first unit contained a very fine sand layer (0–20 cm) and a fine sand layer (20–40 cm) with mean grain sizes ranging from 93 to 155 μm . The second unit was composed of medium silty layers (40–100 cm; 260–320 cm, 360–400 cm) with a D50 value ranging from 16 to 19 μm and fine silty layers (100–260 cm, 320–360 cm) cm with a D50 value ranging from 10 to 15 μm (**Fig. 20c**). The mean grain size of units was 124 and 15 μm , respectively. Samples of BH-2 showed reduced moisture content values (**Fig. 20d**). Here, The uppermost strata in this area, which are primarily made up of fine sand, had low values, slightly around 10%; as a result, the influence of precipitation was not visible here as a result of the poor sand retention

capacity. The water content in the remaining portion of the profile steadily grew from 2.4 m to a consistent value of 20–25% (Fig. 20d). The interpretations of other boreholes drilled on the Tisza levee are found in the supplements under section 1.

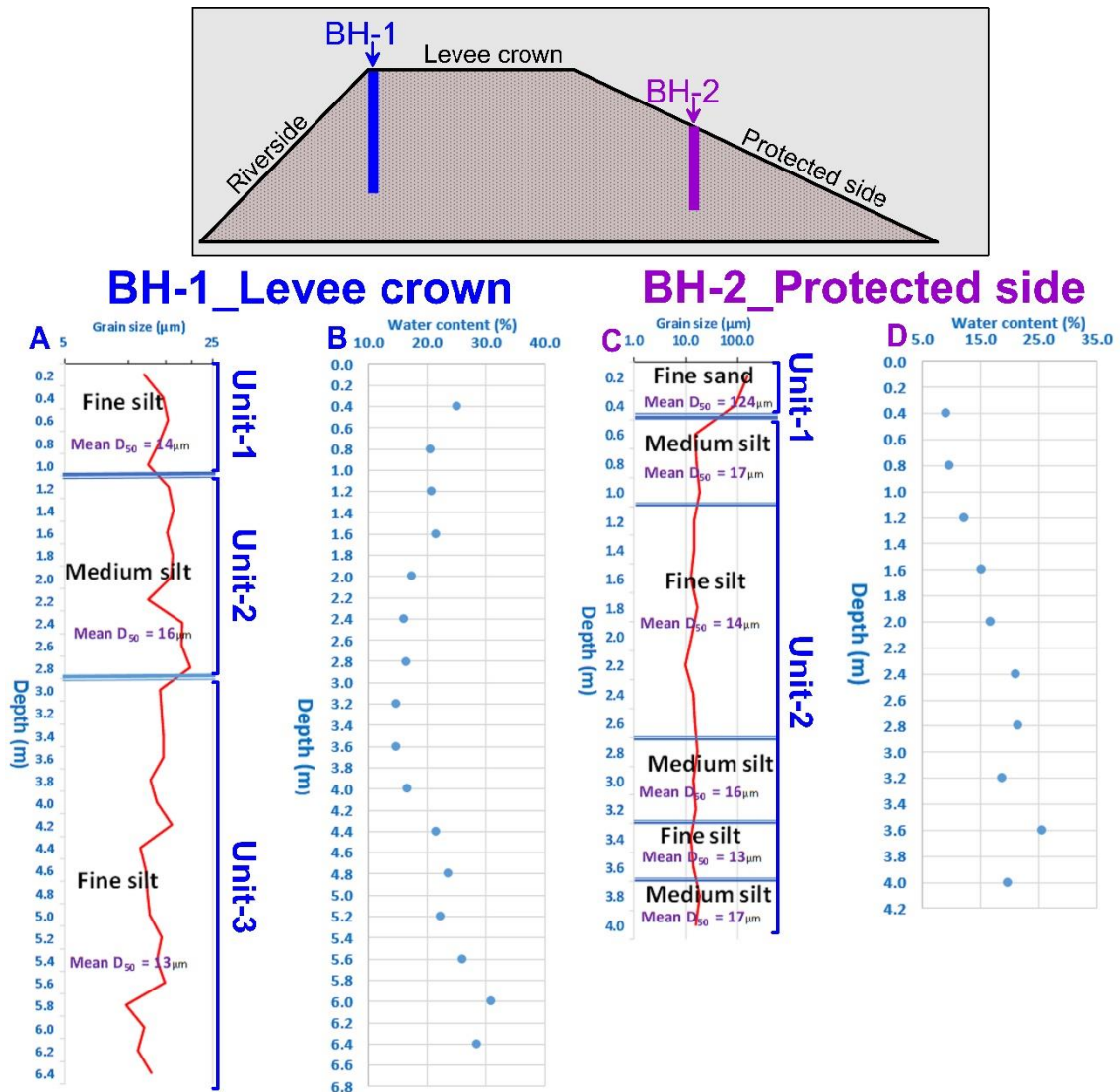


Figure 20: Vertical change of mean grain size (D_{50}) and water content in borehole BH-1 and BH-2 at 13.00 lkm.

The seventh borehole (BH-7) drilled on the levee crown of Tisza River at 37.00 lkm showed six units (Fig. 21a). The first layer consists of a succession of fine and medium silt layers with a D_{50} ranging from 10 µm to 25 µm at depths between 0 and 0.8 m. The second unit consists of a fine silt layer at a depth between 0.8 m and 1.4 m with a mean D_{50} value of 9 µm. The third unit is a medium silt layer from 1.4 m to 1.8 m with a mean D_{50} value of 19 µm. The fourth unit is a fine silty layer at a depth ranging between 2 m to 3 m with a mean D_{50} value of 12 µm. The fifth unit is a medium silt layer from 3 m to 3.6 m with a thin, very fine silty layer in between and a mean D_{50} of 14 µm. The last unit is a fine silty layer at a depth from 3.6 m to 6 m with a mean D_{50} value of 9 µm.

Regarding the water content at BH-7 (**Fig. 21b**), an increasing trend was noticed from the surface until the maximum depth reached by the drilling tool (6 m), with a per cent ranging from 8.3 % to 23.6 %. In more detail, the total depth of the drilling can be subdivided into two units regarding the water content percentage; the top unit, which contains the topmost layers until 3.2 m depth, shows an average per cent of 12.3 % which is considered to be dry fine and medium silt materials and the levee layers starting from 3.2 m until 6 m depth show an average per cent of 21.5 % which is considered wet materials.

The eighth borehole (BH-8) drilled on the levee-protected side slope of Tisza River at 37 lkm exposed a homogeneous composition unit of fine silt (0 – 4 m) with a mean D50 value 10 μm (**Fig. 21c**). In the case water content at BH-8 (**Fig. 21d**), two trends were noticed; a decreasing trend from 18 % to 8 % with an average percent 13.2 % at a depth ranges from the surface until 2.8 m and an increasing trend from 12 % to 17 % with an average percentage 14.4% at a depth ranges from 2.8 m until 4 m.

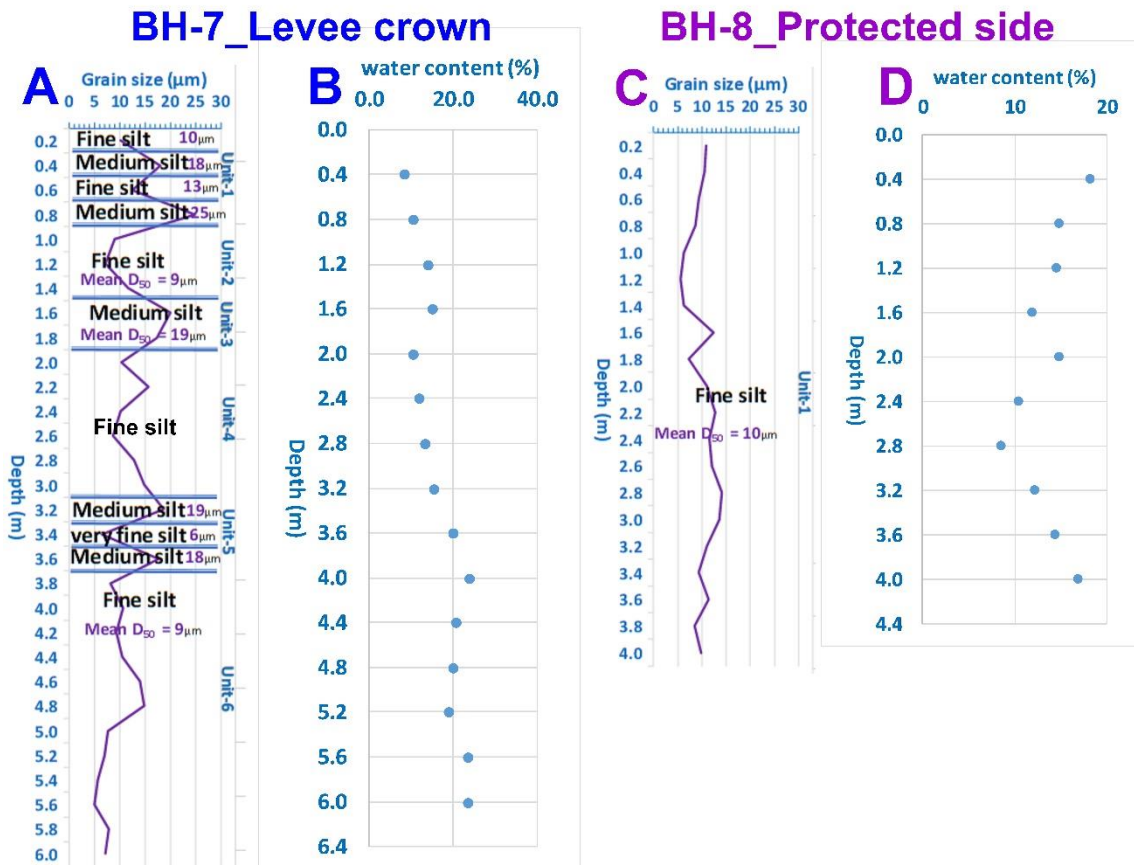
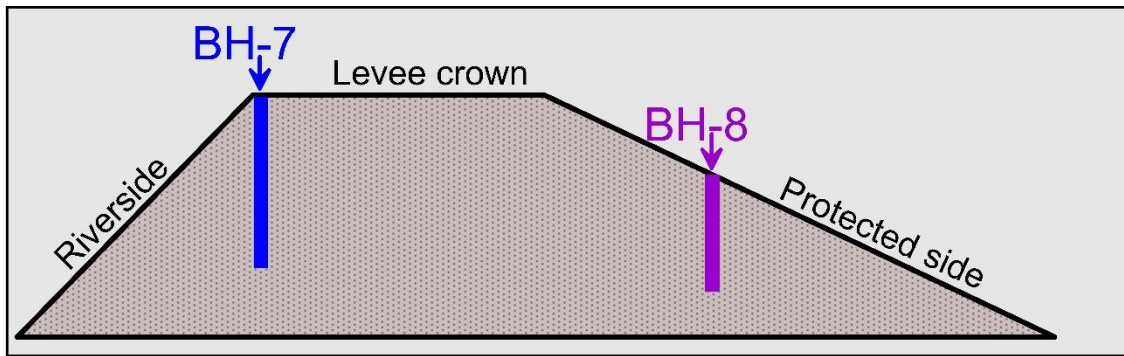


Figure 21: Vertical change of mean grain size (D_{50}) and water content in borehole BH-7 and BH-8 at 37.00 lkm.

The fifteenth borehole (BH-15) drilled on the levee crown of Maros River at 16.00 lkm exhibits six units (**Fig. 22a**). The first three units show a gradual increase in the grain size with depth. They are thin layers of medium silt, coarse silt, and very fine sand with a thickness of 0.2 m for each unit. The mean D_{50} values are $28 \mu\text{m}$, $38 \mu\text{m}$, and $72 \mu\text{m}$, respectively. The fourth unit shows a decrease in the grain size and consists of a thick layer of medium silt at depth ranges from 0.6 m to 3.6 m with a mean D_{50} value of $23 \mu\text{m}$. The gradual decrease in the grain size is continuous in the fifth unit, which shows a fine silt layer with a mean D_{50} $15 \mu\text{m}$ between 3.6 m and 4.8 m. The last unit is the build-up of medium silt with a mean D_{50} value of $16 \mu\text{m}$ and extends from 4.8 m to 6 m.

Regarding the water content at BH-15, two units were exhibited (**Fig. 22b**). From the surface to 3.6 m, a low water content unit with an average per cent 11.7 % was noticed. From a depth of 4 m to 6 m, the second unit exhibited a medium water content with an average per cent 21 %.

The sixteenth borehole (BH-16) drilled on the protected side of Maro's levee at 16.00 lkm exhibits three successive units of fine and coarse-grained sediments (**Fig. 22c**). The first unit is composed of fine silt and extends from the surface until 0.8 m depth with a D50 value 15 μm . The second unit comprises a medium sand layer and extends from 0.8 m to 1.8 m with a mean D50 value of 464 μm . The third unit comprises alteration layers of medium and coarse silt with a mean D50 value of 36 μm and extends from 1.8 m to 3 m. BH-16 showed two units regarding the moisture content percentage (**Fig. 22d**). The first unit that extends from the surface until a depth of 1.6 m seems dry with low water content per cent with an average of 5.7 %. This unit is related to medium sand that did not retain water. The second unit, which extends from 2 m to 2.8 m, exhibits a moderate water content percentage with an average of 16.3 %. The second unit consists mainly of alteration layers of fine-grained sediments.

The seventeenth borehole (BH-17) drilled on the foot of the protected side of Maros levee at 16.00 lkm exhibits five units (**Fig. 22e**). The first unit consists of a thin layer of medium sand (0-0.2 m) with a mean D50 value of 380 μm . The second unit is composed of coarse sand (0.2 m – 0.6 m) with a mean D50 value of 590 μm . The third unit consists of medium sand at depths from 0.6 m to 0.8 m with a mean D50 value of 420 μm . The fourth unit consists of coarse silt at depth ranges between 0.8 m and 1 m with a mean D50 value of 43 μm . The fifth unit exhibits alteration of medium and fine silt layers (1 m – 2 m) with a mean D50 value of 15 μm .

Regarding the moisture content, BH-17 showed two units (**Fig. 22f**). A very dry unit with an average water content per cent of 3 % and extended from the surface until a depth of 0.8 m. The second unit shows a high water content percentage with an average of 25 %, extending from 1.2 m to a depth of 2 m. The first dry unit is related to a coarse-grained material, mainly from medium and coarse sand that did not retain water, while the wet unit is related to fine-grained sediments which retain water. The interpretations of other boreholes drilled on Maros levee are found in the supplements under section 2.

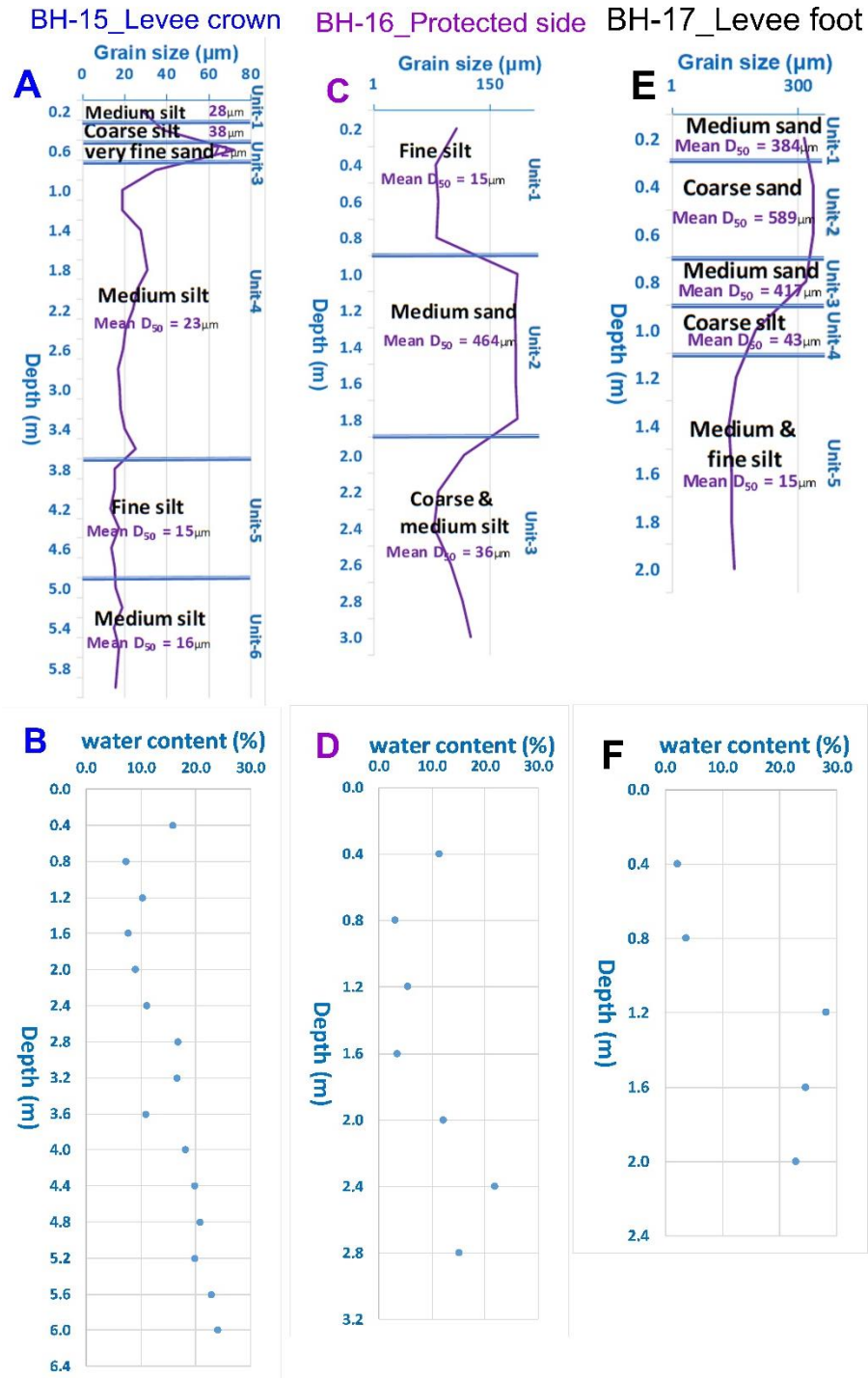
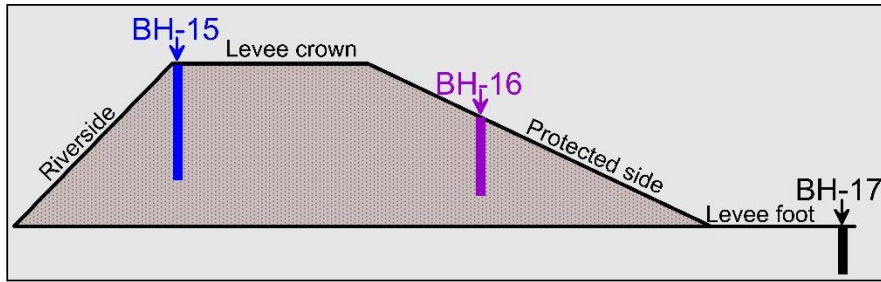


Figure 22: Vertical change of mean grain size (D_{50}) and water content in a, b) BH-15, c, d) BH-16 and e, f) BH-17.

4.2.2 Relationship among resistivity, grain-size and water content of levee materials

Plotting specific resistivity values against water content and mean grain size (D50) values, two of the most important factors defining resistivity, was done for the depths of the sediment samples. Here, one location on Tisza levee (13 lkm), represented by BH-1 and BH-2 and another location on Maros levee (16 lkm), represented by BH-15, BH-16 and BH-17, were chosen as representative data. In the meantime, many high coefficients of determinations and regression curves could be noticed at many of the rest borehole locations drilled on Tisza and Maros levees, and they are explained in detail in the supplement section 3.

No connections could be found when graphing all water content and D50 values for BH-1. Though with a distinct slope and coefficient of determination, it was recognised that if sedimentological units are treated independently, then obvious patterns may be shown (**Fig. 23**). Both water content and particle size had a clear impact on the observed resistivity values in the higher portion of the profile (from 0 to 320 cm). As predicted, the former had an inverse influence on values, whereas the latter had a directly proportionate one. At the same time, fairly negligible connections were visible in the bottom portion of the profile, indicating that resistivity was unaffected by variations in particle size and water content (**Fig. 23**). It must be underlined that the grain size values in this segment fluctuated only within a fairly small range (11–15 μm). The degree of compaction during construction, which also influences the material's porosity, may cause the two units' dissimilar behaviours. Inim et al. (2018). Zhu et al. (2007), Melo et al. 2021, and Seladji et al. (2010) all report that the core of levees is often compacted to a significantly higher degree, which inevitably results in lower resistivity values, which are only marginally influenced by variations in water content.

Since there was only one sample of the highest fine sand layer in borehole BH-2, relationships were only examined for the lower, silty part of the profile. The lack of a correlation between resistivity and grain size in this borehole may be due to the frequent alternation of fine and medium silty materials and the small grain size variation within the layers. However, the water content indicated a significant increase downwards. As a result, particular resistivity was observed to have a strong relationship ($R^2=0.907$) with it (**Fig. 23**). Additionally, this indicates that resistivity measurements at the current resolution could not be used to differentiate thin layers with a little variation in grain size.

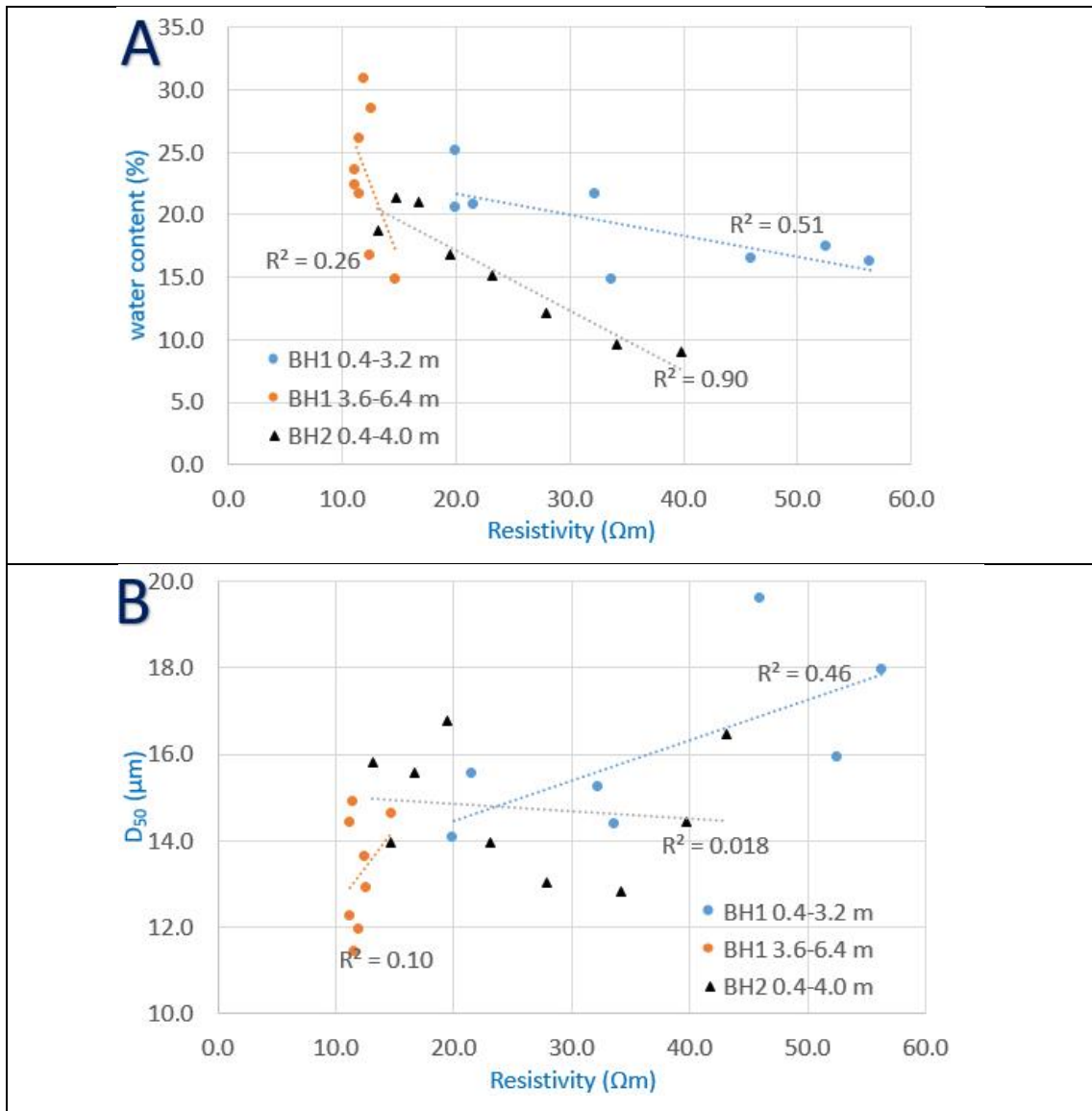


Figure 23: Relationship between A) specific resistivity and water content and B) specific resistivity and grain size in different structural units of the levee body for the boreholes drilled on the levee crown (BH-1) and the protected side (BH-2) at 13.00 lkm of Tisza levee.

Regarding the data obtained from BH-15, BH-16 and BH-17, two relationships were plotted; the first one was between resistivity and water content, and the second one was between resistivity and D50 (**Fig. 24**). Regarding BH-15, the resistivity values were plotted against water content at the depth range from 0.4 m to 6 m and an expected inverse proportional function was obtained with a strong coefficient of determination $R^2 = 0.8$. At the mentioned depth range for BH-15, the resistivity values were plotted against D50 and an expected normal proportional relationship was obtained with a medium coefficient of determination $R^2 = 0.4$. Regarding BH-16, a medium coefficient of determination $R^2 = 0.4$ was obtained from the expected to reverse proportional function between the

resistivity and water content percentage; on the other side, a strong coefficient of determination $R^2 = 0.8$ was obtained from the expected normal proportional function between the resistivity and D_{50} . Regarding BH-17, strong coefficients of determination $R^2 = 0.75$ and 0.9 were obtained from the expected inverse proportional function of resistivity and water content percentage and the expected direct proportional relationship of resistivity and D_{50} , respectively (**Fig. 24**). The other relationships at other drilling locations are found in the supplement.

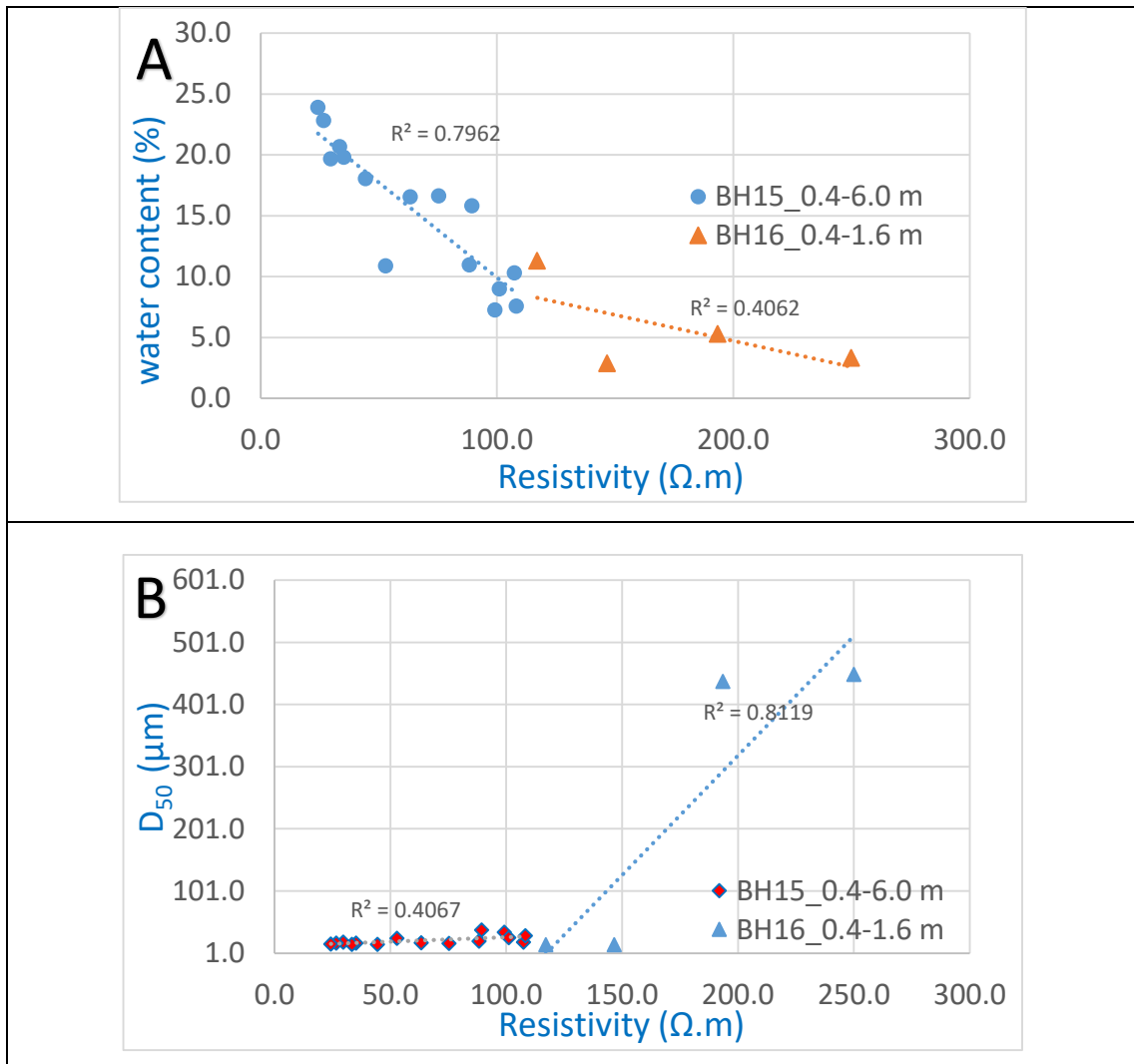


Figure 24: Relationship between A) specific resistivity and water content and B) specific resistivity and grain size in different structural units of the levee body for the boreholes drilled on the levee crown (BH-15) and the protected side (BH-16) at 16.00 lkm of Maros levee.

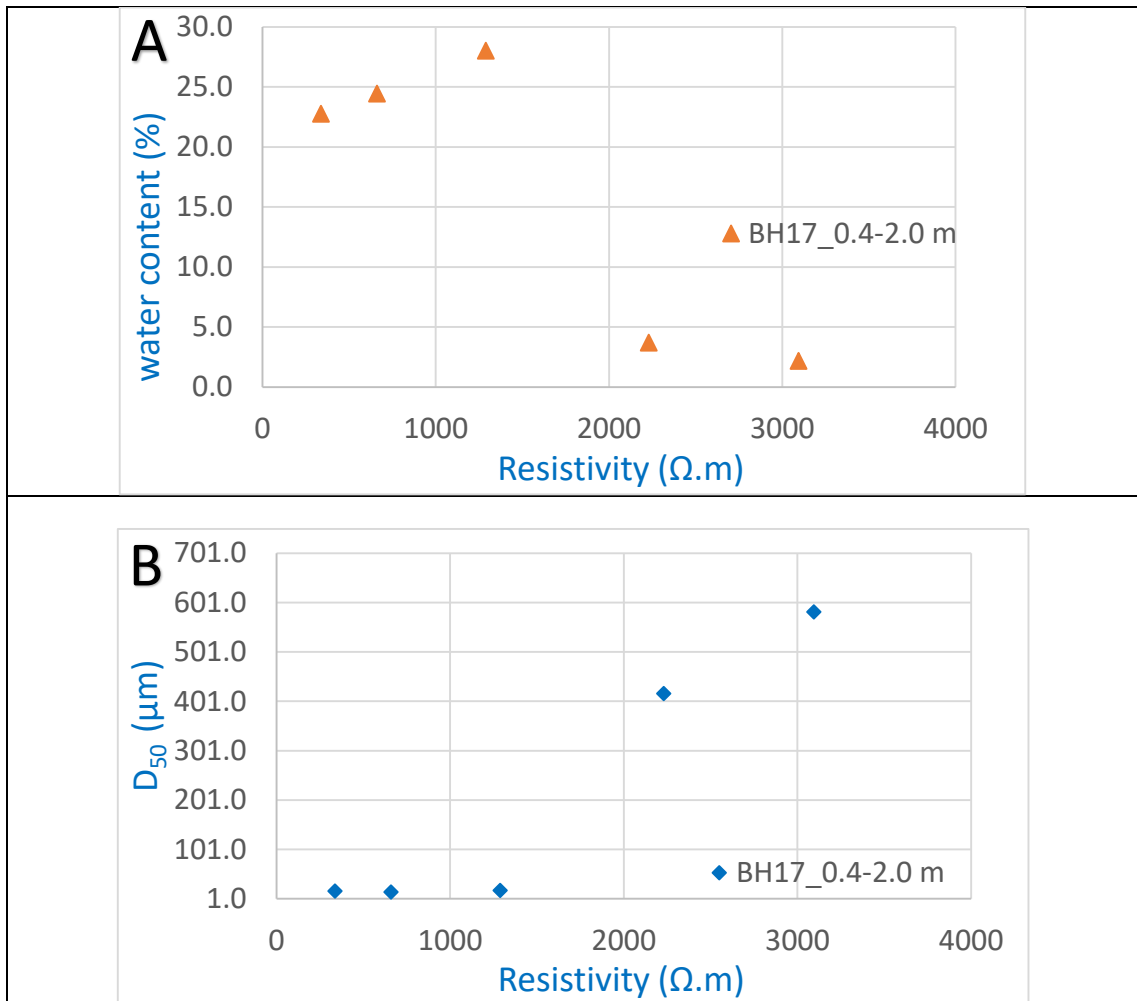


Figure 25: Relationship between A) specific resistivity and water content and B) specific resistivity and grain size in different structural units of the levee body for the borehole drilled on the levee foot (BH-17) at 16.00 lkm of Maros levee.

SPSS statistics carried out two correlations: the resistivity based on ERT profiles and water content and the resistance based on ERT profiles and grain size at each borehole drilled on Tisza and Maros levees. Pearson and Spearman's correlations were used at every borehole, as explained in **Table 2**.

Table 2: Illustrates the correlation results and their related degree of significance between the true resistivity of the samples against the moisture content and the true resistivity of the samples against grain-size (D50) at each borehole location drilled on Tisza and Maros levees.

BH	N/BH	R vs W by Pearson		R vs W by Spearman		R vs D50 by Pearson		R vs D50 by Spearman	
BH-1	16	-0.269	0.314	-0.424	0.101	0.466	0.069	.649**	0.007
BH-2	10	-.934**	0.01	-.842**	0.002	0.471	0.169	0.195	0.59
BH-3	15	0.332	0.226	0.382	0.16	0.263	0.344	0.422	0.117
BH-4	10	-0.452	0.19	-0.527	0.117	0.416	0.232	0.333	0.347
BH-5	15	-0.217	0.438	-0.233	0.404	0.056	0.842	0.025	0.929
BH-6	10	-.765**	0.01	-.733*	0.016	0.601	0.066	.857**	0.002
BH-7	15	-0.127	0.653	0.034	0.904	0.099	0.725	-0.093	0.742
BH-8	10	0.268	0.454	0.281	0.431	-0.413	0.236	-0.309	0.385
BH-9	17	-0.368	0.146	-0.212	0.414	0.182	0.484	0.153	0.557
BH-10	7	.782*	0.038	0.556	0.195	-0.417	0.352	-0.143	0.76
BH-11	17	-0.067	0.797	-0.039	0.881	191	0.463	-0.078	0.765
BH-12	11	0.031	0.927	0.2	0.555	0.194	0.567	0.327	0.326
BH-13	15	0.389	0.152	0.356	0.193	-0.083	0.768	-0.014	0.96
BH-14	7	0.582	0.17	0.667	0.102	0.491	0.263	0.36	0.427
BH-15	15	-.893**	0.01	-.924**	0.01	.638*	0.01	.704**	0.003
BH-16	7	0.677	0.095	0.714	0.071	-0.165	0.724	0.036	0.939
BH-17	5	-0.869	0.056	-0.6	0.285	.952*	0.012	.900*	0.037
BH-18	15	-.776**	0.001	-.941**	0.01	.800**	0.01	.639*	0.01
BH-19	7	-0.295	0.521	-0.214	0.645	0.655	0.11	0.357	0.432

Note: Number of samples/borehole: N/BH, R: resistivity based on ERT profiles. W: water content; D50: mean grain size.

The correlation results showed too much variation in weak, medium and strong. At the same time, the correlations varied depending on their degree of significance, and this is because of the variation in water content among the collected samples. Therefore, I turned to study the correlation between the resistivity based on ERT profiles and the grain size and between the resistivity based on ERT profiles and the water content for all 220 samples. The correlation results between the mentioned parameters are shown in **Table 3**. Even though the low negative correlation between resistivity and water content and the low positive correlation between resistivity and grain size, the degree of significance for both is very high.

Table 3 Correlation results of the 220 samples collected from 19 boreholes

Parameters	No. of samples	Correlation Results	Significance	Correlation coefficients
R vs W	220	-0.3**	<.001	Spearman
R vs D50	220	0.5**	<.001	Spearman

R: resistivity based on ERT profiles W: water content; D50: mean grain size

As the correlation between R and D50 and between R and W at every individual borehole and all the samples showed variation in the results, therefore, I turned to classify all the samples regarding the water content percentage into three classes; the first class includes the samples with a water content range from 0% to 10%, the second class includes the samples with a water content range from 10% to 20%, the third class includes the samples with a water content range from 21% to 30% or more as shown in **Table 4**. The correlation results between resistivity and grain size were significant and positive. The strongest correlation with a degree of significance was noticed in the first class with low water content. This could explain the effect of the water content of the samples on the relationship between resistivity and grain size, in which the increase in the water content in the samples reduces the strength of the relationship between R and D50, as I noticed in the case of the third class of water content samples.

Table 4: Illustrates the correlation results and their related degree of significance between R, D50, at three classes of water content

		R vs D50		
	N	Correlation	Significance	Correlation coefficients
W: 0 % to 10%	34	0.672**	0.01	Pearson
W: 10 % to 20%	92	0.574**	0.01	Pearson
W: 20 % to 30%	94	0.213*	0.05	Pearson

Number of samples at every class: N

4.2.3 Relationship of resistivity and other physical parameters

Aquitard materials are poorly permeable underground layer that limits water flow from the riverside to the protected side. This layer is important in the levee structure from flood risk mitigation issues. In addition to Resistivity, water content percentage, and grain size, analysis of 49 samples gave more information about the different parameters of the levee materials of Tisza and Maros rivers like Saturated hydraulic conductivity (K), Porosity, and Density. The saturated hydraulic conductivity enabled us to study the levee

compositions and classify them into Aquitard and non-Aquitard materials. It was found that 16 out of 21 samples collected from Tisza Levee exhibit Aquitard nature, and 19 out of 29 samples collected from Maros Levee exhibit Aquitard nature, as shown in **Table 5**.

Table 5 Properties of 49 samples collected from 10 different boreholes

	Sample ID	lkm	d	W	D50	ϕ	ρ	K	M	R
		(km)	(cm)	(%)	(μm)	(m/m%)	(g/cm ³)	(mm/h)		($\Omega\cdot\text{m}$)
Tisza levee crown	1	13	270	16.5	18.8	38	1.63	0.007	aquitard	57.2
	2	13	290	16.0	18	39	1.62	0.007	aquitard	43.7
	3	13	300	15.0	16	40	1.59	0.008	aquitard	30.3
	4	13	310	15.0	15.5	36	1.69	0.007	aquitard	24.8
	5	13	570	27.0	14	45	1.47	0.007	aquitard	10.6
	6	13	580	28.0	13.4	44	1.49	0.006	aquitard	10.7
	7	18	300	24.0	12.9	44	1.49	0.006	aquitard	11.9
	8	18	310	24.0	13	35	1.71	0.007	aquitard	12
	9	18	390	22.5	7.5	41	1.56	-	-	12.3
	10	18	510	25.0	12.9	45	1.47	-	-	13
	11	18	520	26.0	12.6	41	1.57	0.007	aquitard	13.2
	12	31.4	150	15.5	12	39	1.63	0.011	aquitard	20.6
	13	31.4	160	16.0	11.9	36	1.69	-	-	17.5
	14	31.4	250	24.0	10.8	38	1.63	0.012	aquitard	10.9
	15	31.4	410	20.0	12.5	44	1.50	0.015	aquitard	9.7
	16	31.4	420	19.5	13	43	1.51	0.013	aquitard	9.9
	17	37	50	8.0	19.5	38	1.64	24.942	not aquitard	22.7
	18	37	60	9.0	21.4	41	1.57	24.375	not aquitard	20
	19	37	270	12.5	16	35	1.72	0.012	aquitard	8.9
	20	37	270	12.5	16	35	1.72	0.011	aquitard	8.8
	21	37	470	20.0	13.8	-	-	0.012	aquitard	10
Maros levee crown	22	3	150	22.0	17.7	44	1.49	3.487	not aquitard	14.7
	23	3	160	22.0	18.7	50	1.31	0.956	not aquitard	14.5
	24	3	290	21.0	13.5	41	1.55	0.013	aquitard	17.45
	25	3	610	33.5	11.7	-	-	-	-	23.7
	26	3	620	34.0	11.9	46	1.43	0.492	not aquitard	23.7
	30	8	190	14.0	33.6	40	1.58	1.246	not aquitard	92
	31	8	200	14.0	34.1	42	1.55	0.266	not aquitard	100.2
	32	8	280	3.0	203.1	48	1.38	0.764	not aquitard	168.2
	33	8	420	18.0	15.8	43	1.50	-	-	233
	34	8	490	23.0	13.3	36	1.69	0.012	not aquitard	217
	35	10	150	27.5	20.8	45	1.46	0.113	not aquitard	24.8

	36	10	160	28.0	21.1	48	1.37	0.013	aquitard	25
	37	10	300	21.0	24.2	48	1.37	0.048	not aquitard	28
	38	10	500	17.5	15.7	47	1.39	0.066	not aquitard	31.6
	39	10	510	17.0	15.6	43	1.50	0.012	aquitard	31.8
	40	16	240	11.0	20.5	48	1.38	-	-	88
	41	16	250	12.5	19	45	1.47	0.011	aquitard	85.11
	42	16	250	12.5	19	48	1.37	1.034	not aquitard	85.11
	43	16	470	21.0	15.7	51	1.3	0.010	aquitard	39
	44	16	480	21.0	15.2	46	1.42	0.688	not aquitard	41
	45	20	250	15.0	15	44	1.49	-	-	34.8
	46	20	250	15.0	15	48	1.39	0.113	not aquitard	34.8
	47	20	260	16.0	15.3	45	1.46	0.200	not aquitard	33
	48	20	430	21.0	18.3	41	1.57	0.113	not aquitard	20
	49	20	440	21.0	18.6	45	1.44	0.036	not aquitard	19
Maros protected side	27	3	150	4.0	339.3	47	1.41	525	not aquitard	442
	28	3	160	4.0	331.8	45	1.44	287	not aquitard	606
	29	3	285	27.0	18.8	46	1.43	0.052	not aquitard	1292

lkm: levee km; d: depth; W: water content; D50: mean grain size, ϕ : porosity; ρ : bulk density; K: saturated hydraulic conductivity; M: material type, and R: resistivity based on ERT profiles.

The correlation among the resistivity of the levee materials and other parameters like water content, grain size (D50), saturated hydraulic conductivity (k), Density and porosity was carried out. The results of the correlations are exhibited in **Table 6**

The correlation between resistivity and water content is negatively low, with a high significance level. The correlation results between resistivity and grain size (D50) are moderately positive and statistically significant. The correlation between resistivity and saturated hydraulic conductivity is positively low, with a high significance level. The correlation between resistivity and porosity is positively low, with a high significance level. The correlation between resistivity and Density is negatively low with a high significance level.

Table 6 Correlation results of the 49 samples collected from 10 different boreholes

Parameters	No. of samples	Correlation	Significance	Correlation coefficients
R vs W	49	-0.378**	0.007	Spearman
R vs D50	49	0.571**	<.001	Spearman
R vs K	49	0.374*	.015	Spearman
R vs ϕ	47	0.339*	0.020	Spearman
R vs ρ	47	-.352*	0.015	Spearman

R: resistivity based on ERT profiles W: water content; D50: mean grain size, K: saturated hydraulic conductivity, ϕ : porosity, ρ : bulk density.

4.3 Mapping the materials along the investigated levees

With the help of sedimentological data, ERT could provide more information about the structures and changes of the materials along the investigated levee sections. In the case of the Tisza levee section and by following up the longitudinal profiles measured on the Tisza levee crown, it is noticed that two materials, medium and fine silt, are the main components of the levee core. Going from north to south, **in Fig. 26b**, the levee sections show four patterns from the crown to the bottom. The first pattern (medium silt, fine silt, and medium silt) is predominant in levee sections from 42-lkm to 40-lkm, in 36-lkm, in 34-lkm, and in 17-lkm. The second pattern (medium silt, and fine silt) is predominant in the levee sections 38-lkm, 33-lkm, from 24-lkm to 19-lkm, and from 16-lkm to 15-lkm. The third pattern (fine silt, medium silt, and fine silt) is predominant in only 37-lkm and 13-lkm. The fourth pattern (fine silt, and medium silt) is predominant in 35-lkm, from 32-lkm to 28-lkm, 18-lkm, and 14-lkm. Regarding the transverse profiles measured on the Tisza levee, both river and protected sides are composed of fine and medium silts, as shown in **Fig. 26a and c**.

In contrast to the investigated Tisza levee section, the investigated Maros levee section is more complicated and shows more variety in the materials from fine silt to coarse sand (fine silt, medium silt, coarse silt, fine sand, medium sand, and coarse sand) and at some parts alteration of fine and medium silt could be noticed. In general, the longitudinal profiles measured on the crown of Maros levee showed that the levee core is composed of medium and fine silts except for three lkm sections showing coarse silt, fine and medium sand as well which are at 8-lkm, 16-lkm, and 22-lkm. going from east to west **Fig. 27b**, the levee sections show five patterns from the crown to the bottom. The

first pattern (medium silt, fine silt, and medium silt) is predominant in levee sections 24-lkm, 20-lkm, and 1-lkm. The second pattern (medium and fine silts) is predominant in the levee sections 23-lkm, 21-lkm, 15-lkm, 9-lkm. The third pattern (alterations of medium and fine silts at the same unit) is predominant in two sections from 19-lkm to 16-lkm and from 13-lkm to 10-lkm. The fourth pattern (fine and medium silts) is predominant in 14-lkm and from 6-lkm to 3-lkm. The fifth pattern (medium silt) is predominant in three sections 15-lkm, 7-lkm, 2-lkm.

Regarding the transverse profiles measured on Maros levee, 17 levee km sections out of the whole investigated sections (24 lkm long) show a sand backfill in the protected side. These sections are from 2-lkm to 9-lkm as shown in, 13-lkm to 19-lkm, at 22-lkm, and 24-lkm, as shown in **Fig. 27a and c**. The rest of the sections show silty materials. The riverside of Maros levee is showing silty composition.

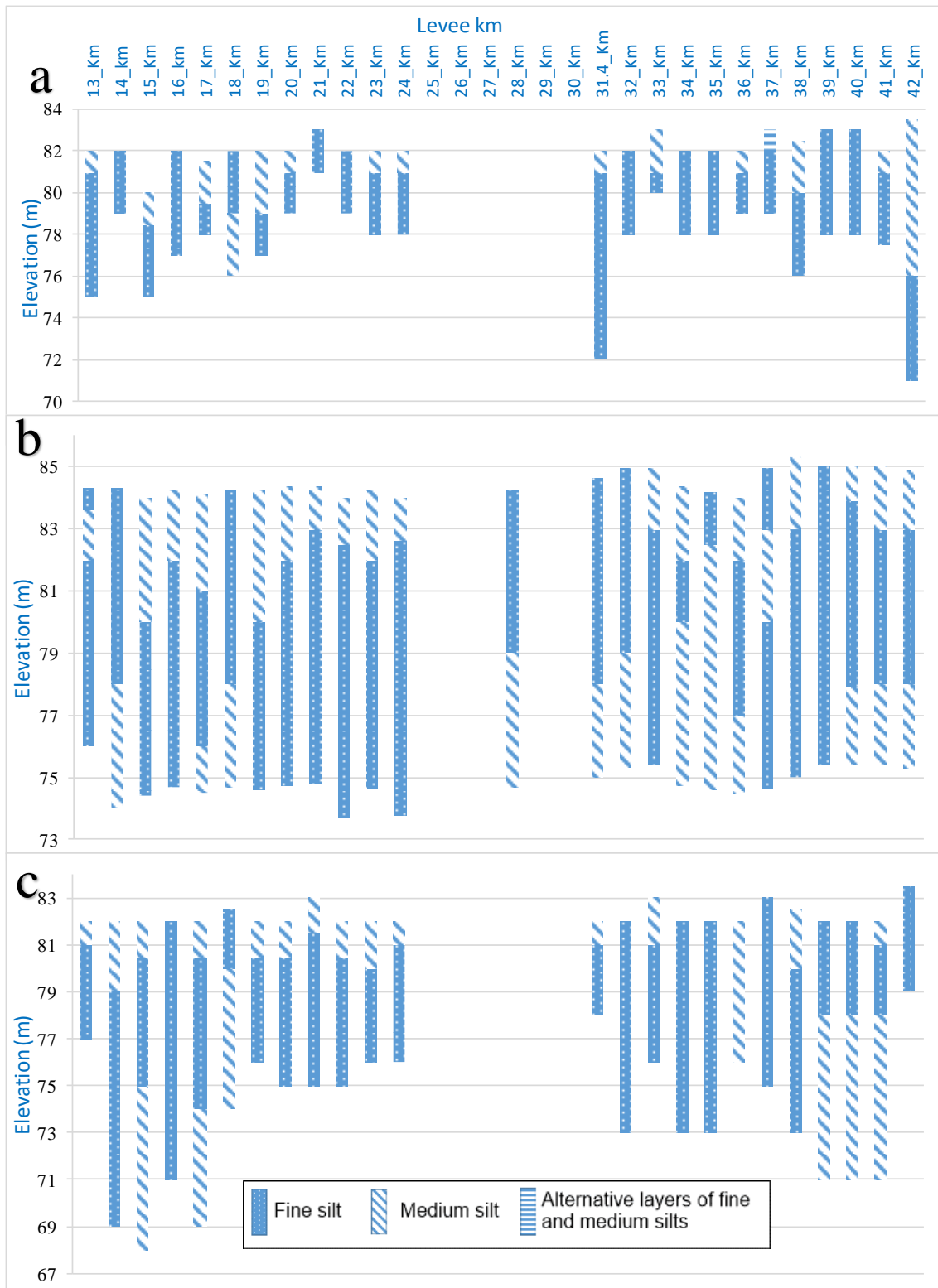


Figure 26: Mapping the composition of the investigated Tisza levee section; A) along the riverside, B) along the levee crown, and C) along the protected side

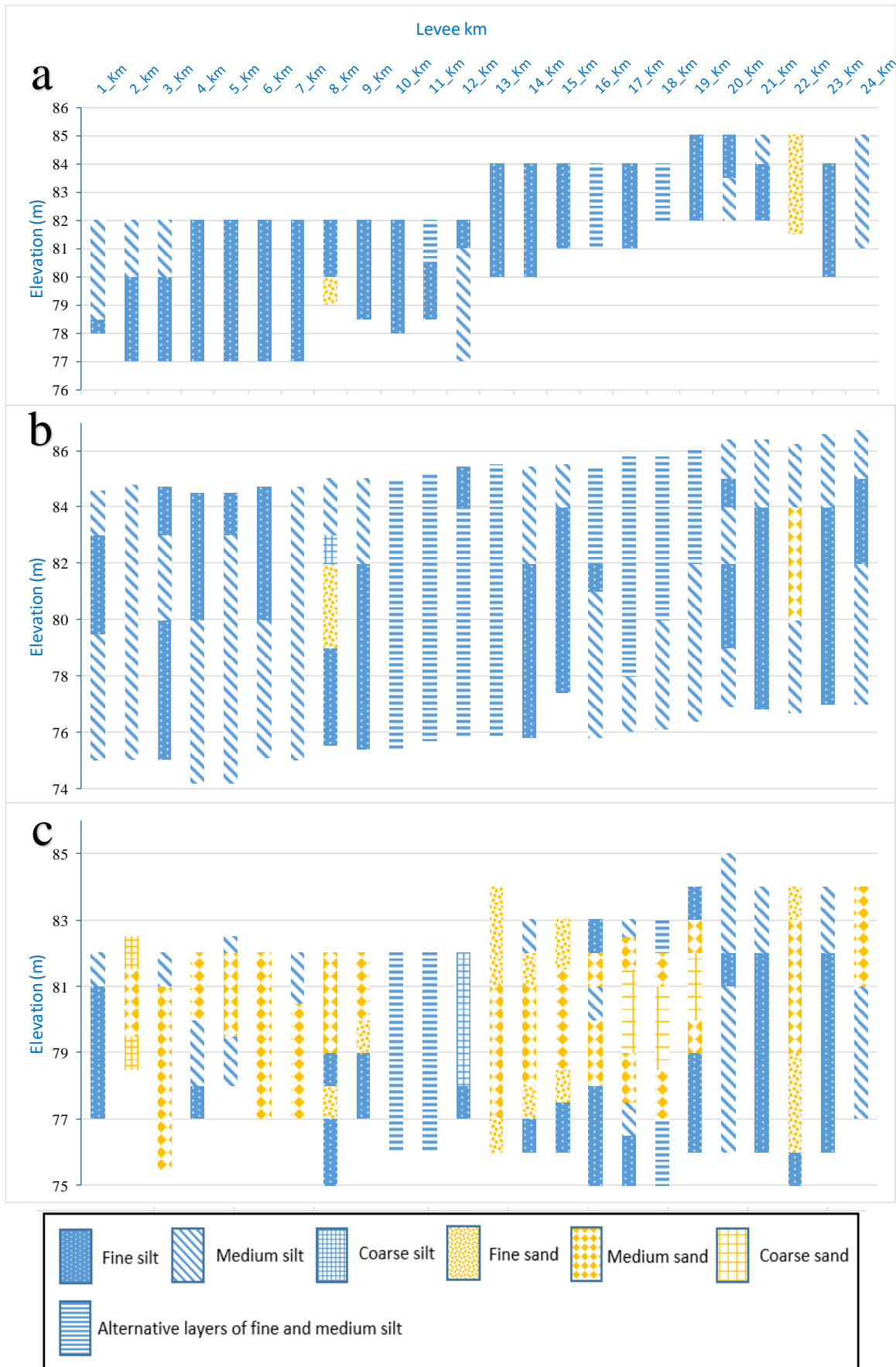


Figure 27: Mapping the composition of the investigated Maros levee section; A) along the riverside, B) along the levee crown, and C) along the protected side

4.4 Elevation change of levees

The elevation values were lower overall in 2017 than in 1976 (**Fig. 28**). In 1976, the levee crown's adjusted mean height was 85.26 metres above sea level; in 2017, it was 85.21 metres above sea level. At first sight, the estimated 5 cm drop in levee crown height is not substantial. However, it must be noted that due to pavement construction and recurrent asphaltting throughout the research period, a little elevation rise could be seen at some sections (**Fig. 28**). In the absence of these parts, the height difference (1976: 85.23 m asl.; 2017: 85.15 m asl.) is -8 cm, which is much more than the anticipated measurement uncertainties. As a result, these parts' annual subsidence rate is 1.3 mm/yr.

Moving average analysis was used to analyse elevation differences in order to more thoroughly explore the spatial variation of changes (1 km window at 200 m increments) (**Fig. 29**). Even on unpaved sections, the drop in height is not uniform; for example, the levee stretch between 32 and 41 km (-16 cm on average) and between 13 and 17 kilometres (-29 cm on average) are more impacted by the elevation decrease. Such spatial differences imply that elevation decrease cannot be just explained by compaction and mass-related subsidence, which should affect the whole region comparably, but rather that additional factors may be involved in non-uniform subsidence.

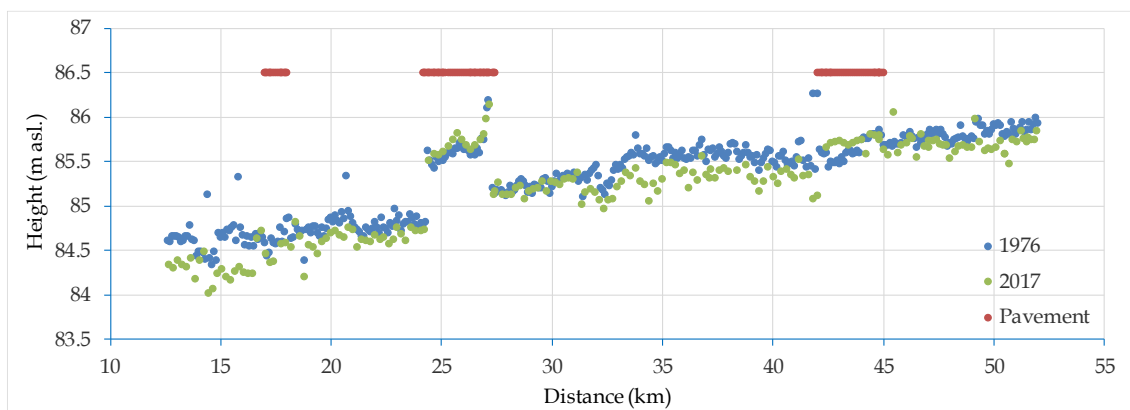


Figure 28: Elevation data of the levee crown in 1976 (blue points) and 2017 (green points). Red lines mark sections where the levee crown is paved.

Similar to the levee crown, elevation readings for the examined segment were lower in 2018 than in 2003 for the levee foot. For comparing the two datasets, points that showed an extreme elevation increase were excluded. These are unambiguously related

to the reinforcement of the levee foot as a matter of constructing a highway bridge over the river between 2009 and 2011.

As a result, the mean height of the levee foot decreased from 78.31 m asl in 2003 to 78.25 m asl in 2018. This results in a 6-centimetre overall drop. The yearly rate of height loss during the 15 years is 3.7 mm/yr, strikingly similar to the 3.7 mm/yr annual height decrease of the levee crown on the same levee section between 1976 and 2017.

Engineering interventions, such as reinforcement, also impact levee foot height, but the change is more uniform, partly because the study period was shorter and fewer elements altered the elevation conditions. The general trend on unpaved sections, such as between 13 and 17 kilometres and between 19 and 24 kilometres (**Fig. 29**), is the same even though the spatial pattern of the levee crown and levee foot elevation decrease is not identical, indicating that the levee crown and foot are moving together and that a subsidence process should be affecting the entire levee body.

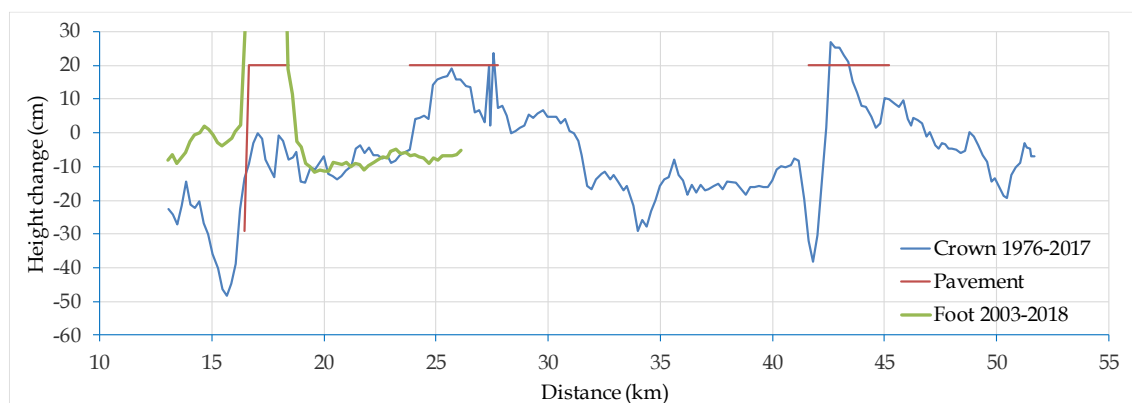


Figure 29: Elevation change of levee crown (blue line) and levee foot (green line) along the investigated sections using a 1 km moving average.

The spatially uneven subsidence in the area is also reinforced by the PSI data, representing not only the levee itself, but also its environs. Surface deformation velocities throughout the analysed 18-year period (1992-2010) varied between +0.5 and -5.0 mm/yr (**Fig. 30**), translating to an average subsidence rate of 1.9 mm/year for the section under investigation (12.5 - 39.0 lkm). Even though a larger section was evaluated in the latter example, this figure is quite similar to the rate computed using levelling and GPS data (1.3 mm/year). When paved areas are excluded from the evaluation, and only portions assessed using both methods are included, the traditional estimate of subsidence is greater (4.2 mm/yr) than the estimates obtained via PSI (2.6 mm/yr). The investigations were conducted during several periods, so vertical velocities may have altered with time, which

might account for the disparity. Even yet, the results of the two approaches corroborate one another, and if the data are accurate, the analysed levee section has experienced substantial subsidence over the previous several decades, with an unequal spatial distribution. As a result, extensive anthropogenic activity may explain deformation and subsidence anomalies (Grenerczy et al., 2021), with intensive oil and natural gas production in the region beginning in the 1970s as a possible source (Kiss et al., 2021).

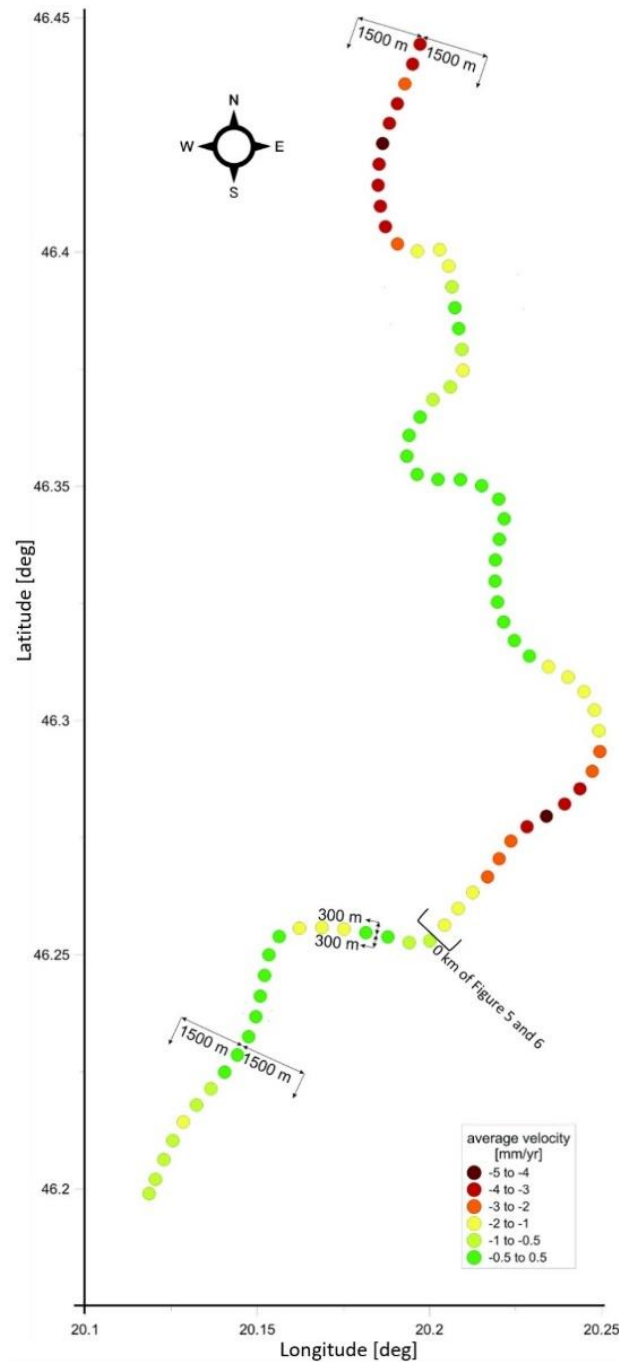


Figure 30: Average deformation velocities between 1992-2010, calculated from PSI data falling within a 1500 m buffer of the levee. Data are averaged for every 500 m sections.

4.5 GPR

4.5.1. Identification of GPR anomalies

Six different types of anomalies, each of which alters the levee structure and affects flood risk differently, were found when the GPR profiles were processed. As noted in **Table 7**, the anomalies found in all the impacted areas were categorised and assessed for their potential to cause flooding, and the number of GPR profiles they would have affected was counted.

The different types of anomalies are explained in detail as follows:







1. **Tensile cracks**: When soil shear strength is exceeded by shear stress, cracks occur (Wei et al., 2020; Lu et al., 2007) , as illustrated in **Fig. 7a**. Tensile cracks on the levee crown were the most typical anomalies seen in GPR profiles. These emerge due to the levee body drying out. They show up as vertical lines on the GPR profiles with a differing dielectric permittivity from the nearby levee materials. An example of this kind of abnormality is shown in GPR profile No. 62 (**Fig. 31a**). Tensile cracks may seal during rainy seasons and reopen during dry ones, causing long-term damage to the levee body. Nearly 30% of the analysed profiles were affected and hundreds of cracks were detected.
2. **Remarkable changes in dielectric permittivity**: The increased (signal band lengthening) or decreased (signal band shortening) water content of levee materials, according to Utsi (2017), can be used to explain this occurrence. In numerous profiles, a notable and abrupt change in the dielectric permittivity in the second layer of the levee structure was subjectively evaluated (**Fig. 31b**). High and low dielectric permittivity may thus also reflect variations in the amount of moisture in the levee material. Since all measurements were taken during a prolonged drought, when the groundwater level was around 10 m below the survey depth, these abrupt changes are more likely due to increased clay (signal band lengthening) or silt/sand (signal band shortening). The presence of widely disparate band lengths in the same profile suggests that changes in levee material are more significant than attenuation, even though attenuation may also impact the banding pattern. Such an abnormality may result in seepage and widespread failure. About 25% of the GPR profiles were impacted, as was seen in several GPR profiles.
3. **Animal burrows**: An animal creates burrows—tunnels or holes—as a place to reside or a temporary haven (a place of safety) (Website 1). Because the dielectric constant of air-filled animal burrows is low ($\epsilon_r = 1$), the reflected signal from the

boundary changes its polarity relative to the incident signal (Smith & Scullion, 1993; Chen & Wimsatt, 2010). Depending on the size of the animal burrow, a positive peak will show in the radar scan over it. They commonly deteriorate, especially in the levee structure (Seed et al., 2006; Wiscomb & Messmer, 2010). This anomaly is one of the most frequent issues that form piping in levee constructions. About 50% of all levee collapses worldwide are caused by piping phenomena (Richards & Reddy, 2010). These characteristics affected about 12% of the profiles. An illustration of an anomaly brought on by animal burrows is shown in **Fig. 31c**.

4. **Layer deformation:** Minor deformations regarding performance limit states are defined by non-discernible shear zones (max deviatoric strain less than 1%) and low gradients (i.e., $i < 1$) throughout the levee and foundation (Khalilzad & Gabr 2011; Khalilzad et al. 2014; Khalilzad et al. 2015). In GPR cross-sections taken on the levee crown, deformation in the levee layers may be seen as a distinct shift in the dielectric permittivity in the top layer between 1 and 2 m, with a significant reflectivity identifying the subsidence region. This anomaly lowers the levee's height, which has a detrimental impact; as a result, the levee must be raised over time. This feature only affected about 2% of the profiles. A layer deformation example is shown in **Fig. 31d**. Signs of this phenomenon were visible in six GPR profiles.
5. **Paleo river channel:** Palaeochannels are the remains of former rivers or stream channels covered or submerged by more recent fluvial sediments. GPR has been used to explore Paleo river channels (Vandenberghe & van Overmeeren, 1999; Skelly et al., 2003; Sowik, 2012). The weak reflections inside this anomaly indicate the currently filled younger layers, whereas the strong reflectors outside reveal a concave form that represents the river's sand-bedded channel. As they let seepage below the levee and may enhance the flood risk, paleo river channels are regarded as one of the major reasons for levee collapse. Water upwelling is a consequence of this phenomenon that can be seen on the levee's protected side. Only in GPR profiles taken on the levee foot can paleo-river channels be seen. An illustration of a paleo river channel may be found in **Fig. 31e**. Five GPR profiles in all were impacted.

6. **Sudden change in stratification:** This phenomenon is characterised by an abrupt decrease in the horizontal levee layers, which may indicate significant changes in the levee's structure. In other words, the construction might have not followed a consistent design 150 years ago. This anomaly might result in areas of widespread failures and exacerbate seepage during floods. In four profiles, abrupt stratification shifts were noticed (**Fig. 31c and f**).

Table 7: Various anomalies detected during interpretation of 2D-GPR cross-sections and their evaluation in terms of flood hazard.

No.	Legend	Name	Evaluation in terms of flood hazard	No. of GPR profiles affected	%
1		Tensile cracks	Enables piping, leading to levee breach or mass failure Cracks might close when the levee gets wet	87	30
2		Remarkable changes in dielectric permittivity	Enables seepage, leading to mass failure	70	25
3		Animal burrows	Enables piping, leading to levee breach or mass failure	33	12
4		Layer deformation	Results in height decrease, overtopping	6	2
5		Paleo river channel	Enables seepage below the levee, leading to water upwelling and the development of sand boils	5	2
6		Sudden change in stratification (dipping layers)	Enables contour line seepage, leading to mass failure	4	1.5

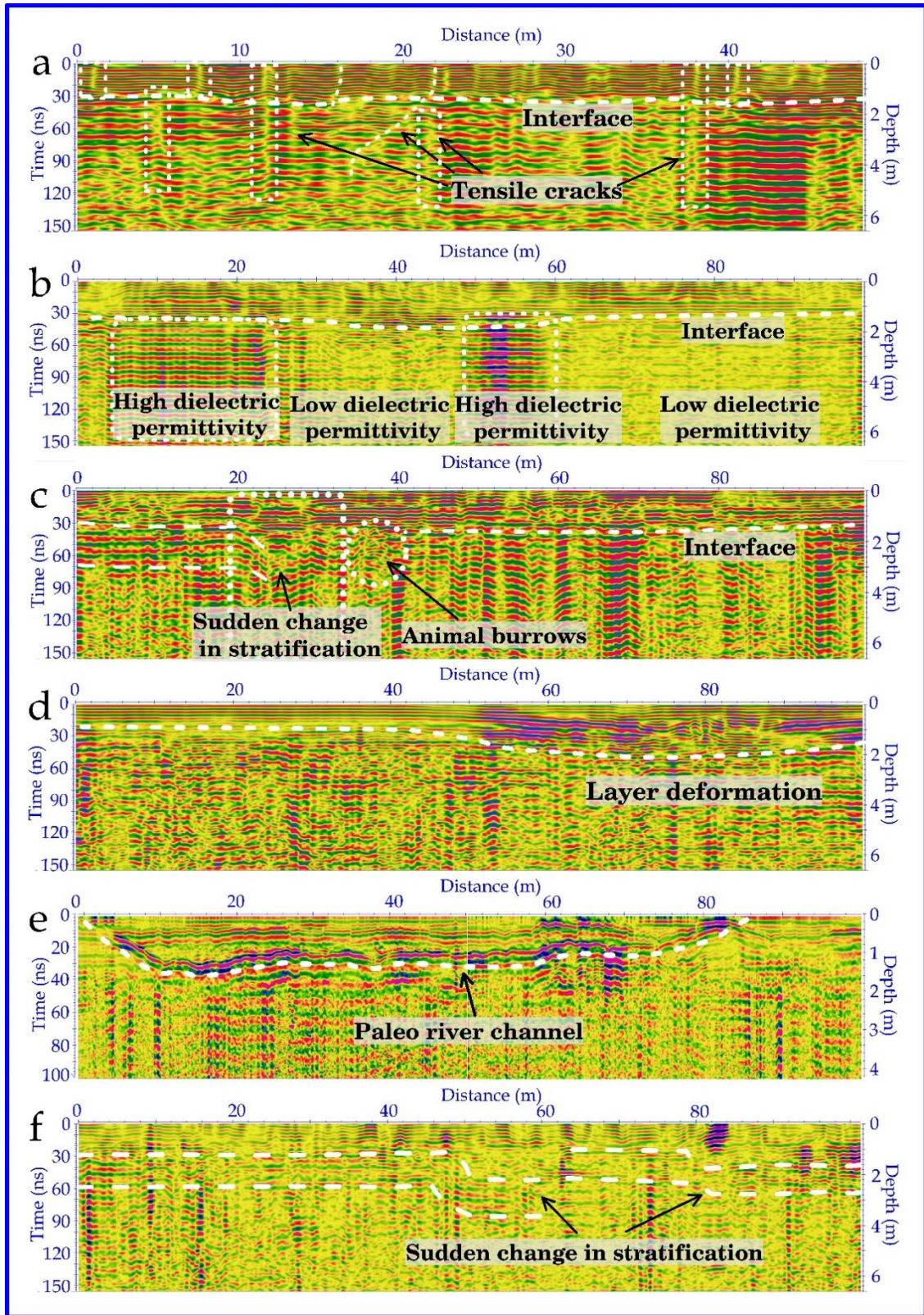


Figure 31 Representative profiles for the identified GPR anomaly types: A) tensile cracks (profile 62, southern zone), B) remarkable changes in dielectric permittivity (profile 24, southern zone), C) animal burrows and sudden change in stratification (profile 54, southern zone), D) layer deformation (profile 18, southern zone), E) paleo-river channel at the levee foot (profile 42, southern zone), and F) sudden change in stratification (profile 60, northern zone).

4.5.2. Spatial distribution of penetration depth and GPR anomalies

Penetration depth, just like changes in dielectric permittivity, is mostly determined by the condition of the levee material. According to the inverse relationship between the velocity of GPR signals and the relative dielectric permittivity of different materials ($v=c/\sqrt{\epsilon_r}$, Annan 1996), the higher penetration depth of the signals meant that this part of the levee is build up of materials that permit the EM waves to pass with higher speed than other parts of the levee. The lower relative dielectric values explain these parts with higher penetration depths. The spatial variation of penetration depth refers to changes in the levee materials, a greater depth indicating higher silt or sand content, a lower depth indicating higher clay content (**Fig. 35b**). The penetration depth of the Southern GPR survey zone ranges from 3.3 m to 4.5 m, with an average of 3.73 m. although values fluctuate, it seems clear that there are three separable zones within this section with increased penetration depth. These three zones are between 14.4 - 15 lkm, 17.5 - 18.8 lkm, and 21.5 - 23 lkm (**Fig. 35b**).

However, compared to the southern measurement zone, there are fewer fluctuations, and just one section of the northern measurement zone demonstrates increased penetration depth between 34 and 35 kilometres. The penetration depth at the northern measurement zone ranges from 3.2 m to 4 m, with an average of 3.4 m. The northern zone is more consistently steady and uniform in its composition overall. The values vary from 3.5 to 4.5 metres, with an average of 3.9 metres displayed as a red line (**Fig. 35b**) for the penetration depth analysis for the profiles recorded on the levee foot. One chart (**Fig. 35c**) showed the results of anomalies from 2D GPR measurement sections.

By comparing the outcomes of penetration depth of GPR signals with the outcomes of anomalies for both southern and northern measurements of the levee, it is noticed that the variation of penetration depths of the signals for the southern zone is due to inhomogeneity of the materials and also due to a large number of anomalies in this zone, in contrary, the penetration depth results show stability for the northern zone and this is due to homogeneity nature of the materials and also due to fewer anomalies detected from GPR profiles in this zone (**Fig. 35c**).

4.5.3. Comparison of applying two different antennas on the Tisza levee section

The 200 MHz GPR antenna's penetration depth along the 3.5 km Tisza levee section under investigation ranged from 3.6 m to 4.4 m, with an average value of 3.9 m. In comparison, the 80 MHz antenna's values varied from 1.8 to 5.6 metres, with 4.0 metres being the average. So, regardless of the centre frequency, there was no discernible difference in average penetration between the two systems. Regarding the 80 MHz antenna, high variance in penetration depths is a sign of measurement uncertainty or low resolution compared to the 200 MHz antenna resolution.

Due to enhanced wave relaxation brought on by polarisation effects, GPR penetration depth in fine-grain media is known to be rather low (Ishida, Makino, 1999; Santamarina et al., 2001; Bittelli et al., 2008). Polarisation results in larger dielectric permittivities and electrical conductivity values, dissipating GPR energy and causing weaker signal reflections. Additionally, high liquid ion concentrations are frequently associated with clayey soils and sediments, promoting energy dissipation (Saarenketo, 1998; Ishida; Makino, 1999). However, the difference in penetration depth due to varying dielectric characteristics might also correspond to variations in the composition of the levee material (Sheishah et al., 2023).

Nearly 25% of the 100 m profiles showed A remarkable change in dielectric values. The locations where the two antenna types detected dielectric changes were identical (**Fig. 32**). Only the 200 MHz antenna could detect the layers and interfaces inside the levee body and minor anomalies. The 80 MHz antenna's vertical resolution needs to be increased for these purposes. In the majority of the profiles, three units were generally found (**Fig. 32a**). The intermediate unit's thickness was 1.32 m, while the uppermost unit's thickness was 1.09 m. Because it extended below the depth of the inquiry, the vertical extension of the third unit could not be mapped.

Smaller anomalies within the uppermost layer were interpreted as tensile cracks caused by the levee material's desiccation. Based on the relationship that the size of the detectable target is roughly 10% of the wavelength (Utsi, 2017) and the equation $\lambda = v/f$, where (λ) is the wavelength, (v) is transmission velocity, and (f) is the centre frequency of the antenna used for the survey, we calculated the minimum size of anomalies the two antennas could detect. This result was 4.3 cm for the 200 MHz antenna at a velocity of 8.5 cm/ns and 10.6 cm for the 80 MHz antennas. The width of the voids discovered by the 200 MHz antenna was above 4.3 and below 10.6 cm (**Fig. 32a**), as no voids could be

identified using the 80 MHz antenna (**Fig. 32b**). At a maximum depth of 1 m, the observed cracks were in the uppermost layer. Four profiles along the survey line had a high density of cracks, which indicates that about 10% of the profiles had this flaw to a significant extent.

Other authors have also used a high-frequency antenna to successfully find small-scale voids and discontinuities in artificial levees (anomaly size 0.1 m or less (see e.g. Di Prinzio et al., 2010; Chlaib et al., 2014). Tensile voids and cracks identified in our study mostly get closed by wetting the levee body during floods, though the largest ones may remain open (Szűcs et al., 2019), which means that their presence can increase the risk of damage. Besides voids, layer deformation and changes in levee composition, marked by sudden changes in dielectric permittivity, are also very important regarding flood hazard. They can contribute to considerable seepage during floods.

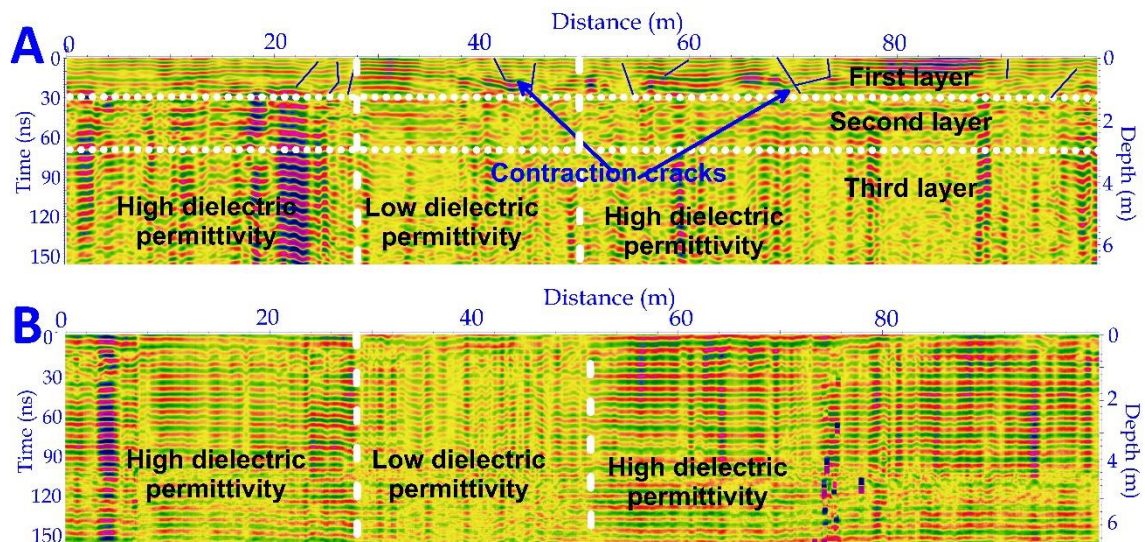


Figure 32: Interpretation and comparison of 100 m GPR profiles made by A) 200 MHz and B) 80 MHz antennae along the same survey line (16.2-16.1 lkm).

4.5.4. Justification of GPR results using recordings of flood phenomena

Along the levee section under study, GPR results were contrasted with piping and moderate seepage records from 2006 and 2010 (**Fig. 33**). The frequency of all GPR anomalies and anomalies related to a remarkable change in dielectric permittivity were used for the spatial comparison. Two factors led to the selection of the latter parameter: 1) it was the second-most prevalent anomaly with sufficient recordings to create a spatial plot, and 2) this sort of anomaly was most frequently observed in the second layer of the levee construction at a height where piping and moderate seepage are typically present. Due to the second issue, anomalies like tensile cracks and animal burrows that only

impact the upper part of the levee needed to be thoroughly considered. Even if the spatial distribution of km-based data on anomalies and flood phenomena does not exactly match, there is a clear distinction between the two investigated zones. A total of 148 and 42 anomalies were found in the southern and northern zones of the studied levee section, respectively, and out of these, 51 and 18 were categorised as a sudden change in dielectric permittivity. In the meantime, the number of 100 m sections affected by piping or moderate seepage regarding the two zones was 26 and 11, respectively. The relationship is particularly clearer if the total number of recordings for a zone is given as a percentage of all recordings. In the southern and northern zones, the proportionate values of piping and moderate seepage were 70% and 30%, respectively. Very similar values were obtained when remarkable changes in dielectric permittivity were considered (74% vs. 26%), and a somewhat different, but still comparable distribution was experienced when each type of anomaly were taken into account (78% vs. 22%).

Despite discrepancies in the pattern of recordings, it is still impossible to predict the frequency of flood phenomena from GPR anomalies. However, if longer sections are investigated, the trend becomes clear, and GPR can be used to assess the potential of seepage and piping phenomena.

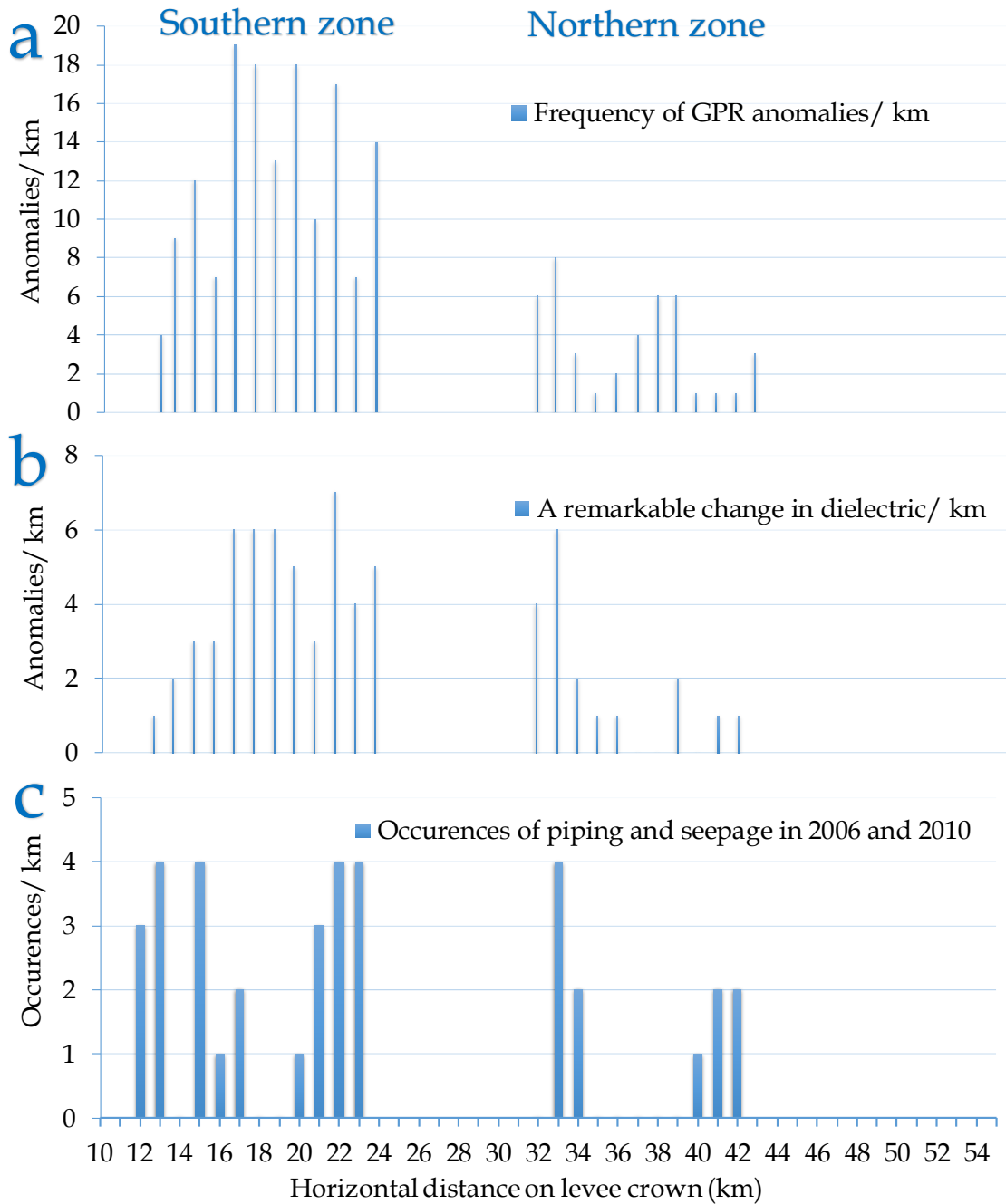


Figure 33: A) Spatial frequency of anomalies identified from GPR profiles measured on the levee crown each one 1Km, B) a special frequency of a remarkable change in dielectric each 1km section, and C) Occurrence of concentrated seepage (piping phenomenon) each one Km during two flood periods in 2006 and 2010.

5. Evaluation of levee health

The previous results could help to understand the structure and composition of the two investigated levee sections. The contrast in the resistivity values of the investigated levee materials was visible; therefore, the interfaces between layers could be detected using ERT, as it was documented (e.g. Kearey et al., 2013; Sheishah et al., 2022; Sheishah et al., 2023).

5.1 Evaluation of levee materials

The number of all water content samples collected at every 0.4 m depth was 220 samples. These samples were sorted regarding the grain size to investigate the dominant class among the seven different grain size classes forming the body of both Tisza and Maros levees. The analysis showed that fine silt is the most prominent class forming the body of both investigated levee systems with a proportion of 55.6 %, then medium silt with a proportion of 31.2 %, then medium sand with a proportion of 6.3 %, then coarse silt with a proportion of 4.5 %. The other classes, like very fine silt, fine sand, and coarse sand, represent a minor proportion ranging between 0.4% and 1.3 %, as shown in **Table 8**. It is noticed that fine-grained materials, which are fine and medium silts (with a total proportion = 87 %), represent the highest proportion among the seven classes, which means that the building materials of both Tisza and Maro's levees are good in terms of flood protection.

Table 8 Classification of the 220 samples regarding the grain-size and their proportion

Class	Proportion
fine silt	55.6 %
medium silt	31.2 %
coarse silt	4.5 %
medium sand	6.3 %
very fine silt, fine sand, and coarse sand	Between 0.4% and 1.3 %

The present study shows a range of specific resistivity values for different sediments forming the investigated levees with variable water content. Based on ERT measurements in the investigated Tisza and Maros levee sections, the quartile was utilized to calculate the specific resistivity range of different materials. Samples collected at every 0.4 m depth were used in this classification. The results showed seven sedimentary classes for the investigated levees; (1) fine silt which is characterized by a D50 range between 11

μm and $14 \mu\text{m}$ and a moisture content between 16 % and 24 % has a resistivity range between $15 \Omega\text{m}$ and $39 \Omega\text{m}$ with an average of $24 \Omega\text{m}$ and standard deviation 86, (2) Medium silt which is characterized by a D_{50} between $16 \mu\text{m}$ and $19 \mu\text{m}$ and a moisture content between 11 % and 22 % has a resistivity range between $25 \Omega\text{m}$ and $63 \Omega\text{m}$ with an average of $34 \Omega\text{m}$ and standard deviation 191, (3) Coarse silt which is characterized by a D_{50} between $34 \mu\text{m}$ and $38 \mu\text{m}$ and a moisture content between 12 % and 16 % has a resistivity range between $90 \Omega\text{m}$ and $128 \Omega\text{m}$ with an average of $97 \Omega\text{m}$ and standard deviation 116, (4) Fine sand which is characterized by a D_{50} between $109 \mu\text{m}$ and $164 \mu\text{m}$ and a moisture content between 4 % and 7 % has a resistivity range between $108 \Omega\text{m}$ and $199 \Omega\text{m}$ with an average of $173 \Omega\text{m}$ and standard deviation 93, (5) Medium sand which is characterized by a D_{50} between $332 \mu\text{m}$ and $430 \mu\text{m}$ and a moisture content between 3 % and 5 % has a resistivity range between $276 \Omega\text{m}$ and $798 \Omega\text{m}$ with an average of $518 \Omega\text{m}$ and standard deviation 525. (6 and 7) Very fine silt is represented by one sample with a D_{50} of $6.5 \mu\text{m}$ and a moisture content of 22.7 % and has a resistivity of $13.5 \Omega\text{m}$. One drilling sample from the levee foot of 16 lkm of Maros levee represents coarse sand. It is characterized by a D_{50} $582 \mu\text{m}$ and a moisture content of 2.2 % and has a resistivity of $3095 \Omega\text{m}$. The main classes are represented in **Fig. 34**.

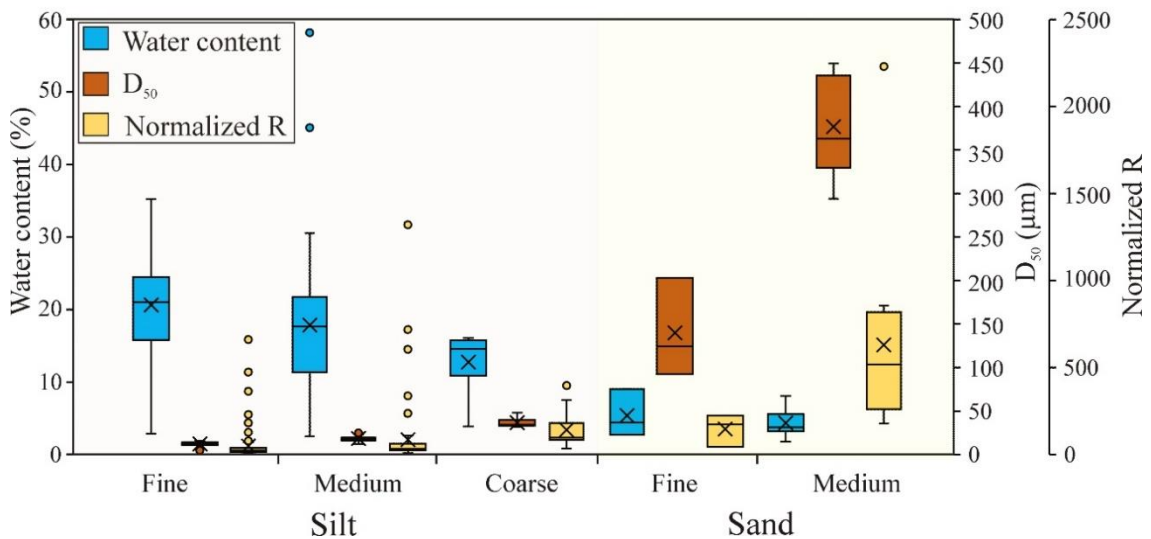


Fig. 34 Classification of the materials of the investigated Tisza and Maros levees regarding the grainsize and their related water content and normalised resistivity.

Nevertheless, as water content showed much greater variability, and still, the effect of grain size could be recognized, it is possible to detect general compositional changes along the investigated levee systems as water content showed a considerable variation in the profiles.

The mentioned resistivity values of Tisza levee materials indicate that the levee is built up from fine-grain sediments based on the low values given for alluvial materials by former researchers (Keller & Frischknecht, 1966; Waxman et al., 1968; Abu-Hassanein et al., 1996; Giao et al., 2003; Loke, 2004; Tabbagh et al., 2007; Sheishah et al., 2023). Also, the values of the levee body core are close to or even lower than those reported by Busato et al. (2016), who found that in an earthen levee composed mainly of clayey sand and having low moisture conditions, resistivity values ranged between 50–100 Ωm . Similarly, fine-grained materials in a dam structure had a specific resistivity below 100 Ωm (Himi et al., 2018; Jodry et al., 2019). Schwartz et al. 2008 and Kalinski and Kelly 1993 estimated 2D field-scale soil moisture distribution utilizing time-series data of 1D TDR soil moisture and 2D electrical resistivity imaging (ERI) in a heterogeneous setting. They proposed a relationship between resistivity and fine-grained sediments. Datsios et al. (2017) measured the electrical resistivity of sand, and it showed a value of 1350 Ωm or more in dry soil. This value can be matched with the resistivity of the sandy layer (with a resistivity up to 2200 Ωm) detected on the protected side of the Maros levee.

As was shown previously by several authors, the physical properties of the sediment, such as grain size, porosity, and water content, can greatly affect specific resistivity values (Popescu et al., 2016; Alpaslan & Bayram, 2020).

There is a link between electrical resistivity values and porosity as the soil compaction process increases bulk density, reduces the volume of large pores and, in turn, affects the physical properties of the soils as stated by (Robain et al., 1996; Alakukku 1996; Richard et al., 2001; Pereira et al., 2007). A normal relationship is proposed between resistivity and coarse-grained materials (Keller & Frischknecht, 1966). Therefore, it is realized that besides the compaction parameter mentioned above, the lower porosity percentage is one of the essential factors behind the noticed lower resistivity values measured on the Tisza levee section. In contrast to the Tisza levee section, the higher resistivity values regarding the Maros levee might be due to the higher porosity percentage related to its coarse-grained composition. Sediments with higher water content normally show lower resistivity values (Loke, 2004). Soil compaction of the levee materials is mainly characterized by increased soil bulk density and reduced macroporosity. Therefore, compacted soils should have lower electrical resistivity values (Zhu et al., 2007). The dry density influences the resistivity of fine-grained soil (Beck et al., 2011). It is also a promising tool for identifying structural differences due to soil compaction (García-tomillo et al., 2018; Jerabek et al., 2017).

ERT results, confirmed by sedimentological data, showed that the core of the two investigated levee sections was different in the sense that the levee along the Tisza is composed of fine silt, while the levee along the Maros of medium silt and of fine and medium silt. From flood safety, the dominance of fine silt is advantageous, as it is highly aquitard based on hydraulic conductivity measurements.

Regarding the structure of the Tisza levee, the core is composed of fine silt, however below the levee body, a medium silt zone can be identified in the northern zone and at some sections in the southern zone of the levee, which can be an area of increased seepage during floods, being undesirable from the aspect of flood safety. Medium silt units were also identified on the riverside, in the form of a thick blanket, on the protected side as part of reinforcement, and even on the crown of some levee sections. On the protected side, applying less impervious materials is accepted to control seepage. However, riverside blankets are supposed to be composed of highly impervious materials to inhibit borrowing (USACE, 2000).

Regarding the levee section investigated along the Maros River, the levee core mainly comprises silty sediments. In more detail, medium silt could be considered the main composition of the levee core; in some sections, fine silt and other sections show alteration layers of fine and medium silt. A fine silt unit was identified on the riverside part of the levee. This layer is important in increasing the imperviousness of the structure; thus, during high water levels, the overlying medium silt layer can transfer water towards the protected side. However, a relatively thin fine silt blanket over the riverside and the levee crown can provide sufficient protection against the development of intensive seepage.

Unlike the Tisza, most of the protected side of the Maros levee section is built up of a sand backfill, covered by a thin fine and medium silt layer. High porosity, sandy layers on the protected side can ease water drainage from the levee body during floods and can be advantageous from the aspect of flood protection. However, as the riverside structure also contains a non-aquitard medium silt layer, the seepage rate can be very intensive and is only moderated by a thin fine silt layer on both sides. Based on the drillings, a fine silt layer is situated below the sandy unit at some sections, though ERT measurements were unable to detect it due to the very high resistivity of coarse-grained sand, which masks nearby lower values.

5.2 Evaluation of levee defects

The majority of authors (Masannat (1980), Borgatti et al. (2017), Di Prinzio et al. (2010), Mazzini and Simoni (2008), and Chlaib et al. (2014)) investigated and analysed animal burrows to evaluate levee of health; however, in the case of our study, the flood phenomena affecting levee health are related to other types of defects in addition to animal burrows. Because one defect is insufficient to capture the current state of the investigated levee, many types of defects must be integrated and analysed concurrently to establish a relationship between flood occurrences and various defects. Tensile cracks were discovered in the investigated levee section along with other sorts of anomalies, and they mostly get closed by wetting the levee body during floods. The larger ones, however, could still be open (Szűcs et al., 2019), which increases the likelihood of damage since leaking through cracks frequently results in piping, which is the primary cause of levee failure occurrences (Huang et al., 2014; Cleary et al., 2015; Antoine et al., (2015)). Several GPR profiles taken on the levee foot correspond with Ritambhara et al. (2021) revealed the presence of paleo-river channels, and a unique reflector feature explained the old banks and the younger sediments that filled these channels. Because it might result in the growth of sand boils on the levee's protected side, , thus increasing flood risk (Nagy, 2000; Ojha et al., 2001; Tímár, 2020). Several GPR profiles taken on the levee crown showed surface deformation. According to Kiss et al. 2021, one of the primary causes of artificial levee height decrease is surface deformation caused by subsidence or uplift.

5.3 Structural assessment by comparing different geophysical data

On the levee's protected side, The structure and composition of the levee itself significantly affect flood risk. Since each approach has benefits and drawbacks regarding penetration depth, resolution, or acquisition time, the results of the methods used were combined to provide a reliable evaluation of the investigated levee section's structure and composition.

It was clear from the combined use of GPR and ERT in the investigated sections of Tisza Levee as well as the drilling-provided control data that the interfaces between the main units could be detected by the two geophysical techniques concerning a representative profile (**Fig. 35a and b**). Even with a 1 m electrode spacing, longitudinal and transverse ERT profiles could only fully identify the top interface at a depth of less than 1 m (**Figs. 35b and c**). On the transversal ERT profile. However, it is possible to detect the layer that, in some places, covers the levees. Meanwhile, the second interface

at around 3 m shows up nearly in the same spot on the ERT and GPR profiles (**Fig. 35d**). The lack of a significant change in water content at this level implies that the combination of approaches can detect even small changes in composition (shift from medium to fine silt).

Each method has demonstrated that there are three main units within the levee body at the location of the representative profile: 1) fine silt, clayey levee core; 2) a medium silt layer designed to increase the height of the structure; and 3) a fine silt blanket on top to prevent seepage (**Fig. 35**). A thin (0.4 m) sand sheet was also found on the protected side as shown in **Fig. 35c**, however, this could only be found using drilling data. ERT could not resolve the sand cover because the vertical resolution was only about 0.5 m, even with a 1 m electrode spacing.

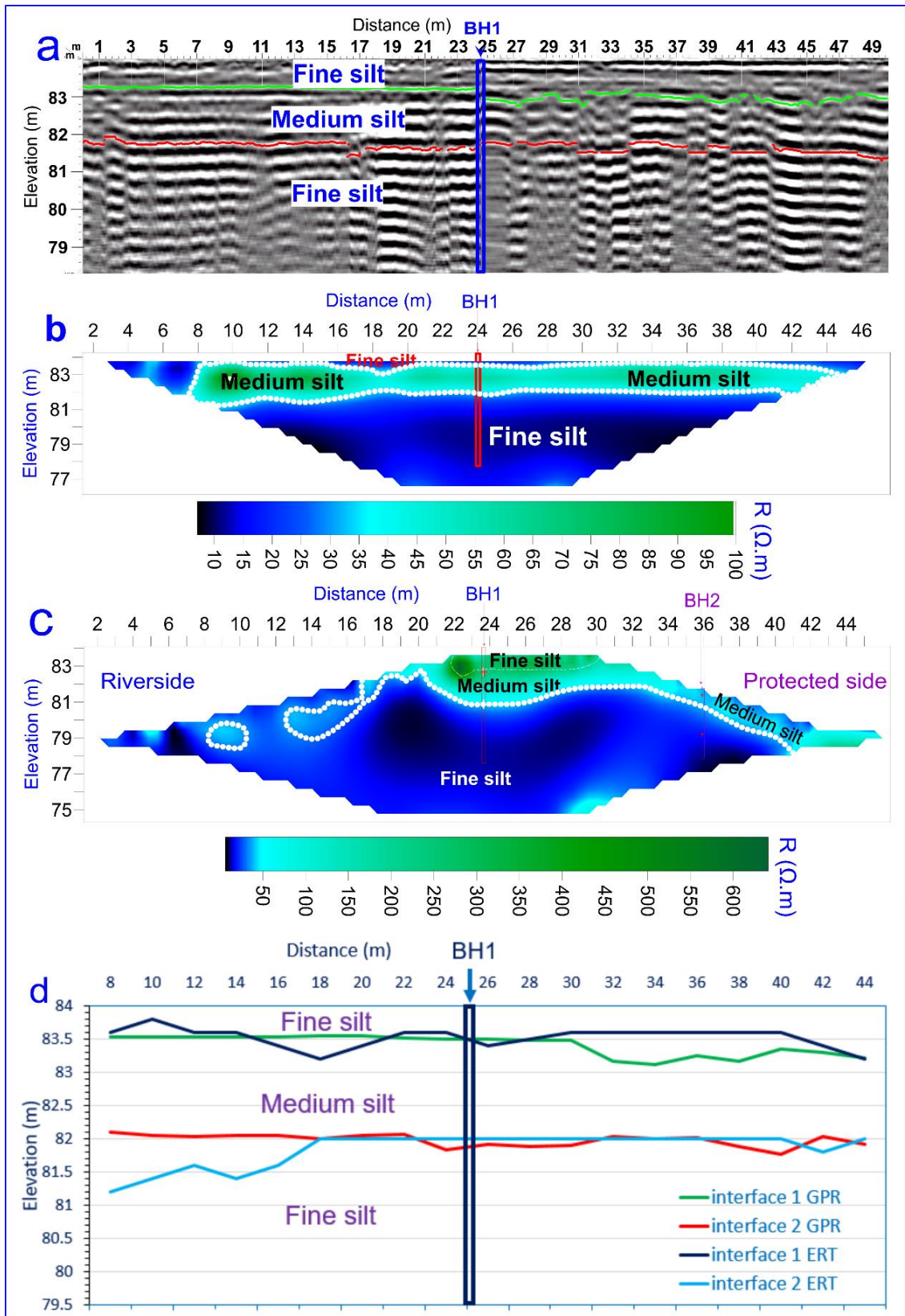


Fig. 35 Combination of a) GPR, b and c) ERT results in the same profile to determine d) the depth of interfaces.

The levee's structure at the investigated profile is advantageous from the perspective of flood safety in that there are fewer layers than those reported elsewhere (Zorkóczy, 1987; Schweitzer, 2001; Szlávik, 2003), making the occurrence of contour seepage along structural interfaces less likely (Szűcs et al., 2019). The ERT profile may also be used to identify a clayey wedge, a crucial structural component in reducing sub-levee seepage at the riverside foot of the levee (USACE 2000, Szűcs et al. 2019). On the other hand, a discontinuity appears in the fine silt blanket at the riverside edge of the levee crown (**Fig. 35c**). The significant gradient of resistivity shift between the levee's top and body makes interpretation still challenging. This attribute may contribute to the observed piping during more intense flood events.

Two interfaces at depths of ~ 1 m and 2 m can be identified at a selected section of the Tisza levee (3.4 km), where two different centre frequency antennas were applied and showed similar results (**Fig. 36**), on the majority of the levees investigated by GPR, the structure of the top layers does not change significantly. Since the GPR data point to a very comparable structure in the upper 4 m of the levee body, the structure identified in the levee body at the ERT profiles can be extended to these sections.



Figure 36 An example of the longitudinal change of structural interfaces along the investigated levee section based on GPR data (a representative section with 3.4 km long of Tisza levee)

5.4 Overall analysis of levee health

Along the investigated Tisza levee section, similar defects were detected by combined use of GPR and GPS, just like in the case of the study provided by Tanajewski and Bakula (2016), but in a 40 km section of the investigated levee. Measuring PSI offered a fast way of detecting surface deformation along the investigated levee, especially when GPS supports it and levelling data; however, GPR and ERT data can also provide better ideas about the levels of healthy sections of the levee.

The combined results of the levelling data from 1976 and GPS data measured in 2017 were spatially fitted to GPR penetration depth data, the distribution of GPR anomalies detected on the levee crown and the dominance of materials forming the levee core identified on ERT profiles. We assessed the risk potential at every km of the investigated levee section by combining the data I obtained. Subsequently, scores of levee health levels were added up, and for each 1 km section, a potential level of levee health value was assigned: scores 4 and 5 meaning very low and low and scores 7 and 8, meaning high and very high risky sections or very high level of levee health potential (**Fig. 37**).

Going from north to south, an increasing trend can be seen in levels of levee health scores (**Fig. 37**). VLLLH and LLLH sections are predominant in most of the northern zone except for one 1km section with an MLLH (at 34-Lkm). In contrast to the northern zone, in the southern zone, mostly MLLH sections from 21 lkm to 18 lkm and HLLH sections from 17 lkm to 14 lkm can be identified, and even very high levels of levee health section (VHLLH) occur (at 13 lkm), while LLLH sections are restricted only to the first part of this zone at (23 Lkm and 22 Lkm). Accordingly, the mean level of levee health score in the southern zone is 6.25, while in the northern zone, it is 4.6, referring to the overall worse condition of the previous section. Consequently, the southern levee zone can be considered more prone to flood phenomena and failure during floods.

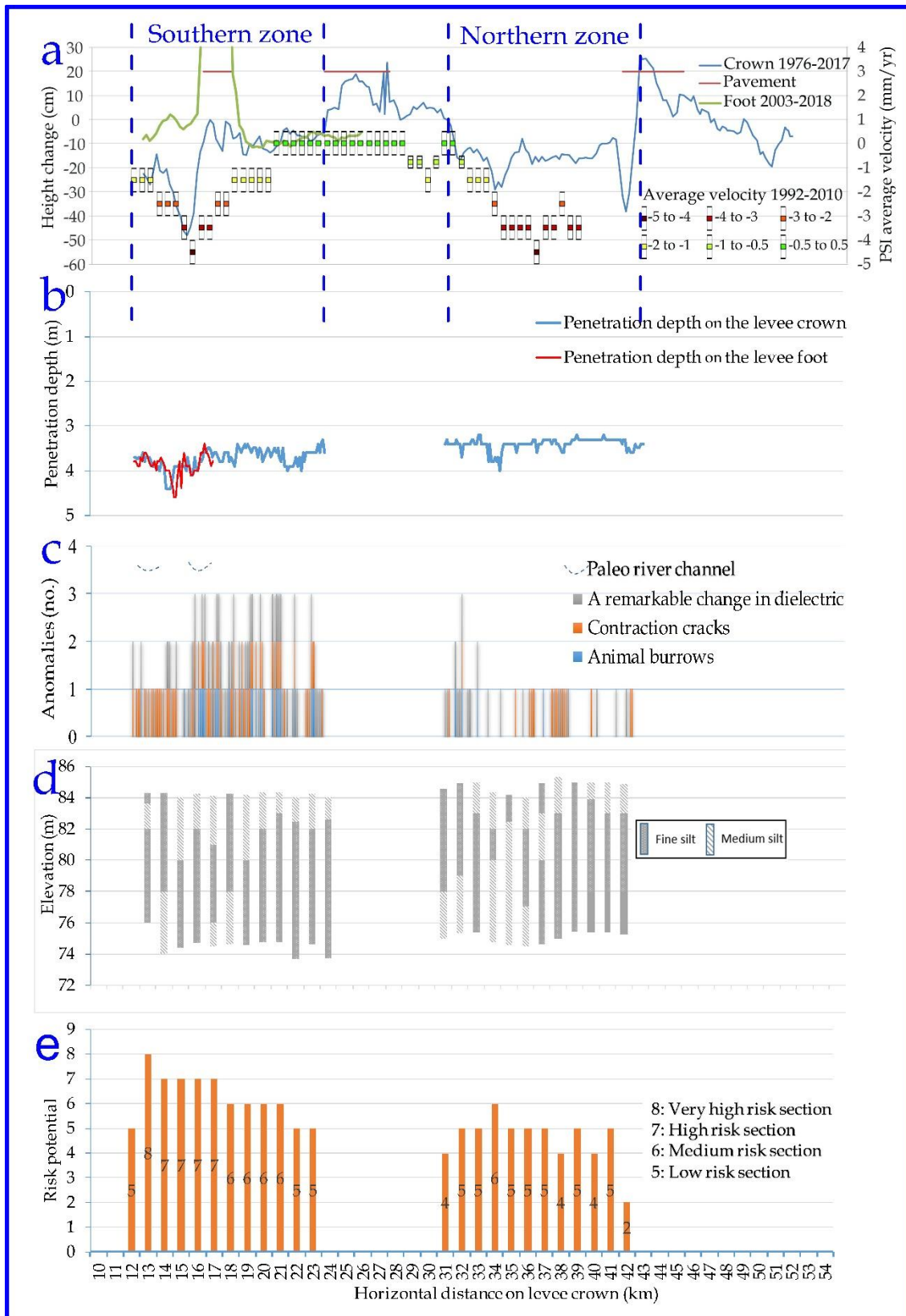


Fig. 37: The spatial distribution of parameters influencing flood risk related to the levee in the study area. A) Moving average of elevation change between 1976-2017, B) Penetration depth of GPR signals, C) types and spatial frequency of anomalies identified on GPR profiles taken on the levee crown, d) dominant materials of the levee core identified on ERT profiles, and e) risk evaluation for each 1 km section of the levee

6. Conclusion

Based on ERT results with a precise analysis of grain size and their related physical parameters (saturated hydraulic conductivity, porosity, density, and water content) used for monitoring the materials of two different levee sections along the Tisza and Maros rivers, it is concluded that the investigated section of the Tisza levee showed low resistivity values, indicating the fine-grained materials' conductivity. In contrast, the investigated section of the Maros levee showed high resistivity values, indicating the resistivity nature of larger grain-size sediments forming this section, especially noticed on the protected side of the levee from the transversal ERT profiles. The main components of investigated Tisza levee section, including the core and both sides, are medium and fine silts. However, the situation of the investigated Maros levee section shows more variation of different materials: fine, medium, coarse silt, and fine, medium, and coarse sand. The materials and their resistivity range are generally similar, forming the core of the Tisza and Maros levees. Regarding the analysis of different physical properties of the two levee systems like resistivity, porosity, density, water content, grain size, and saturated hydraulic conductivity, the materials of the Maros levee could be distinguished well and showed more variation when it is compared to the building materials of Tisza levee.

It is concluded that combining the use of GPS, PSI, ERT, and GPR with data validation obtained from flood phenomena recordings and drilling information is an effective approach to examine the levee condition in terms of flood risk and its flood resistance capacity based on the focused research carried out on the Tisza levee section using several geophysical techniques. Comparison of archive levelling data and GPS measurements, reinforced by PSI surface deformation analysis, allowed the quantification of changes in levee elevation with time. At the same time, GPR was useful for detecting the most frequent anomalies and mapping levee defects. On the other hand, ERT successfully identified the levee materials and classified them in terms of levels of levee health.

Using elevation and surface deformation velocity data, it was found that between 1976 and 2017, the height along the examined levee crown and levee foot significantly decreased. The function of subsidence as a matter of surface deformation is strengthened because different datasets for various periods on various levee areas all point in the same direction. If mass-related sinking and compaction are generally considered, the levee

crown should be more significantly impacted than the levee foot. It is clear from PSI data that regional surface deformation is a major cause of elevation variations along the levee. It is also a serious problem regarding the risk of flooding since it affects the absolute height of the levee locally.

The radar signal penetration depth in most GPR cross-sections was constrained, allowing for detecting anomalies up to three to four metres. Following the categorization of anomalies, the investigated sections could be evaluated in terms of flood risk. Tensile cracks and a remarkable change in dielectric permittivity were the most frequent anomalies among all other identified defects. Changes in dielectric permittivity due to these also indicate compositional diversity, which is crucial for flood safety. The differences in penetration depth caused by the levee material's dielectric characteristics are another indicator of the spatial change in the investigated levee's heterogeneity. Lower clay content was critical in preventing seepage at several sections, particularly in the southern zone, where a considerable change in the penetration depth was noticed. Thus, based on the GPR data, it was found that the health of the southern zone is worse than that of the northern zone.

It was noticed that, among the various flood phenomena recordings since 1970, piping and moderate seepage could be compared to GPR data since they primarily affect the upper part of the levee body and fall within the known GPR penetration depth. Along the investigated levee segment, these have been the flood occurrences that have occurred the most frequently. I discovered that the frequency and spatial distribution of GPR anomalies closely matches flood occurrences, making it feasible to forecast the presence of seepage and piping during floods using GPR scans.

By combining several types of outcomes, high, medium, and low flood risk sections could be recognised from the perspective of the levee condition. Generally, the southern zone received a much higher risk score than the northern zone, meaning the risk of failure during floods is considerably greater here. This information is very important for the maintenance of the levee and can also aid the planning of interventions during flood events.

GPR, ERT and drilling results with different spatial resolutions and penetration depths were compared and combined to assess the structure and composition of a levee section exhibiting various unwanted flood phenomena. From a methodological aspect, GPR can be applied to investigate the upper 3-4 m structures at the usual dimensions and composition of the levees along the Lower Tisza River. The use of low frequency 80 MHz

GPR does not increase penetration depth significantly. In contrast, higher frequency 200 MHz GPR is capable of detecting not only structural interfaces but various defects as well in the upper layers. Concerning ERT, at 1 m electrode spacing, it is possible to capture structural changes. Still, penetration depth covers only the levee body, and no information can be obtained from sub-levee conditions. This requires an increase in spacing. Although water content has a primary role in determining the obtained specific resistivity values, based on the present study, it is still possible to detect structural units composed of slightly different materials.

Considering the above, the optimum measurement strategy for the future is first to perform longitudinal surveys using GPR, by which major changes in levee structure can be detected, and sections for more time-consuming ERT measurements can be easily identified. By determining the specific resistivity range of fine and medium silt among various moisture conditions at the study site using a limited number of boreholes, it is possible later to separate aquitard (clay) and non-aquitard (sand) materials without drilling the levees of the Lower Tisza River.

The increased frequency of seepage and piping at the investigated site can be explained by the primarily silty composition of the levee body. The number of structural units is low, which is advantageous in terms of contour seepage; however, the fine silt/clayey cover on the riverside slope of the structure might not be continuous; therefore, the identified medium silt layer in the upper half at the levee body of some sections can also contribute to increased seeping and piping during floods, to which tensile cracks in the topmost layer of the structure can also contribute. In the meantime, sub-levee conditions, i.e. a coarser sedimentary unit, are also precursors of seepage phenomena.

In all, our investigation proved adequate for evaluating levee health and can be extended to longer sections along the Tisza and other rivers.

7. Acknowledgements

I want to first of all thank Allah for His grace throughout my PhD research. Alhamdulillah.

Undoubtedly, my profound gratitude goes to my supervisor, Dr. Sipos for his patience and guidance during these past four years. You were not just my supervisor, but mentor as well. I cherish all the times we spent on the field together and the pieces of advice to be both a good academic and person. This dissertation is mainly due to your support and direction. I thank all those who played various roles to ensure that I could begin my studies especially my lovely parents and my lovely wife. May Allah continue to brighten your corner wherever you go.

I want to acknowledge the Egyptian missions and the Hungarian Government for granting me the Stipendium Hungaricum Scholarship to undertake my doctoral studies in Hungary. Secondly, I thank all my professors and my colleagues at my home institute in Egypt (NRIAG). May the good Lord continue to brighten your corner wherever you go.

To all the lecturers, staff and colleague PhD researchers of the Department of Geoinformatics, Physical and Environmental Geography of the University of Szeged, I am appreciative of your warm reception throughout my stay in Hungary. You really made me feel welcome, and a part of one big family, not forgetting my lovely colleagues from different nationalities in Szeged. My sincere thanks also go to the students of the department who helped me in the field during measurements. Together, we overcame both the harsh summer heat and the cold winter chills. To all the staff of ATIVIZIG who provided the validation data to make this research a reality, I cannot thank you enough. Your support will never be forgotten. I also thank the support of Geo-Sentinel under the project No. 4000119892/17/I-NB. I also thank the additional support for GPR measurements that was provided by Roden Ltd. under project 2018-1.1.2-KFI-2018-00029, funded by the National Research, Development and Innovation Fund, Hungary. My thanks go to Gyula Grenczy for his help in PSI data. My sincere thanks also go to Dávid Gergely Páll and Sándor Kovács for their contribution during GPR data acquisition, and Gergő Gál for his help during GPS data collection. I acknowledge Szabolcs Gáti for his contribution to ERT measurements. I thank Dávid Filyó and Gergő Magyar for their immense help during drilling. I also thank Istvan Fekete for his assistance in measuring the laboratory samples. Especial thankfulness goes to professor Károly Barta for his guidance in borehole sample analysis.

8. References

- Abu-Hassanein Z. S., C. H. Benson, and L. R. Blotz, 1996. "Electrical resistivity of compacted clays," *Journal of Geotechnical Engineering - ASCE*, vol. 122, pp. 397-406. [https://doi.org/10.1061/\(ASCE\)0733-9410\(1996\)122:5\(397\)](https://doi.org/10.1061/(ASCE)0733-9410(1996)122:5(397))
- Amissah, G. J., Kiss, T., & Fiala, K. (2018). Morphological evolution of the Lower Tisza River (Hungary) in the 20th century in response to human interventions. *Water (Switzerland)*, 10 (7), 14–19.
- Annan, A.P., 1996, Transmission dispersion and GPR. *JEEG*, Vol. 0, January 1996, pp. 125–136. <https://doi.org/10.4133/JEEG1.B.125>.
- Antoine, R., Fauchard, C., Fargier, Y., & Durand, E. (2015). Detection of leakage areas in an earth embankment from GPR measurements and permeability logging. *International Journal of Geophysics*, 2015. <https://doi.org/10.1155/2015/610172>.
- Alpaslan, N., & Bayram, M., 2020. *Landslide study with 2D electrical resistivity tomography (ERT): A case study from Turkey*. *Carpathian Journal of Earth and Environmental Sciences*, 15(2), 391–403. <https://doi.org/10.26471/cjees/2020/015/139>
- Alakukku, L., 1996. Persistence of soil compaction due to high axle load traffic. I. Short-term effects on the properties of clay and organic soils. *European Journal of Soil Science*, 37, 211–222. [https://doi.org/10.1016/0167-1987\(96\)01017-3](https://doi.org/10.1016/0167-1987(96)01017-3)
- Asch, T.H., Deszcz-Pan, M., Burton, B.L., Ball, L.B., 2008. *Geophysical characterisation of American River levees, Sacramento, California, using electromagnetics, capacitively coupled resistivity, and dc resistivity*. USGS Open File Report (2008-1109, 12 pp). <https://pubs.usgs.gov/of/2008/1109/index.html>
- Bakula, K., Salach, A., Wziątek, D.Z., Ostrowski, W., Górski, K., Kurczyński, Z., 2017. *Evaluation of the accuracy of lidar data acquired using a UAS for levee monitoring: preliminary results*. *Int. J. Remote Sens.* 38 (8–10), 2921–2937. <https://doi.org/10.1080/01431161.2016.1277044>
- Beck, Y.L., Lopes, S. P., Ferber, V., and Côte, P., 2011. Microstructural Interpretation of Water Content and Dry Density Influence on the DC-Electrical Resistivity of a Fine-Grained Soil. *Geotechnical Testing Journal*, 34(6):694–707. <https://doi.org/10.1520/GTJ103763>
- Bittelli, M., Salvatorelli, F., Rossi Pisa, P., 2008. Correction of TDR-based soil water content measurements in conductive soils. *Geoderma* 143, 133–142. <https://doi.org/10.1016/j.geoderma.2007.10.022>
- Boga, L., & Nováky, B. (1986). Magyarország vizeinek műszaki-hidrológiai jellemzése. A felszíni vízkészlet mutatói: Maros. Vízgazdálkodási Intézet, Budapest, 32
- Borgatti, L., Forte, E., Mocnik, A., Zambrini, R., Cervi, F., Martinucci, D., Zamariolo, A. (2017). Detection and characterization of animal burrows within river embankments utilizing coupled remote sensing and geophysical techniques: Lessons from River Panaro (northern Italy). *Engineering Geology*, 226(March), 277–289. <https://doi.org/10.1016/j.enggeo.2017.06.017>
- Borsos, B., & Sendzimir, J. (2018). The Tisza River: Managing a Lowland River in the Carpathian Basin. *Riverine Ecosystem Management*, 541–560. https://doi.org/10.1007/978-3-319-73250-3_28
- Busato, L., Boga, J., Peruzzo, L., Himi, M., Cola, S., Bersan, S., & Cassiani, G. (2016). Combined geophysical surveys for the characterization of a reconstructed river embankment. *Engineering Geology*, 211, 74–84. <https://doi.org/10.1016/j.enggeo.2016.06.023>

- Chakraborty, S., Mukhopadhyay, S., 2019. Assessing flood risk using analytical hierarchy process (AHP) and geographical information system (GIS): application in Coochbehar district of West Bengal, India. *Nat. Hazards* 99, 247–274. <https://doi.org/10.1007/s11069-019-03737-7>.
- Chen, Y., & Alexander, D. (2022). Integrated flood risk assessment of river basins: Application in the Dadu river basin, China. *Journal of Hydrology*, 613(PB), 128456. <https://doi.org/10.1016/j.jhydrol.2022.128456>
- Chen, Y., Liu, R., Barrett, D., Gao, L., Zhou, M., Renzullo, L., Emelyanova, I., 2015. A spatial assessment framework for evaluating flood risk under extreme climates. *Sci. Total Environ.* 538, 512–523.
- Chlaib, H. K., Mahdi, H., Al-Shukri, H., Su, M. M., Catakli, A., & Abd, N. (2014). Using ground-penetrating radar in levee assessment to detect small-scale animal burrows. *Journal of Applied Geophysics*, 103, 121–131. <https://doi.org/10.1016/j.jappgeo.2014.01.011>
- Cleary, P.W., Prakash, M., Mead, S., Lemiale, V., Robinson, G.K., Ye, F., Ouyang, S., Tang, X., 2015. A scenario-based risk framework for determining consequences of different failure modes of earth dams. *Nat. Hazards* 75, 1489–1530. <https://doi.org/10.1007/s11069-014-1379-x>.
- Constable, S.C., Parker, R.L., Constable, C.G., 1987. Occam's inversion: a practical algorithm for generating smooth models from electromagnetic sounding data. *Geophysics* 52, 289–300. <https://doi.org/10.1190/1.1442303>
- Cosenza P., E. Marmet, F. Rejiba, Y. Jun Cui, A. Tabbagh, and Y. 2006. Charlery, "Correlations between geotechnical and electrical data: A case study at Garchy in France," *Journal of Applied Geophysics*, vol. 60, pp. 165-178. <https://doi.org/10.1016/j.jappgeo.2006.02.0030>
- Crawford, M.M., Bryson, L.S., 2018. *Assessment of active landslides using field electrical measurements.* *Eng. Geol.* 233, 146–159. <https://doi.org/10.1016/j.enggeo.2017.11.012>
- Daniels, D.J., 2004. Ground penetrating radar, seconded. Institution of Engineering and Technology. https://books.google.hu/books?hl=en&lr=&id=16PV-fhKasoC&oi=fnd&pg=PR15&ots=u-bFZkV5rj&sig=8WN2SwUH6Z2KpfJhOFya2G5wrDI&redir_esc=y#v=onepage&q&f=false
- Di Prinzio, M., Bittelli, M., Castellarin, A., & Pisa, P. R. (2010). Application of GPR to the monitoring of river embankments. *Journal of Applied Geophysics*, 71(2–3), 53–61. <https://doi.org/10.1016/j.jappgeo.2010.04.002>
- Datsios, Z. G., Mikropoulos, P. N., & Karakousis, I., 2017. *Laboratory characterisation and modelling of DC electrical resistivity of sandy soil with variable water resistivity and content.* *IEEE Transactions on Dielectrics and Electrical Insulation*, 24(5), 3063–3072. <https://doi.org/10.1109/TDEI.2017.006583>.
- De Groot-Hedlin, C., Constable, S., 1990. Occam's inversion to generate smooth, two dimensional models from magnetotelluric data. *Geophysics* 55, 1613–1624. <https://doi.org/10.1190/1.1442813>.
- de Brito, M.M., Evers, M., H"ollermann, B., 2017. Prioritization of flood vulnerability, coping capacity and exposure indicators through the Delphi technique: a case study in Taquari-Antas basin. Brazil. *Int. J. Disaster Risk Reduct.* 24, 119–128. <https://doi.org/10.1016/j.ijdrr.2017.05.027>.
- Dezert, T., Fargier, Y., Palma Lopes, S., & Côte, P., 2019. Geophysical and geotechnical methods for fluvial levee investigation: A review. *Engineering Geology*, 260(March 2018), 105206. <https://doi.org/10.1016/j.enggeo.2019.105206>

- Farzamian Mohammad, Fernando A. Monteiro Santos, Mohamed A. Khalil, 2015. Application of EM38 and ERT methods in estimation of saturated hydraulic conductivity in unsaturated soil. *Journal of Applied Geophysics* 112. 175–189. <https://doi.org/10.1016/j.jappgeo.2014.11.016>
- Fargier, Y., Lopes, S. P., Fauchard, C., François, D., & CÔte, P. (2014). DC-Electrical Resistivity Imaging for embankment dike investigation: A 3D extended normalization approach. *Journal of Applied Geophysics*, 103, 245–256. <https://doi.org/10.1016/j.jappgeo.2014.02.007>
- François, D., Mériaux, P., and Monnet, J. (2016). *Méthodologie de reconnaissance et de diagnostic de l'érosion interne des ouvrages hydrauliques en remblai*. Presses des Ponts: Publications IREX, Paris. OCLC: 966418274.
- Fukue, M., Minatoa, T., Horibe, H. and Taya, N., 1999. The micro-structure of clay given by resistivity measurements. *Eng. Geol.* 54, 43-53.
- Fetter, C. W. (2001). *Properties of aquifers*. Applied hydrogeology, 625p. University of Wisconsin, Oshkosh. https://arjzaidi.files.wordpress.com/2015/09/unimasr-com_e7ce669a880a8c4c70b4214641f93a02.pdf
- Galli L., (1976) *Az árvízvédelmi földművek állékonyságának vizsgálata*. Budapest: Országos Vizügyi Hivatal, available at: https://library.hungaricana.hu/hu/view/VizugyiKonyvek_078/?pg=57&layout=s (in Hungarian)
- Giao, P. H., Chung, S. G., Kim, D. Y., and Tanaka, H. 2003. *Electric imaging and laboratory resistivity testing for geotechnical investigation of Pusan clay deposits*. *Journal of Applied Geophysics*, 52(4):157–175. [https://doi.org/10.1016/S0926-9851\(03\)00002-8](https://doi.org/10.1016/S0926-9851(03)00002-8)
- Goyal, V.C., Gupta, P.K., Seth, P.K. and Singh, V.N., 1996. Estimation of temporal changes in soilmoisture using resistivity method. *Hydro. Proces.* 10, 1147-1154. (14) (PDF) *Electrical resistivity survey in soil science: A review*. Available from: https://www.researchgate.net/publication/222649758_Electrical_resistivity_survey_in_soil_science_A_review [accessed Jul 18 2022].
- GSSI, 2018 RADAN 7 software, accessible at: <https://www.geophysical.com/software>.
- Gupta, S.C. and Hanks, R.J., 1972. Influence of water content on electrical conductivity of the soil. *Soil Sci. Soc. Am. Proc.* 36, 855-857.
- Gábris, Gy, Nador, A., 2007. Long-term fluvial archives in Hungary: response of the Danube and Tisza rivers to tectonic movements and climatic changes during the Quaternary: a review and new synthesis. *Quaternary Science Reviews* 26, 2758e2782. <https://doi.org/10.1016/j.quascirev.2007.06.030>
- García-Tomillo, A., Figueiredo, T.De, Dafonte, J.D., Almeida, A., Paz-González, A., 2018. Effects of machinery trafficking in an agricultural soil assessed by Electrical Resistivity Tomography (ERT). *Open Agric.* 3, 378–385. <https://doi.org/10.1515/opag-2018-0042>
- Grenerczy, Gy., Farkas, P., & Frey, S. (2021). Ground motion map of Hungary (Version v20210322). Zenodo. <https://doi.org/10.5281/zenodo.4625653>.
- Hadzick Z.Z., A.K. Guber, Y.A. Pachepsky, R.L. Hill, 2011. Pedotransfer functions in soil electrical resistivity estimation. *Geoderma* 164. 195–202. <https://doi.org/10.1016/j.geoderma.2011.06.004>
- Hudson, P. F., Middelkoop, H., & Stouthamer, E. (2008). Flood management along the Lower Mississippi and Rhine Rivers (The Netherlands) and the continuum of geomorphic adjustment. *Geomorphology*, 101(1–2), 209–236. <https://doi.org/10.1016/j.geomorph.2008.07.001>

- Himi, M., Casado, I., Sendros, A., Lovera, R., Rivero, L., & Casas, A. (2018). Assessing preferential seepage and monitoring mortar injection through an earthen dam settled over a gypsiferous substrate using combined geophysical methods. *Engineering Geology*, 246(September), 212–221. <https://doi.org/10.1016/j.enggeo.2018.10.002>.
- Hibert, C., Grandjean, G., Bitri, A., Travelletti, J., Malet, J.-P., 2012. *Characterising landslides through geophysical data fusion: example of the La Valette landslide (France)*. *Eng. Geol.* 128, 23–29. <https://doi.org/10.1016/j.enggeo.2011.05.001>
- Huang, W.-C., Weng, M.-C., Chen, R.-K., 2014. Levee failure mechanisms during the extreme rainfall event: a case study in Southern Taiwan. *Nat. Hazards* 70, 1287–1307. <https://doi.org/10.1007/s11069-013-0874-9>.
- Ihrig D. 1973. A magyar vízszabályozás története (The history of Hungarian River Engineering). OVH, Budapest, p. 398. (in Hungarian).
- Inim IJ, Tijani MN, Affiah UE (2018) Experimental assessment of electrical properties of lateritic soils as an alternative non-destructive method for compaction monitoring. *International Journal of Geotechnical Engineering* 12(3): 252-257, DOI: 10.1080/19386362.2016.1270792.
- Ishida, T., Makino, T., 1999. Effects of pH on dielectric relaxation of montmorillonite, allophane, and imogolite suspensions. *J. Colloid Interface Sci.* 212, 152161.
- Jerabek, J., Zúmr, D., Dost'ál, T., 2017. Identifying the plough pan position on cultivated soils by measurements of electrical resistivity and penetration resistance. *Soil Tillage Res.* 174, 231–240. <https://doi.org/10.1016/j.still.2017.07.008>.
- Jodry, C., Palma Lopes, S., Fargier, Y., Sanchez, M., & Côte, P., 2019. 2D-ERT monitoring of soil moisture seasonal behaviour in a river levee: A case study. *Journal of Applied Geophysics*, 167, 140–151. <https://doi.org/10.1016/j.jappgeo.2019.05.008>
- Jol, H. M. (Ed.). (2009). *Ground penetrating radar theory and applications*. elsevier.
- Kalinski, R. J. and Kelly, W. E., 1993. *Estimating water content of soils from electrical resistivity*. *Geotechnical Testing Journal*, 16(3):323–329. DOI: 10.1520/GTJ10053J
- Karl L, Fechner T, Francois, S., and Degrande, G. (2008). Application of surface waves for the geotechnical characterisation of dykes. In: *Near Surface 2008–14th EAGE European meeting of environmental and engineering geophysics*
- Keller, G.V. and Frischknecht F.C., 1966. *Electrical methods in geophysical prospecting*. Pergamon Press Inc., Oxford: pp 517.
- Khalilzad, M. A. Gabr and M. E. Hynes (2014), "Effects of Woody Vegetation on Seepage-Induced Deformation and Related Limit State Analysis of Levees," *International Journal of Geomechanics*, vol. 14, no. 2, pp. 302-312,.
- Khalilzad and M. A. Gabr (2011), "Deformation-Based Limit States for Earth Embankments,," in *Geo-Frontiers Congress*, Dallas, Texas,.
- Khalilzad, M. A. Gabr and M. E. Hynes (2015), "Assessment of Remedial Measures to Reduce Exceedance Probability of Performance Limit States in Embankment Dams," *Computers and Geotechnics*, pp. 213-222.
- Kirch, W. (2008). Pearson's Correlation Coefficient. In: *Encyclopedia of Public Health*. Springer, Dordrecht. https://doi.org/10.1007/978-1-4020-5614-7_2569
- Knox, R. L., Morrison, R. R., & Wohl, E. E. (2022). Identification of artificial levees in the contiguous United States. *Water Resources Research*, 58(4), e2021WR031308. <https://doi.org/10.1029/2021WR031308>
- Kearey, P., Brooks, M., & Hill, I. 2013. *An introduction to geophysical exploration*. John Wiley & Sons. Department of Earth Sciences University of Bristol 281 Pages.

- https://faculty.ksu.edu.sa/sites/default/files/AN_INTRODUCTION_TO_GEOPHYSICAL_EXPLORATION_brooks_0_0.pdf
- Kiss, T., Nagy, J., Fehérvári, I., Amissah, G. J., Fiala, K., & Sipos, G. (2021). Increased flood height driven by local factors on a regulated river with a confined floodplain, Lower Tisza, Hungary. *Geomorphology*, 389, 107858. <https://doi.org/10.1016/j.geomorph.2021.107858>
- Kiss, T., Fiala, K., Gy, Sipos, Szatmári, G., 2019b. Long-term hydrological changes after various river regulation measures: are we responsible for flow extremes *Hydrol. Res.* 50 (2), 417–430. <https://doi.org/10.2166/nh.2019.095>.
- Kiss T., Hernesz P., Sümeghy B., Györgyövícs K., Sipos Gy. 2014: The evolution of the Great Hungarian Plain fluvial system – fluvial processes in a subsiding area from the beginning of the Weichselian. *Quaternary International* 388, 142-155. <https://doi.org/10.1016/j.quaint.2014.05.050>.
- Kiss, T., Hernesz, P., Sipos, Gy, 2012. Meander cores on the floodplain the early Holocene development of the low-floodplain along the Lower Tisza Region, Hungary. *Journal of Environmental Geography* 5, 1-10. <https://doi.org/10.14232/jengeo-2012-43802>
- Kiss, T., Fiala, K., Gy, Sipos, 2008. Altered meander parameters due to river regulation works, Lower Tisza, Hungary. *Geomorphology* 98 (1–2), 96–110.
- Kovács, D. (1979). *Árvízvédelem, folyó-és tószabályozás, víziutak Magyarországon* (Flood control, regulation of rivers and lakes and waterways in Hungary). National Water Management Authority (OVH), Budapest.
- Lyu, H.M., Sun, W.J., Shen, S.L., Arulrajah, A., 2018. Flood risk assessment in metro systems of mega-cities using a GIS-based modeling approach. *Sci. Total Environ.* 626, 1012–1025.
- Lászlóffy, W., 1982. *The Tisza*. Akadémiai Kiadó, Budapest, p. 610 (in Hungarian).
- Lee, B., Oh, S., & Yi, M. J. (2020). Mapping of leakage paths in damaged embankment using modified resistivity array method. *Engineering Geology*, 266(December 2019), 105469. <https://doi.org/10.1016/j.enggeo.2019.105469>
- Levesque, R. (2007). *SPSS programming and data management: A guide for SPSS and SAS users*.
- Loke, M. H., 2004. *Tutorial: 2-D and 3-D Electrical Imaging Surveys*, 2004 Revised Edition. *Tutorial: 2-D and 3-D Electrical Imaging Surveys*, (July), 136.
- Lóczy, D., Kis, É., Schweitzer, F., 2009. Local flood hazards assessed from channel morphometry along the Tisza River in Hungary. *Geomorphology* 113, 200–209. <https://doi.org/10.1016/j.geomorph.2009.03.013>
- LACZAY I. (1975): A Maros szabályozása. In: *A Maros Vízrajzi Atlasza*, VITUKI, Budapest; 20–21.
- McCarter, W.J., 1984. The electrical resistivity characteristics of compacted clays. *Geotech.* 34, 263-267.
- Melo, L. B. B. de, Silva, B. M., Peixoto, D. S., Chiarini, T. P. A., de Oliveira, G. C., & Curi, N. (2021). Effect of compaction on the relationship between electrical resistivity and soil water content in Oxisol. *Soil and Tillage Research*, 208(November 2019). <https://doi.org/10.1016/j.still.2020.104876>
- Mezősi, G. (2022). *Natural Hazards and the Mitigation of their Impacts*. Springer International Publishing AG, Switzerland, p. 260. <https://doi.org/10.1007/978-3-031-07226-0>
- Michot, D., Dorigny, A. and Benderitter, Y., 2000. Mise en évidence par r ésistivité électrique desécoulements préférentiels et de l'assèchement par le maïs d'un calcisol de Beauce irrigué.*C.R.Acad.Sci.*, 332, 29-36. (14) (PDF) Electrical resistivity

- survey in soil science: A review. Available from: <https://www.researchgate.net/publication/222649758> Electrical resistivity survey in soil science A review [accessed Jul 18 2022].
- Masannat, Y.M., 1980. Development of piping erosion conditions in the Benson area, Arizona, U.S.A. Q. J. Eng. Geol. Hydrogeol. 13, 53–61.
- Mazzini, E., Simoni, G., 2008. Relazione Descrittiva: Evento di Piena del 20 maggio 2008 del Torrente Samoggia. Regione Emilia-Romagna — Servizio Tecnico Bacino Reno (in Italian).
- Morelli, G., Francese, R., 2013. *A fast and integrated geophysical imaging system for large-scale levee monitoring*. In: *Symposium on the Application of Geophysics to Engineering and Environmental Problems*, (Denver, Colorado, 17–21 March 2013). Doi: [10.4133/segeep2013-261.1](https://doi.org/10.4133/segeep2013-261.1)
- Nagy, L. (2000): Az árvízvédelmi gátak geotechnikai problémái = Geotechnical problems of levees. *Vízügyi Közlemények*, 82(1), 121–146. (in Hungarian). https://adt.arcanum.com/hu/view/VizugyiKozlemenyek_2000/?pg=0&layout=s
- NAGY, L., TÓTH, S. (2001) - Detailed Technical Report on the collation and analysis of dike breach data with regards to formation process and location factors. Investigation of Extreme Flood Processes & Uncertainty – Additional Partners IMPACT-ADD Contract No.: EVG1-CT-2001-00037
- Ojha C.S.P, Singh V.P., and Adrian D.D. (2001). Influence of Porosity on Piping Models of Levee Failure. *ASCE, Journal of Geotechnical and Geoenvironmental Engineering*, 120 (12), pp. 1071-1074.
- Olhoeft, G. R. (1998). Electrical, magnetic and geometric properties that determine ground penetrating radar performance. In *Proceedings of GPR* (Vol. 98, pp. 177-182).
- Oludayo, I. (2021). Effect of Grain Size Distribution on Field Resistivity Values of Unconsolidated Sediments. 7(1), 12–18.
- OVF 2014. Árvízi kockázati térképezés és stratégiai kockázatkezelési terv készítése (Flood risk mapping and strategic risk management plan), project report of the National Water Directorate Hungary, accessible at: http://www.vizugy.hu/vizstrategia/documents/B91A47EC-E3B8-4D58-A15F-3E522958BEE8/Orszagos_elontes_1e_web.pdf
- Pereira, J.O., Defossez, P. & Richard, G. 2007. Soil susceptibility to compaction as a function of some properties of a silty soil as affected by tillage system. *European Journal of Soil Science*, 58, 34–44. <https://doi.org/10.1111/j.1365-2389.2006.00798.x>
- Perri, M. T., Boaga, J., Bersan, S., Cassiani, G., Cola, S., Deiana, R., Simonini, P., & Patti, S., 2014. River embankment characterisation: The joint use of geophysical and geotechnical techniques. *Journal of Applied Geophysics*, 110, 5–22. <https://doi.org/10.1016/j.jappgeo.2014.08.012>
- Popescu, M., Şerban, R. D., Urdea, P., & Onaca, A. 2016. *Conventional geophysical surveys for landslide investigations: Two case studies from Romania*. *Carpathian Journal of Earth and Environmental Sciences*, 11(1), 281–292.
- Pozdnyakova A. and L. Pozdnyakova, 2002. Electrical fields and soil properties, *Proceedings of 17th World Congress of Soil Science*, Thailand, vol. 14-21, pp. 1558, August 2002.
- Radzicki, K., Gołębiowski, T., Ćwiklik, M., & Stoliński, M. (2021). A new levee control system based on geotechnical and geophysical surveys including active thermal sensing: A case study from Poland. *Engineering Geology*, 293(July). <https://doi.org/10.1016/j.enggeo.2021.106316>

- Rónai, A., 1985. Az Alföld negyedidőszaki földtana (Quaternary Geology of the Great Hungarian Plain). *Geologica Hungarica, Series Geologica* 21 (in Hungarian).
- Rahimi, S., Wood, C. M., Coker, F., Moody, T., Bernhardt-Barry, M., & Mofarraj Kouchaki, B. (2018). The combined use of MASW and resistivity surveys for levee assessment: A case study of the Melvin Price Reach of the Wood River Levee. *Engineering Geology*, 241(May), 11–24. <https://doi.org/10.1016/j.enggeo.2018.05.009>
- Richards, K.S., Reddy, K.R., 2010. New approach to assess piping potential in earth dams and levees. *ASCE NEWS*, 51(6) (pp. A1, A4, A5, and A10).
- Ritambhara K. Upadhyay, Naval Kishore & Mukta Sharma (2021) Delineation and mapping of palaeochannels using remote sensing, geophysical, and sedimentological techniques: A comprehensive approach, *Water Science*, 35:1, 100-108, DOI: 10.1080/23570008.2021.1941691
- Robain, H., Descloitres, M., Ritz, M., and Atangana, Q. Y., 1996. A multiscale electrical survey of a lateritic soil system in the rain forest of Cameroon. *Journal of Applied Geophysics*, 34(4):237–253. [https://doi.org/10.1016/0926-9851\(95\)00023-2](https://doi.org/10.1016/0926-9851(95)00023-2)
- Sandmeier (2016) geophysical software - REFLEXW guide. Introduction to the processing of GPR-data within REFLEXW, 23p. https://www.sandmeier-geo.de/Download/gpr_2d_import_processing.pdf
- Sandmeier geophysical Software, 2016. Reflex v8. <http://www.sandmeier-geo.de/reflexw.html>.
- Schweitzer F. 2002, Pleisztocen. In: Karatson D. (szerk.) Pannon enciklopédia Kertek, Budapest, 130-135. <https://docplayer.hu/1721975-A-magyarorszag-i-folyoszabalyozasok-geomorfologiai-vonatkozasai.html>
- Seed, R.B., Bea, R.G., Abdelmalak, R.I., Athanasopoulos, A.G., Boutwell, G.P., Bray, J.D., Briaud, J.-L., Cheung, C., Cobos-Roa, D., Cohen-Waeber, J., Collins, B.D., Ehrensing, L., Farber, D., Hanemann, M., Harder, L.F., Inkabi, K.S., Kammerer, A.M., Karadeniz, D., Kayen, R.E., Moss, R.E.S., Nicks, J., Nimmala, S., Pestana, J.M., Porter, J., Rhee, K., Riemer, M.F., Roberts, K., Rogers, J.D., Storesund, R., Govindasamy, A.V., Vera-Grünauer, X., Wartman, J.E., Watkins, C.M., Wenk Jr., E., Yim, S.C., 2006. Investigation of the performance of the New Orleans flood protection systems in Hurricane Katrina on August 29, 2005. Volume I: Volume I: Main Text and Executive Summary, Final Report, p. 690. https://digitalcommons.calpoly.edu/cgi/viewcontent.cgi?article=1032&context=ce_n_v_fac
- Sentenac, P., Benes, V., Budinsky, V., Keenan, H., & Baron, R. (2017). Post flooding damage assessment of earth dams and historical reservoirs using non-invasive geophysical techniques. *Journal of Applied Geophysics*, 146, 138–148.
- Szlávik, L. Az Alföld árvízi veszélyeztetettsége (Flood hazard in the Great Hungarian Plain). In *A Víz Zerepe és Jelentősége (Role and Significance of Water in the Great Hungarian Plain)*; Pálfai, J., Ed.; Nagyalföld Alapítvány: Békéscsaba, Hungary, 2000; pp. 64–84. (In Hungarian).
- Szűcs P; Nagy L; Ficsor J; Kovács S; Szlávik L; Tóth F; Keve G; Lovas A; Padányi J; Balatonyi L; Baross K; Sziebert J; Ficzer A; Göncz B; Dobó K (2019) *Árvízvédelmi ismeretek = Flood Protection*, available at: <http://hdl.handle.net/20.500.12944/13490> (in Hungarian).
- Saarenketo, T., 1998. Electrical properties of water in clay and silty soils. *J. Appl. Geophys.* 40, 73–88.

- Samouelian, A. Cousin, I., Tabbagh, A. Bruand, A. and Richard, G. (2005). Electrical resistivity survey in soil science: a review. *Soil and Tillage Research*, vol. 83, pp. 173-193.
- Santamarina, J.C., Klein, K.A., Fam, M.A., 2001. *Soils and Waves: Particulate Materials Behavior, Characterisation and Process Monitoring*. John Wiley and Sons, New York.
- Schweitzer, F. (2001). A magyarországi folyószabályozások geomorfológiai vonatkozásai = Geomorphological aspects of Hungarian river regulation works. *Földrajzi értesítő*, 50(1-4), 63-72. (in Hungarian)
- Seladji, S., Cosenza, P., Tabbagh, A., Ranger, J., & Richard, G. (2010). The effect of compaction on soil electrical resistivity: A laboratory investigation. *European Journal of Soil Science*, 61(6), 1043–1055. <https://doi.org/10.1111/j.1365-2389.2010.01309.x>.
- Siddiqui, F.I and Osman, S.B.A.S (2012). Integrating Geo-Electrical and Geotechnical Data for Soil Characterization *International Journal of Applied Physics and Mathematics*. Vol. 2, pp. 104-106.
- Sheishah, D., Kiss, T., Borza T., Fiala K., Kozák P., Abdelsamei E., Tóth C., Grenczy G., Páll, D. G., & Sipos G. (2023a).. Mapping subsurface defects and surface deformation along the artificial levee of the Lower Tisza River, Hungary. *Natural Hazards journal* 117, 1647–1671 (2023). <https://doi.org/10.1007/s11069-023-05922-1>
- Sheishah, D., Sipos, G., Barta, K., Abdelsamei, E., Hegyi, A., Onaca, A., & Abbas, A. M. (2023b). Comparative evaluation of the material of the artificial levees. *Journal of Environmental Geography*, 16(1–4), 1–10. <https://doi.org/10.14232/jengeo-2023-44452>
- Sheishah, D., Sipos, G., Hegyi, A., Kozák, P., Abdelsamei, E., Tóth, C., Onaca, A., & Páll, D. G. (2022). Assessing the Structure and Composition of Artificial Levees Along the Lower Tisza River (Hungary). *Geographica Pannonica*, 26(3), 258–272. <https://doi.org/10.5937/gp26-39474>
- Smith, S.S., Scullion, T., 1993. Development of ground-penetrating radar equipment for detecting pavement condition for preventive maintenance. Technical Report, Project H-104 A, Strategic Highway Research Program. Natural Resources Defense Council, Washington, DC, USA, p. 177. <https://ui.adsabs.harvard.edu/abs/1993STIN...9511904S/abstract>
- Sudha K., M. Israil, S. Mittal, and J. Rai, 2009."Soil characterisation using electrical resistivity tomography and geotechnical investigations," *Journal of Applied Geophysics*, vol. 67, pp. 74-79.
- Schwartz, B. F., Schreiber, M. E., and Yan, T. 2008. *Quantifying field-scale soil moisture using electrical resistivity imaging*. *Journal of Hydrology*, 362(3):234–246. <https://doi.org/10.1016/j.jhydrol.2008.08.027>
- Schweitzer, F. (2009). Strategy or disaster: Flood prevention related issues and actions in the Tisza River basin. *Hungarian Geographical Bulletin*, 58(1), 3–17.
- Szlávik L. (2003): Az elmúlt másfél évszázad jelentősebb Tisza-völgyi árvizei és az árvízvédelem szakaszos fejlesztése. = Significant floods of the Tisza in the last one and a half century and the gradual improvement of flood protection. *Vízügyi Közlemények, Special Issue* (4), 31-43. (in Hungarian)
- Tabbagh, J., Samouëlian, A., Tabbagh, A., and Cousin, I., 2007. *Numerical modelling of direct current electrical resistivity for the characterisation of cracks in soils*. *Journal of Applied Geophysics*, 62(4):313–12 323. <https://doi.org/10.1016/j.jappgeo.2007.01.004>

- Tímár, A. (2020). Árvízvédelmi töltések potenciális veszélyforrásai a Körösök vidékén= Potential Sources of Danger of Flood Protection Dams in the Körös River Area. *HADMÉRNÖK*, 15(1), 107-119. <https://doi.org/10.32567/hm.2020.1.8>
- Tresoldi, G., Arosio, D., Hojat, A., Longoni, L., Papini, M., & Zanzi, L., 2019. Long-term hydrogeophysical monitoring of the internal conditions of river levees. *Engineering Geology*, 259 (August 2018), 105139. <https://doi.org/10.1016/j.enggeo.2019.05.016>
- Tanajewski, D., & Bakula, M. (2016). Application of Ground penetrating radar Surveys and GPS Surveys for Monitoring the Condition of Levees and Dykes. *Acta Geophysica*, 64(4), 1093–1111. <https://doi.org/10.1515/acgeo-2016-0006>.
- Tellman, B., Sullivan, J.A., Kuhn, C., Kettner, A.J., Doyle, C.S., Brakenridge, G.R., Erickson, T.A., Slayback, D.A., 2021. Satellite imaging reveals increased proportion of population exposed to floods. *Nature* 596, 80.
- Tobin, G. A. (1995). The levee love affair: A stormy relationship? *JAWRA Journal of the American Water Resources Association*, 31(3), 359–367. <https://doi.org/10.1111/j.1752-1688.1995.tb04025.x>
- Utsi, E. C. (2017). Ground penetrating radar Theory and Practice. In-Ground penetrating radar Theory and Applications. Butterworth-Heinemann publication Elsevier, 209 p. <https://www.scribd.com/book/345718688/Ground-Penetrating-Radar-Theory-and-Practice>
- USACE – U.S. Army Corps of Engineers (2000). EM 1110-2-1913, Engineering and Design - Design and Construction of Levees. Department of the Army, USACE, Washington, DC. <https://www.yumpu.com/en/document/view/346990/departement-of-the-army-em-1110-2-1913-us-army-corps-of>
- Waxman, M. H., Smits, L. J. M., 1968. *Electrical conductivities in oil-bearing shaly sands*. *Society of Petroleum Engineers Journal*, 8(02):107–122. <https://doi.org/10.2118/1863-A>
- Wohl, E. (2005). Disconnected rivers: Human impacts to rivers in the United States. *Reviews in Engineering Geology*, 16, 19–34.
- Wiscomb, G.W., Messmer, T.A., 2010. Pocket Gophers. Utah State University Extension service and College of Natural Resources 6. https://digitalcommons.usu.edu/cgi/viewcontent.cgi?article=3303&context=wild_facpub
- Wei, X., Gao, C., & Liu, K. (2020). A Review of Cracking Behavior and Mechanism in Clayey Soils Related to Desiccation. *Advances in Civil Engineering*, 2020, 19–27. <https://doi.org/10.1155/2020/8880873>.
- Website 1: <https://education.nationalgeographic.org/resource/burrow>.
- Wohl, E. (2017). Connectivity in rivers. *Progress in Physical Geography*, 41(3), 345–362. <https://doi.org/10.1177/0309133317714972>.
- Willner, S.N., Otto, C., Levermann, A., 2018. Global economic response to river floods.
- Xu, Z., Chen, H., Ren, M., Cheng, T., 2020. Progress on disaster mechanism and risk assessment of urban flood/waterlogging disasters in China. *Adv. Water Sci.* 31, 713–724.
- Yoon G. L. and Park J. B., 2001. "Sensitivity of leachate and fine contents on electrical resistivity variations of sandy soils," *Journal of Hazardous Materials*, vol. 84, pp. 147-161.
- Yu, D., Xie, P., Dong, X.H., Hu, X.N., Liu, J., Li, Y.H., Peng, T., Ma, H.B., Wang, K., Xu, S. J., 2018. Improvement of the SWAT model for event-based flood simulation on a sub-daily timescale. *Hydrol. Earth Syst. Sci.* 22, 5001–5019.

- Zhu, J.J., Kang, H.Z., Gonda, Y., 2007. Application of Wenner configuration to estimate soil water content in pine plantations on sandy land. *Pedosphere* 17, 801–812. [https://doi.org/10.1016/S1002-0160\(07\)60096-4](https://doi.org/10.1016/S1002-0160(07)60096-4).
- Zorkóczy, Z., 1987. *Árvízvédelem = Flood protection*. Budapest: Országos Vízügyi Hivatal (in Hungarian).

9. Abstract

Artificial levees along alluvial rivers are major components of flood risk mitigation. This is especially true in the case of Hungary, where more than one-third of the country is threatened by floods and protected by an over 2940-km-long levee system. Most of the levees were built in the 19th century. Since then, several natural and anthropogenic processes, such as compaction, erosion, Etc., could contribute to these earth structures' slow but steady deformation. Meanwhile, as construction works were scarcely documented, the structure and composition of artificial levees are not well known. Therefore, the present analysis aimed to use different geophysical techniques to validate their efficiency in mapping structural differences, possible compositional deficiencies, potential defects and sections where elevation decrease and compare the compositional and structural variations of two very different levee sections along a 24 km section of the River Tisza and a 24 km section of the River Maros. Investigations were conducted by real-time kinematic GPS (RTK-GPS), Ground penetrating radar (GPR), Electrical Resistivity Tomography (ERT) and drillings. Onsite data acquisition was complemented with an analysis using a Persistent Scatterer Synthetic Aperture Radar (PSI) to assess general surface deformation. The higher frequency 200 MHz GPR data have shown that levee structures can significantly vary even in a few km on sections with the same construction history.

Based on electrical resistivity tomography results with a precise analysis of grain size and their related physical parameters used for monitoring the materials of two different levee sections along the Tisza and Maros rivers, we noticed that the main components of investigated Tisza levee section are medium and fine silts, however, the situation of the investigated Maros levee section shows more variation of different materials which are fine, medium, and coarse silt, moreover, fine, medium, and coarse sand. The investigated section of the Tisza levee showed low resistivity values, indicating the fine-grained materials' conductivity. In contrast, the investigated section of the Maros levee showed high resistivity values, indicating the resistivity nature of higher grain size sediments forming this section, especially noticed on the protected side of the levee.

It was possible to capture structural changes and resolving the thin layers by 1 m electrode spacing ERT profile. In turn, at a larger spacing it was possible to get information on the sedimentary base below the levee body. The selected levee section

could be assessed in terms of its structure and composition and major units within the levee body and their composition could be resolved by the applied methods.

In general, there is a similarity in the materials and their resistivity range which form the core of Tisza and Maros levees, however, the situation on their both sides is not the same. Regarding the analysis of different physical properties of the two levee systems like resistivity, porosity, density, water content, grain size, and saturated hydraulic conductivity, the materials of the Maros levee could be distinguished well and showed more variation when it is compared to the materials of Tisza levee. It means that the physical properties of levee materials are very important, and they are recommended when carrying out further levee investigations.

From the physical properties mentioned above, it was found that some of them show a connection with resistivity except hydraulic conductivity parameter that did not show a direct connection, however the latter could exhibit the aquitard nature of Tisza levee materials and the non-aquitard nature of Maros levee materials which illustrates the difference in levee composition in terms of flood risk or flood safety.

Based on height measurements, the mean elevation of the levee crown decreased by 8 cm in a 40-year time span. However, elevation decrease could reach up to 30 cm at some locations. Sections affected by structural anomalies, compositional changes, and increased surface subsidence are especially sensitive to floods when measurement results are compared to flood phenomena archives.

GPR profiles showed several anomalies, including structural and compositional discontinuities and local features. They were classified into six types regarding to the flood risk; tensile cracks (enables piping, leading to levee breach or mass failure, cracks might close when the levee gets wet), remarkable changes in dielectric permittivity (enables seepage, leading to mass failure), animal burrows (enables piping, leading to levee breach or mass failure), layer deformation (results in height decrease, overtopping), paleo river channel (enables seepage below the levee, leading to water upwelling and the development of sand boils), sudden change in stratification or dipping layers (enables contour line seepage, leading to mass failure). The penetration depth of GPR varied between 3 and 4 m.

The combined results of the levelling data from 1976 and GPS data measured in 2017 were spatially fitted to GPR penetration depth data, the distribution of GPR anomalies detected on the levee crown and the dominance of materials forming the levee core identified on ERT profiles. The risk potential at every km of the investigated levee

section was assessed by combining the results. Subsequently, scores of levee health levels were added up, and for each 1 km section, a potential level of levee health value was assigned. The mean level of levee health score in the southern zone is 6.25, while in the northern zone, it is 4.6, referring to the overall worse condition of the previous section. Consequently, the southern levee zone can be considered more prone to flood phenomena and failure during floods.

The survey approach outlined in the present thesis can be applied extensively along lowland levee systems in the region and elsewhere.

Keywords: Alluvial rivers, Tisza River, Maros River, levee assessment, levee composition, flood risk, surface deformation, Electrical Resistivity Tomography (ERT), Ground penetrating radar (GPR), Elevation change, Persistent Scatterer Synthetic Aperture Radar (PSI), Drillings.

10. Supplements

10.1 Supplement section 1: Rest of the interpreted ERT data measured on Tisza levee

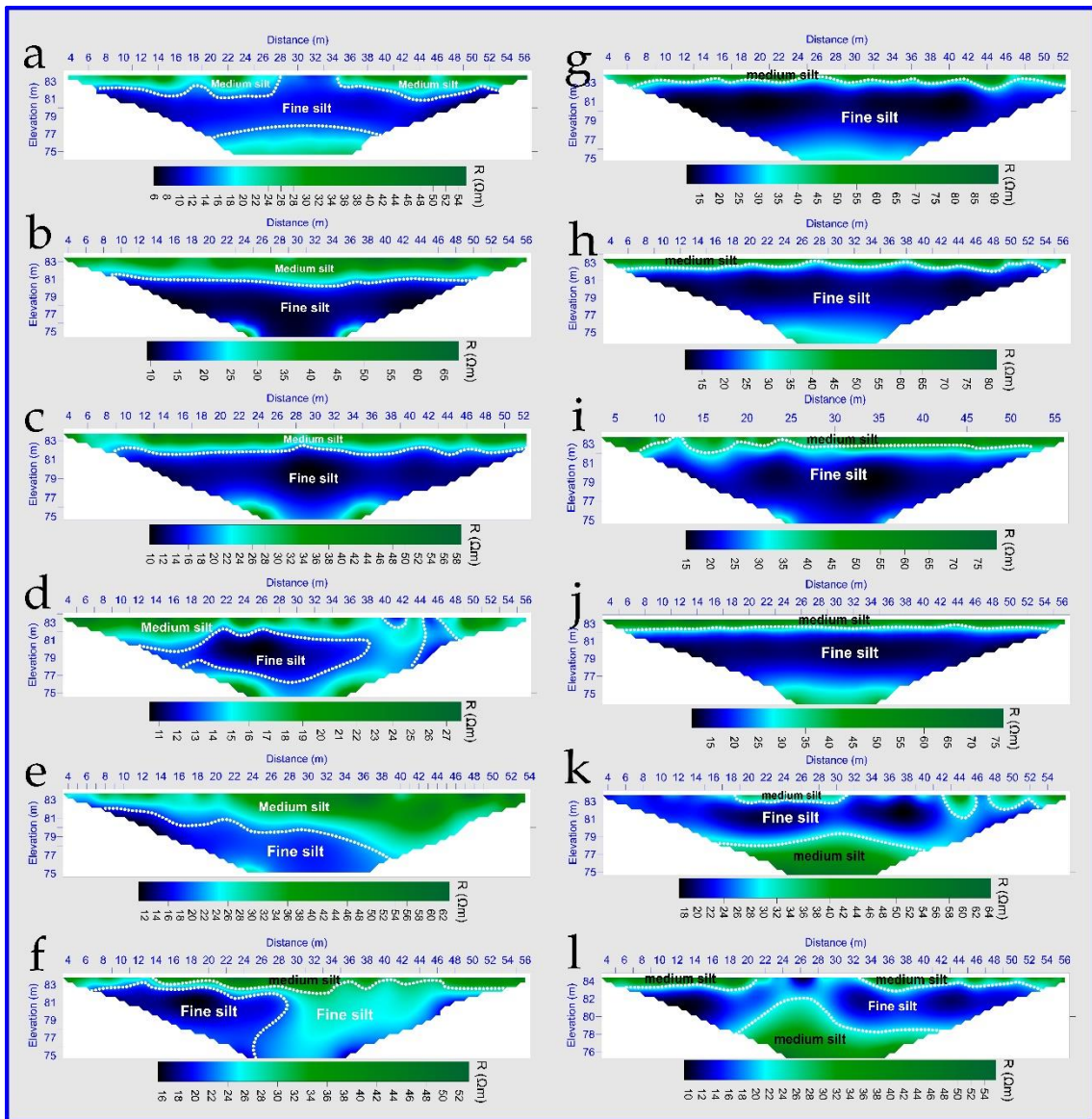


Figure 1 Longitudinal profiles measured along Tisza levee at a) 14 lkm, b) 15 lkm, c) 16 lkm, d) 17 lkm, e) 19 lkm, f) 20 lkm, g) 21 lkm, h) 22 lkm, i) 23 lkm, j) 24 lkm, k) 28 lkm, l) 32 lkm

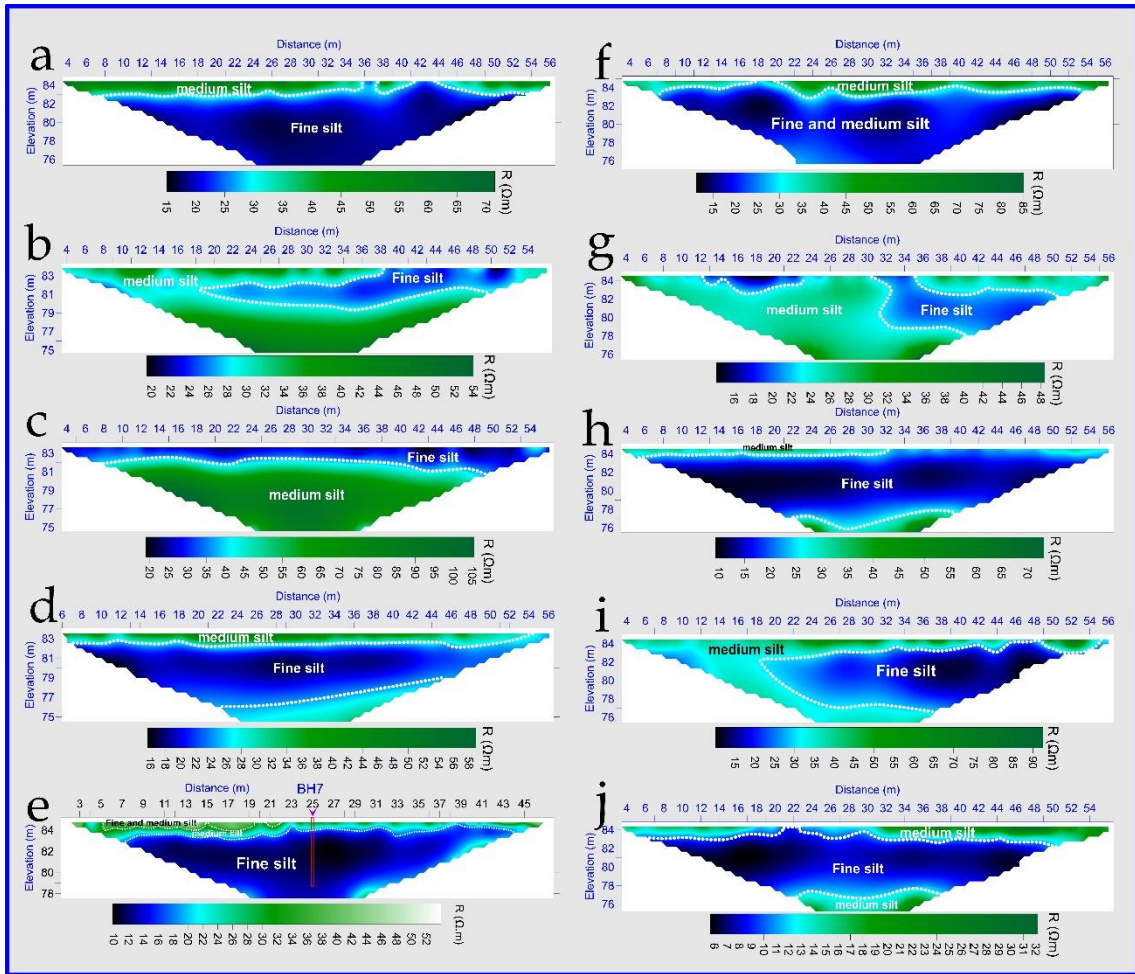


Figure 2 Longitudinal profiles measured along Tisza levee at a) 33 lkm, b) 34 lkm, c) 35 lkm, d) 36 lkm, e) 37 lkm, f) 38 lkm, g) 39 lkm, h) 40 lkm, i) 41 lkm, j) 42 lkm

Grain-size analysis for BH-3 and BH-4

The third borehole (BH-3) drilled on the levee crown of Tisza river at 18.00 lkm, exposed homogeneous composition of fine silt from the surface until the maximum depth reached by the drilling tool (6 m) (**Fig. 3c**) with a D50 value ranging between 10 μm and 14 μm and the average is 12 μm except 0.2 m thin layer of very fine silt at depth between 3.8 m to 4 m which shows a D50 value 6 μm .

The fourth borehole (BH-4), drilled on the levee protected slope of Tisza river at 18.00 lkm, exposed three units (**Fig. 3e**). The first unit contained a fine silt layer (0-3 m) with a mean D50 ranging from 12 μm to 16 μm . The second unit contained a medium silt layer (3 m – 3.8 m) with a mean D50 ranging from 16 μm to 18 μm . The third unit contained a fine silty layer (3.8 m to 4 m) with a mean D50 value 14 μm .

Water content analysis for BH-3 and BH-4

Concerning samples of borehole BH-3 collected at 18.00 lkm of Tisza river, a relative high water content was noticed from the surface until the maximum depth reached by the drilling tool (6 m) with a per cent ranging between 21% and 26%. The higher values indicate almost the total height of the levee at this point was highly saturated with water (**Fig. 3d**).

In case of samples collected from BH-4 drilled on the protected side of Tisza levee at 18.11 lkm, a variation in the water content percentage could be noticed with depth. The topmost layer until a depth of 1.6 m show lower moisture content with an average 14 %, then the water content increased and remained stable from 2 m until 2.4 m with an average 18 %, then a gradual decrease from 2.4 m until 3.2 m with an average percent 12 %, after that the water content increased at 3.6 m and 4 m with an average percent 20.3 %. The fluctuation in water content percentage with depth from low to high then low again was noticed at the same unit consisting of fine silt materials while the higher water content was adjacent to a medium silt unit (**Fig. 3f**).

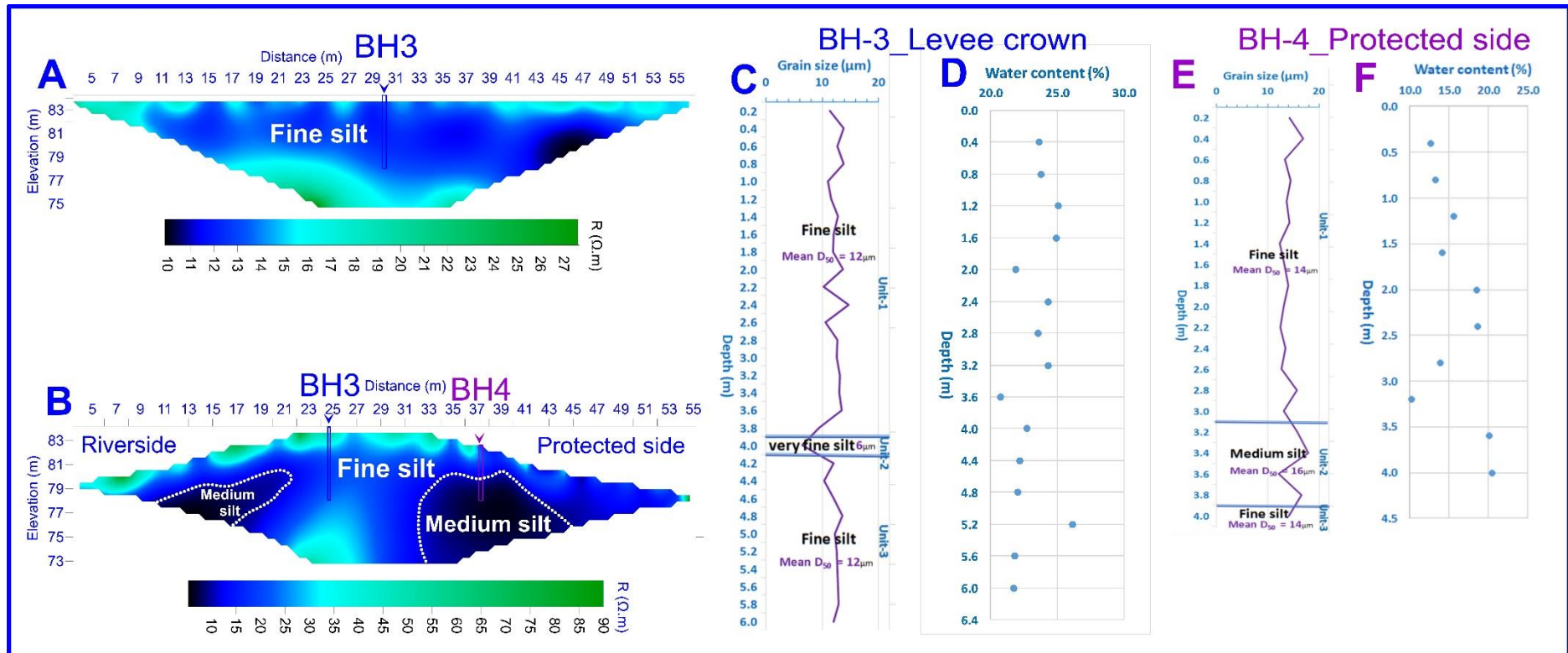


Figure 3 ERT profile measured A) longitudinally on the crown at 18.00 lkm of Tisza levee of length 60 m, B) ERT profile measured Transversely on the levee crown at 18.00 lkm of length 60 m, C) First borehole (BH-3) drilled on the levee crown and mean grainsize D50 values were chosen for layer classification, D) Water content analysis with depth of the first borehole, E) second borehole (BH-4) drilled on the protected side and mean grainsize D50 values were chosen for layer classification, and F) Water content analysis with depth of the second borehole

10.2 Supplement section 2: Rest of the interpreted ERT data measured on Maros levee

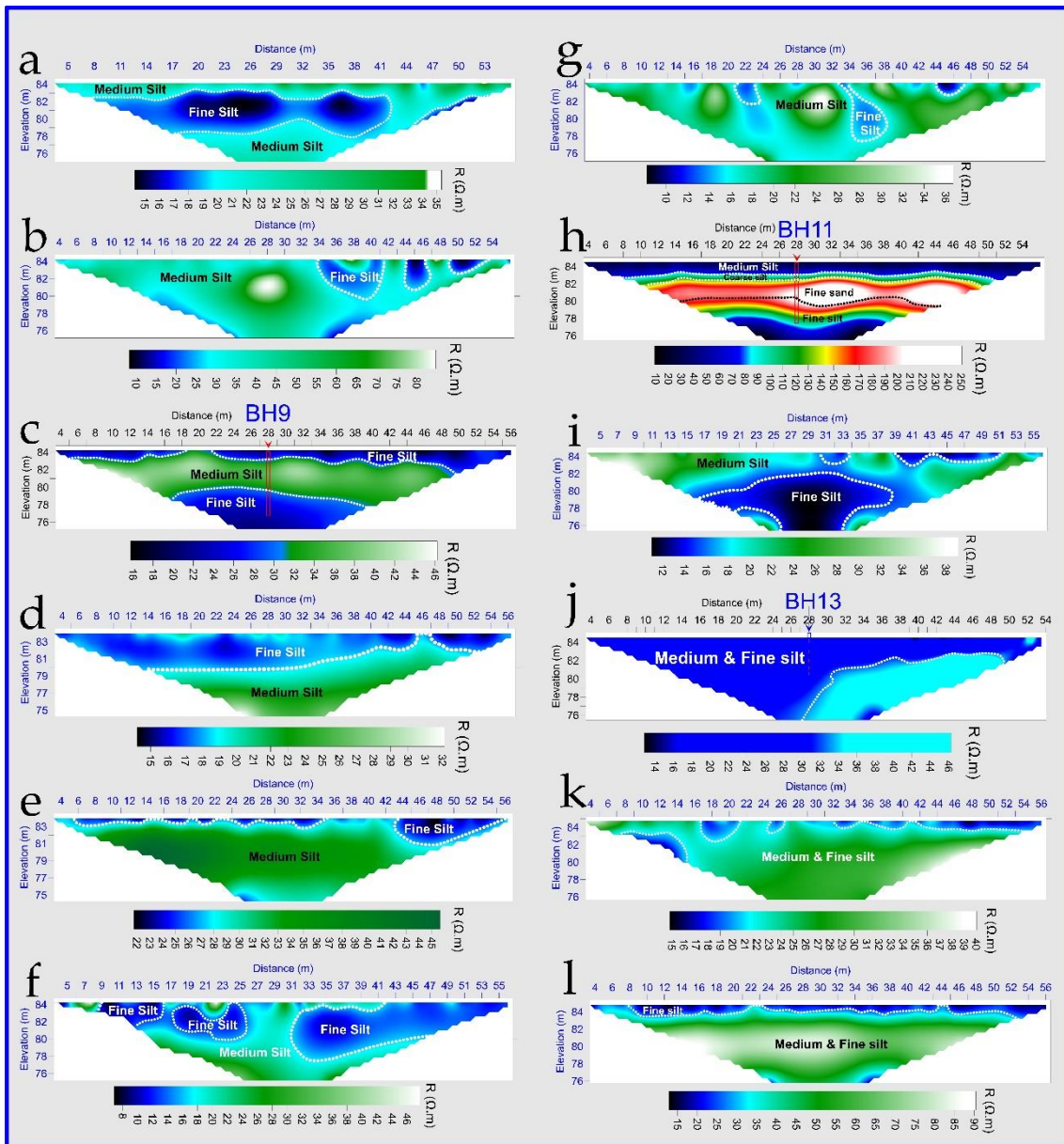


Figure 4 Longitudinal profiles measured along Maros levee at a) 1 lkm, b) 2 lkm, c) 3 lkm, d) 4 lkm, e) 5 lkm, f) 6 lkm, g) 7 lkm, h) 8 lkm, i) 9 lkm, j) 10 lkm, k) 11 lkm, l) 12 lkm

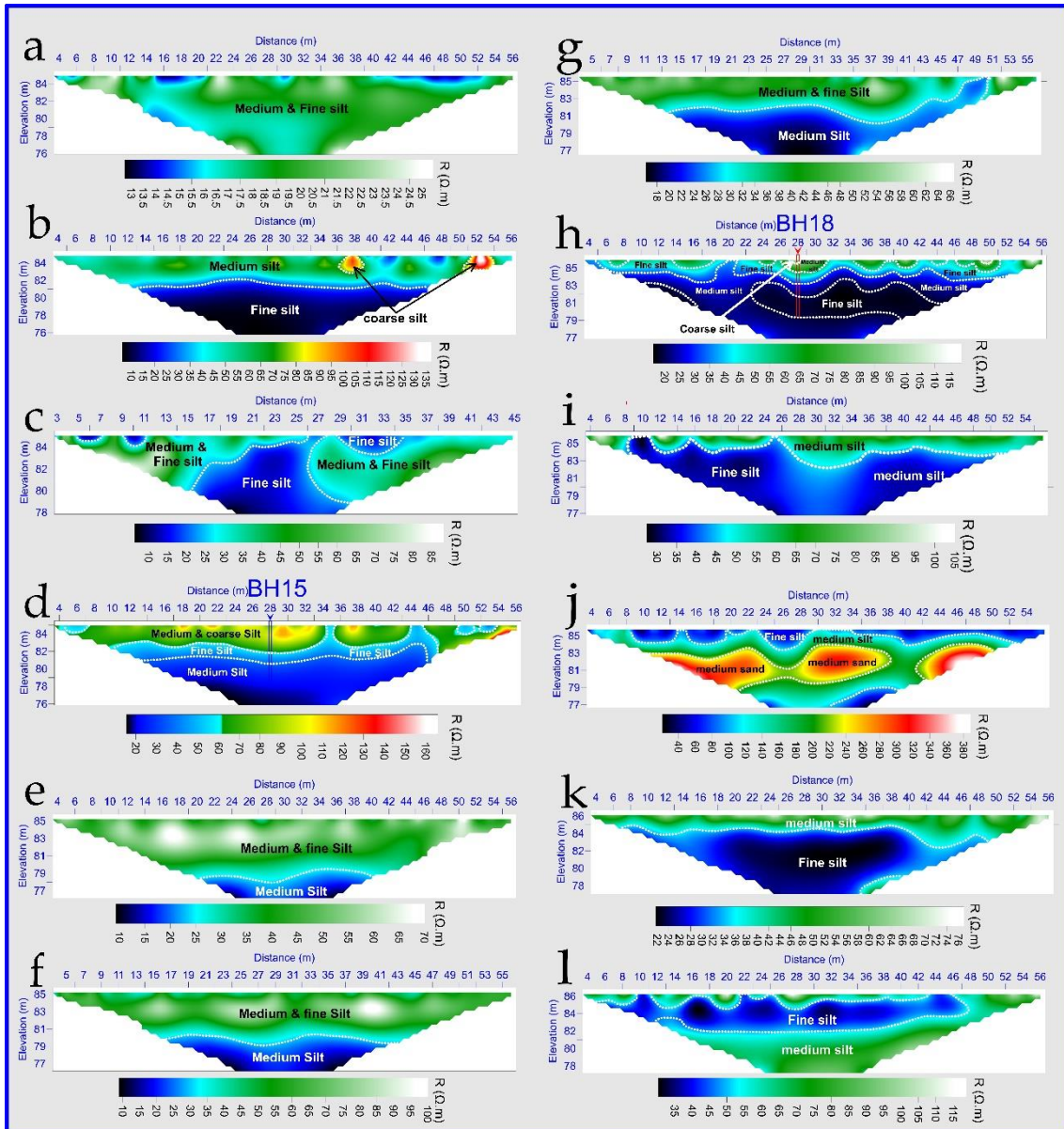


Figure 5 Longitudinal profiles measured along Maros levee at a) 13 lkm, b) 14 lkm, c) 15 lkm, d) 16 lkm, e) 17 lkm, f) 18 lkm, g) 19 lkm, h) 20 lkm, i) 21 lkm, j) 22 lkm, k) 23 lkm, l) 24 lkm

Grain-size analysis for BH-9 and BH-10

The ninth borehole (BH-9), drilled on the levee crown of Maros river at 3.00 lkm, exposed three units (**Fig. 6c**). The first unit contained a fine silty layer (0 - 0.8 m) with a D50 value ranging between 12 and 14 μm , a thick layer of medium silt (1 - 4.4 m) with a D50 value ranging from 16 to 24 μm and a fine silty layer again below 4.4 m with a D50 value ranging between 12 and 15 μm . Unit means grain sizes were 13, 24 and 14 μm , respectively. It was noticed from the second and third units that the grain-size curve reflects sudden changes at some points, but these are not that significant to move the D50 value into another grain-size class. Consequently,

we did not separate further sedimentary units at BH-9. The overall evaluation from BH-9 indicates that the fine-grained sediments are predominant components of the Maros levee body.

The tenth borehole (BH-10) drilled on the protected side of the Maros levee at 3.00 lkm exhibited five units (**Fig. 6e**); a fine silty layer from the surface until a 0.2 m depth with a D50 value of 15 μm , a medium silty layer at depths between 0.2–0.4 m with a D50 value 16 μm , a very fine sandy layer with a D50 value 104 μm , a thick medium sandy layer at depths between 0.6–2.2 m with a D50 value ranging from 292 to 453 μm with a mean grain size value 358 μm and a fine silty layer below 2.2 m with a D50 value ranging between 12 and 13 μm . The five units exhibit an increasing grain-size trend with depth, meaning that the coarse-grained sediments as sandy materials are the main compositions of the protected side of the Maros levee at the investigated section.

Water content analysis for BH-9 and BH-10

The ninth borehole (BH-9) drilled on the levee crown of Maros river at 3.00 lkm can be classified regarding the water content into two units. Each unit exhibits stability of water content percentage with depth (**Fig. 6d**). **The first unit extends from the surface until 4 m and shows a high water content with an average per cent of 21.4 %.** the second unit extends from 4.4 m until the maximum depth reached by the drilling tool (6.8 m) and shows a much higher water content percentage with an average of 30.8%.

The tenth borehole (BH-10) drilled on the protected side of Maros levee at 3.00 lkm (**Fig. 6f**) exhibits low water content values from the surface until a depth of 2 m with a per cent from 2 % to 10 %; however, below a depth of 2 m, higher values could be noticed between 27 % and 33.5 %. This means that the topmost layer was dry and did not affect by rains at the time of sample collection.

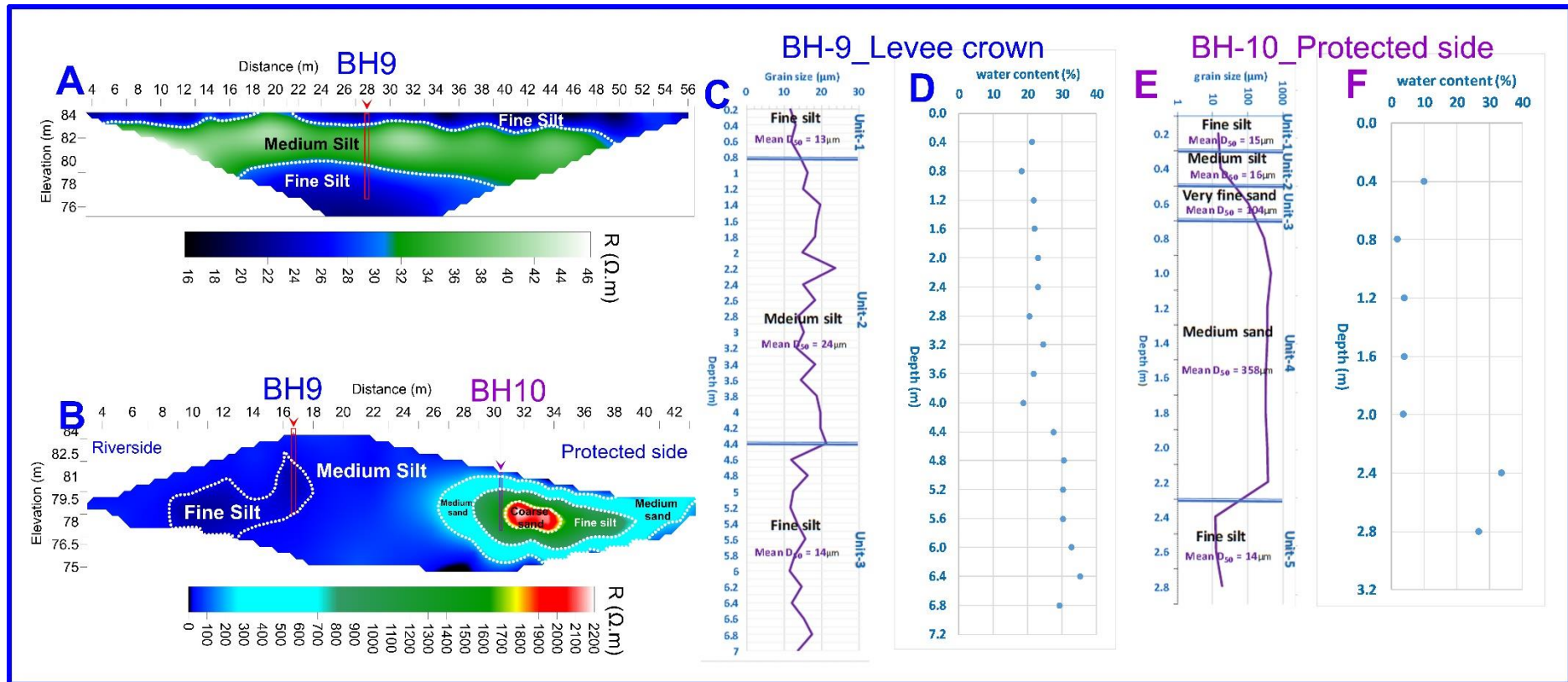


Figure 6 ERT profile measured A) longitudinally on the crown at 03.00 lkm of Maros levee of length 60 m, B) ERT profile measured Transversely on the levee crown at 03.00 lkm of length 48 m, C) First borehole (BH-9) drilled on the levee crown and mean grainsize D50 values were chosen for layer classification, D) Water content analysis with depth of the first borehole, E) second borehole (BH-10) drilled on the protected side and mean grainsize D50 values were chosen for layer classification, and F) Water content analysis with depth of the second borehole

Grain-size analysis for BH-11 and BH-12

The eleventh borehole (BH-11) drilled on the levee crown of Maros river at 8.00 lkm, exhibited four units (**Fig. 7c**). The first unit contains medium silt layer and extends from the surface until 1.4 m depth with a mean D50 value 15 μm . The second unit is formed of coarse silt layer (1.4 m-2 m) with a mean D50 value 31 μm . The third unit consists of fine sand layer at a depth extends from 2 m to 3.8 m with a mean D50 value 91 μm . The fourth unit consists of fine silt layer and extends from 3.8 m until 7 m with a D50 value 12 μm . In the first three units, the grain-size curve reflects sudden changes at some points, but these are not that significant to move the D₅₀ value into another grain size class. Consequently, we did not separate further sedimentary units at BH-11.

The twelveth borehole drilled on the levee protected side slope of Maros river at 8.00 lkm exhibits five units (**Fig. 7e**). The first unit is a very thin layer of fine silt (0 – 0.2 m) with a mean D50 value 14 μm . The second unit consists of a thick layer of medium sand (0.2 m – 2.8 m) with a mean D50 value 365 μm . The third unit is a very thin layer of fine sand (2.8 m – 3.00 m) with a mean D50 value 217 μm . The fourth unit is medium silt layer (3.00 m – 3.6 m) with a mean D50 value 19 μm . The fifth unit consists of fine silt layer with a mean D50 value 12 μm .

Water content analysis for BH-11 and BH-12

The eleventh borehole (BH-11) drilled on the crown of Maros levee at 8.00 lkm exhibits four increasing water content trends with depth. The first trend ranges from 12 % to 24 % at a depth from 0.4 m to 1.2 m. The second trend ranges from 12.6 % to 16.1 % at a depth from 1.6 m to 2.4 m. The third trend ranges from 2.7 % to 12.2 % at a depth from 2.8 m to 4 m. The fourth trend ranges from 24 % to 33.3 % at a depth from 4.4 m until 6.4 m. By comparing the water content data with the adjacent sedimentological units, we found that even the fine sand unit has a higher porosity than the three classifications of silt (fine, medium, and coarse silts), it shows the lowest water content range below 12 % that can be interpreted as the lowest capacity of sand to retain water, while silt materials can retain water in a higher degree (**Fig. 7d**).

The twelveth borehole (BH-12) drilled on the protected side of Maros levee at 8.00 lkm (**Fig. 7f**) exhibits two different units regarding the moisture content. A very dry unit which extends from the surface until 2.8 m with an average water content percent 5 % and a very wet unit which extends from 3.2 m until 4.4 m with an average water content percent 40 %. By

comparing the water content results with the adjacent sedimentological units we can notice the medium sand has a higher porosity than silt classifications, however, its capacity to retain water is very low, therefore we received a very low water content percentage with an average of 5 %. The water content and sedimentological units matching of BH-12 is similar to the case of BH-11.

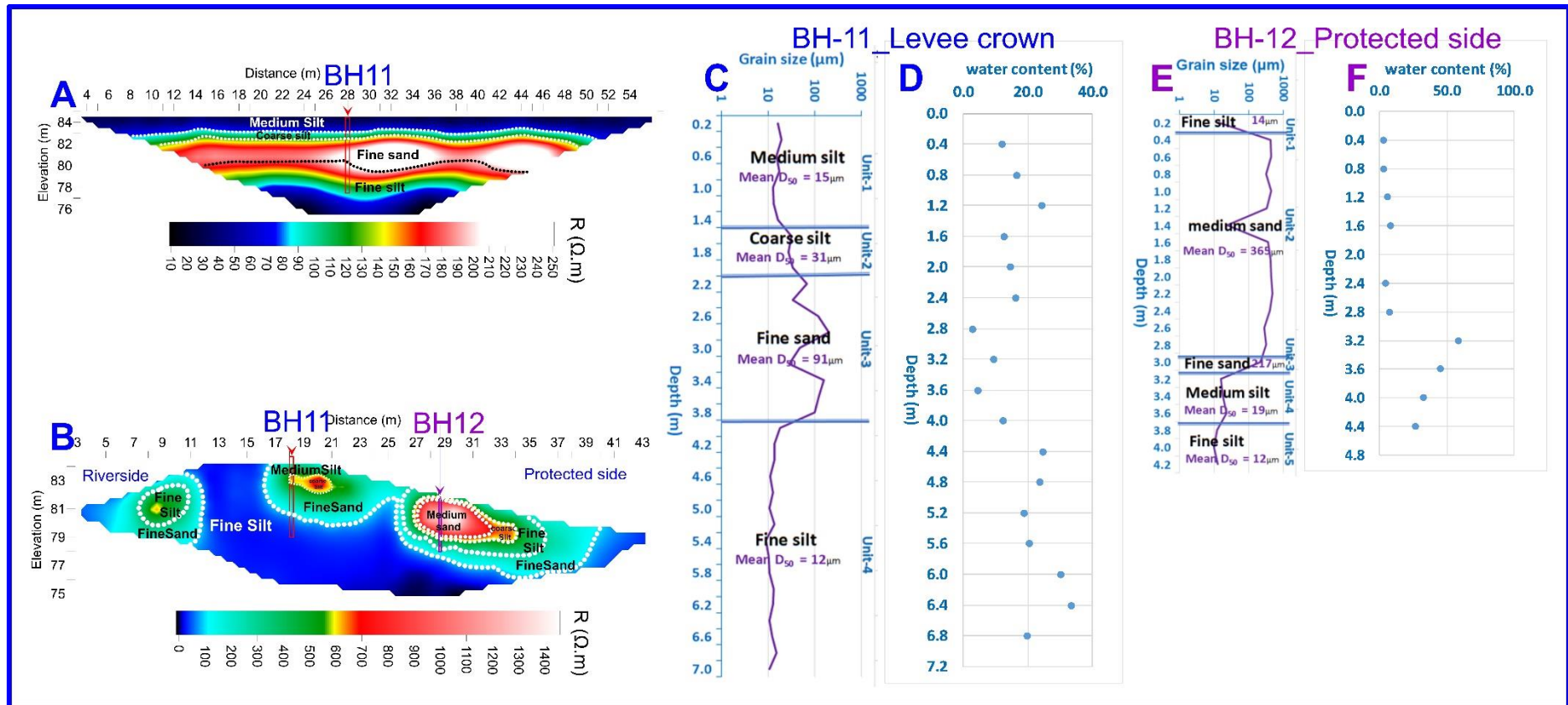


Figure 7 ERT profile measured A) longitudinally on the crown at 08.00 lkm of Maros levee of length 60 m, B) ERT profile measured Transversely on the levee crown at 08.00 lkm of length 48 m, C) First borehole (BH-11) drilled on the levee crown and mean grainsize D50 values were chosen for layer classification, D) Water content analysis with depth of the first borehole, E) second borehole (BH-12) drilled on the protected side and mean grainsize D50 values were chosen for layer classification, and F) Water content analysis with depth of the second borehole

Grain-size analysis for BH-13 and BH-14

The thirteenth borehole (BH-13) drilled on the levee crown of Maros river at 10.00 lkm exhibits seven units and shows a succession of fine grained sediments in the range of fine and medium silts in general (**Fig. 8c**). In more details, the first unit consists of fine silt layer and extends from the surface until 0.8 m depth with a mean D50 value 15 μm . The second unit consists of medium silt layer at depth range from 0.8 m to 2 m with a mean D50 value 19 μm . The third unit is fine silt layer (2 m – 3 m) with a mean D50 16 μm . The fourth unit is a very thin layer of coarse silt and extends from 3 m to 3.2 m with a mean D50 36 μm . The fifth unit consists of a fine silt layer (3.2 m – 3.8 m) with a mean D50 13 μm . The sixth unit consists of a medium silt layer at a depth ranges from 3.8 m to 4.4 m with a mean D50 value 19 μm . The seventh unit is fine silt layer and extends from 4.4 m to 6 m with a mean D50 value 15 μm .

The fourteenth borehole (BH-14) drilled on the levee protected side of Maros river at 10.00 lkm exhibits five units (**Fig. 8e**). Unlike the expected coarse grained materials at the protected side of Maros levee, this borehole shows a fine grained sediments and the units are medium silt, fine silt, medium silt, fine silt, and medium silt with a mean D50 values 20 μm , 14 μm , 31 μm , 15 μm , 20 μm respectively. The depth ranges for these units are 0 – 0.2 m, 0.2 – 1.2 m, 1.2 m – 1.8 m, 1.8 m – 2.6 m, and 2.6 m – 3 m respectively.

Water content analysis BH-13 and BH-14

The thirteenth borehole (BH-13) drilled on the crown of Maros levee at 10.00 lkm exhibits two units regarding the water content percentage (**Fig. 8d**). The first unit extends from the surface until a depth of 2.8 m and shows a high water content percentage with an average percent of 28 %. The second unit extends from 3.2 m to 6 m and exhibits a medium water content percentage with an average percent of 18 %. High and medium water content percentage is related to fine grained sediments forming the levee at the drilling point which are mainly successive units of fine and medium silts.

The fourteenth borehole (BH-14) drilled on the protected side of Maros levee at 10.00 lkm (**Fig. 8f**) exhibits medium water content percentage ranging between 12 % and 22 % with an average percent of 16 %. These values are adjacent to alternate units of fine and medium silts forming the protected side of levee.

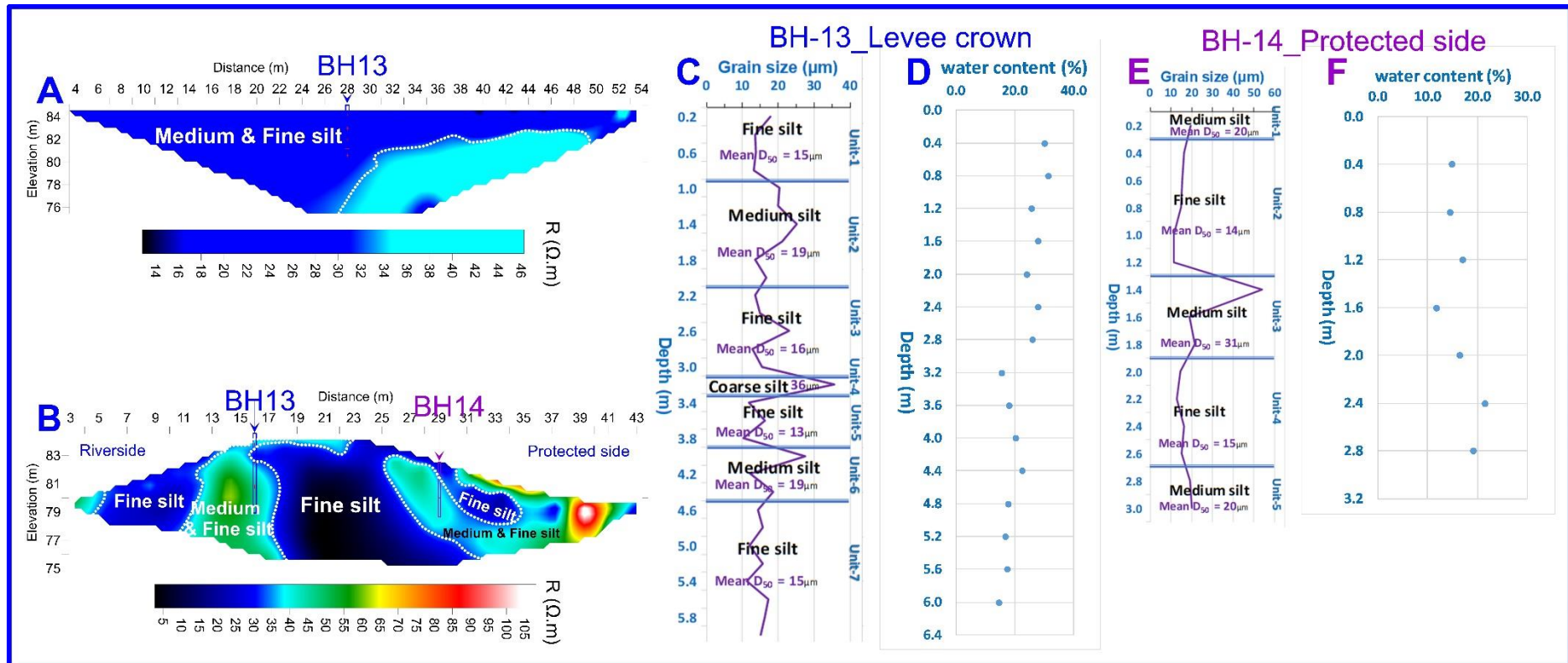


Figure 8 ERT profile measured A) longitudinally on the crown at 10.00 lkm of Maros levee of length 60 m, B) ERT profile measured Transversely on the levee crown at 10.00 lkm of length 48 m, C) First borehole (BH-13) drilled on the levee crown and mean grainsize D50 values were chosen for layer classification, D) Water content analysis with depth of the first borehole, E) second borehole (BH-14) drilled on the protected side and mean grainsize D50 values were chosen for layer classification, and F) Water content analysis with depth of the second borehol

Grain-size analysis for BH-18 and BH-19

The eighteenth borehole (BH-18) drilled on the levee crown of Maros river at 20.00 lkm shows six units (**Fig. 9c**). The first unit consists of a thin layer of medium silt (0-0.2 m) with a mean D50 value 72 μm . The second unit consists of coarse silt layer (0.2 m – 0.8 m) with a mean D50 value 45 μm . The third unit consists of medium silt layer at a depth ranges from 0.8 m to 1.8 m with a mean D50 value 18 μm . The fourth unit is composed of a fine silt layer at a depth ranges from 1.8 m to 3.2 m with a mean D50 value 13 μm . The fifth unit consists of a medium silt layer with a mean D50 value 18 μm . the sixth unit consists of a fine silt layer with a mean D50 value 11 μm .

The nineteenth borehole (BH-19) drilled on the protected side of Maros river at 20.00 lkm exhibits two units (**Fig.9e**). The first unit consists of a thick layer of medium silt and extends from the surface until 2.6 m depth with a mean D50 value 22 μm . The second unit is a fine silt layer at a depth ranges from 2.6 m to 3.00 m with a mean D50 value 11 μm .

Water content analysis for BH-18 and BH-19

The eighteenth borehole (BH-18) drilled on the crown of Maros levee at 20.00 lkm exhibits a gradual increase of water content with depth (**Fig. 9d**). The water content percent ranges from 11.4 % to 30.5 %. The levee composes mainly of alternate units of medium and fine silt from the surface until the maximum depth reached by the drilling tool (6m).

The nineteenth borehole drilled on the protected side of Maros levee at 20.00 lkm exhibits a very low water content percentage. The percent ranges from 2.5 % to 4.8 % with an average of 3.6 %. These values are related to medium and fine silt forming the protected side at the drilling location (**Fig. 9f**).

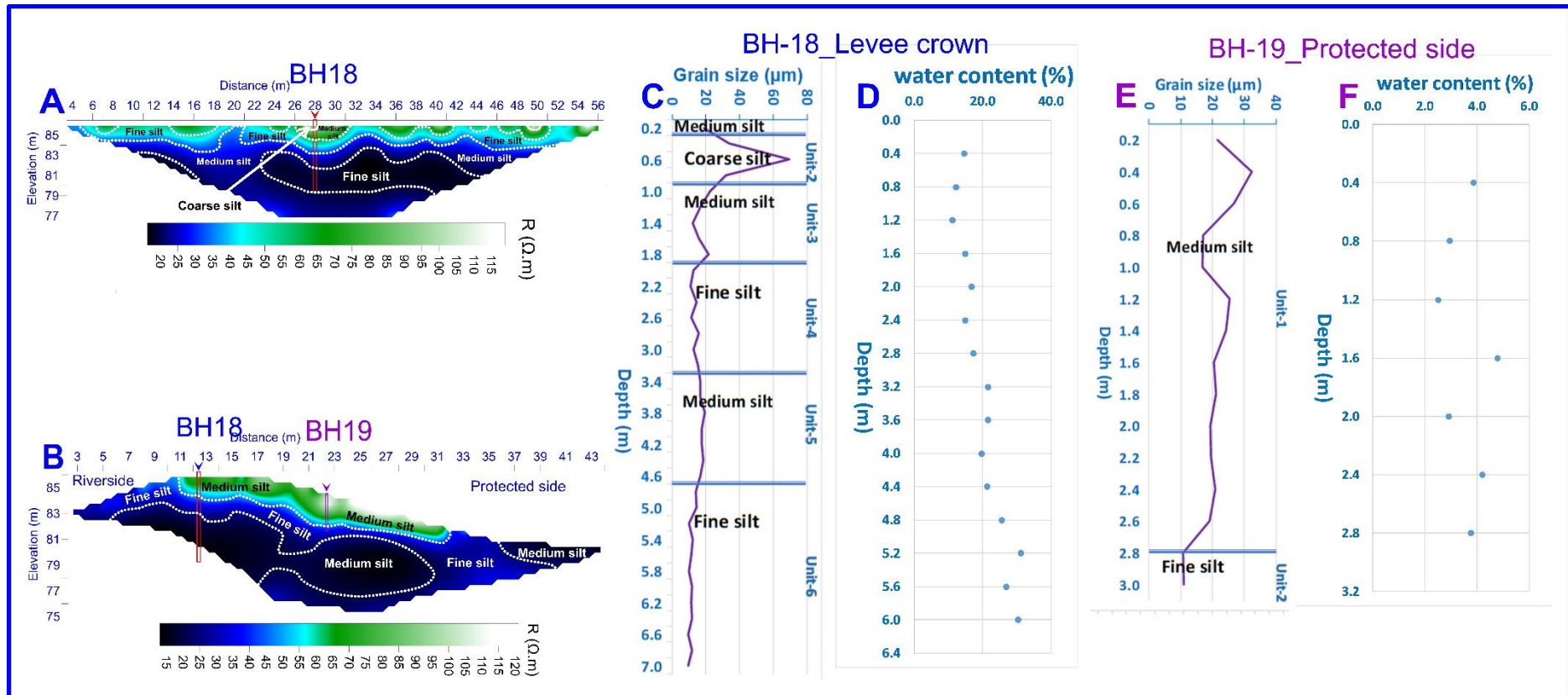
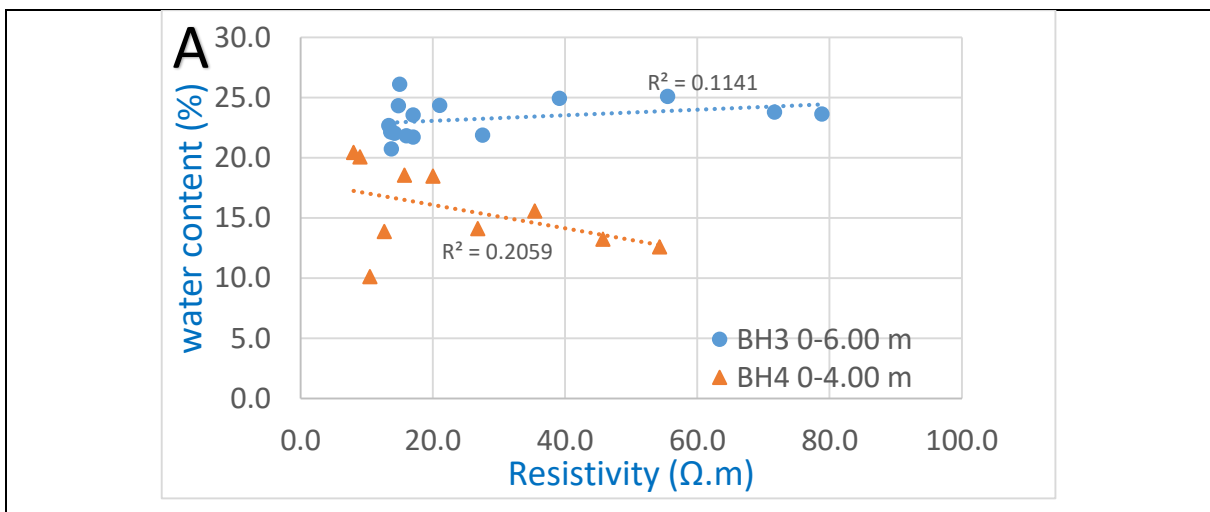


Figure 9 ERT profile measured A) longitudinally on the crown at 20.00 lkm of Maros levee of length 60 m, B) ERT profile measured Transversely on the levee crown at 20.00 lkm of length 48 m, C) First borehole (BH-18) drilled on the levee crown and mean grainsize D50 values were chosen for layer classification, D) Water content analysis with depth of the first borehole, E) second borehole (BH-19) drilled on the protected side and mean grainsize D50 values were chosen for layer classification, and F) Water content analysis with depth of the second borehole

10.3 Supplement section 3: Rest of relationships among physical properties for the other boreholes

Regarding BH-3 and BH-4, all water content and D50 values were plotted against the resistivity for the maximum depth reached by the drillings (6 m in case of BH-3 and 4 m in case of BH-4) and a clear trends could be identified with a weak coefficient of determination. In case of BH-3, an unexpected direct proportional function could be noticed between water content and resistivity because of the homogeneity nature of fine silt forming all the levee body while the expected inverse relationship could be verified in case of BH-4 between the same parameters with a coefficient of determination ($R^2 = 0.2$). Regarding the D50 and resistivity relationships for both BH-3 and BH-4, a direct proportional function could be realized with a weak coefficient of determination $R^2 = 0.06$ and 0.17 respectively. although the weak coefficient of determination between them, the resistivity is still affected by the fine grained composition of levee body and protected side (fine and medium silt) **Fig 10**.



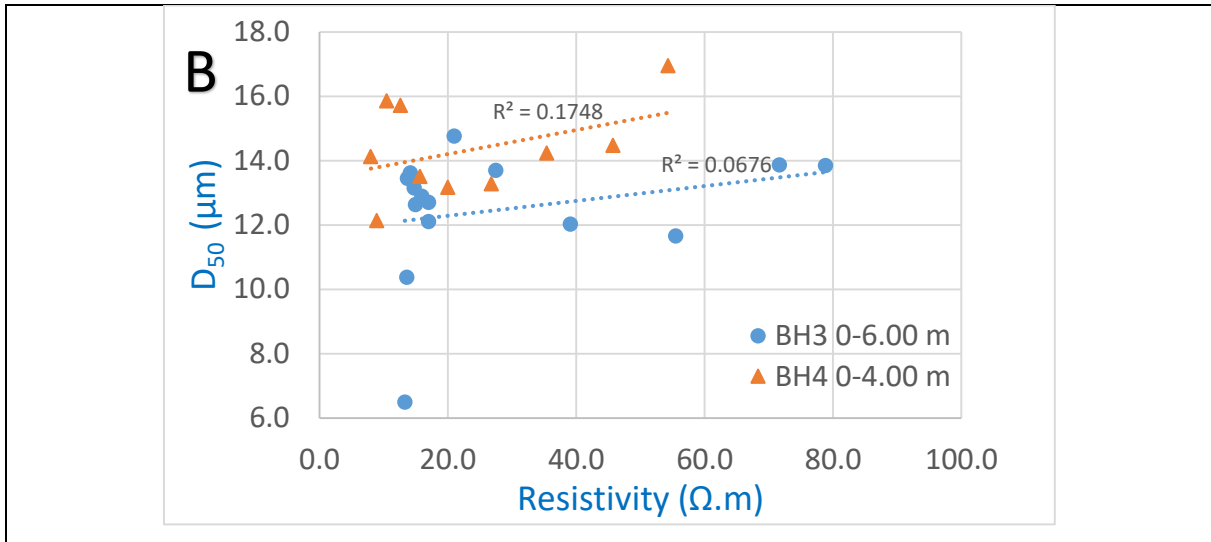
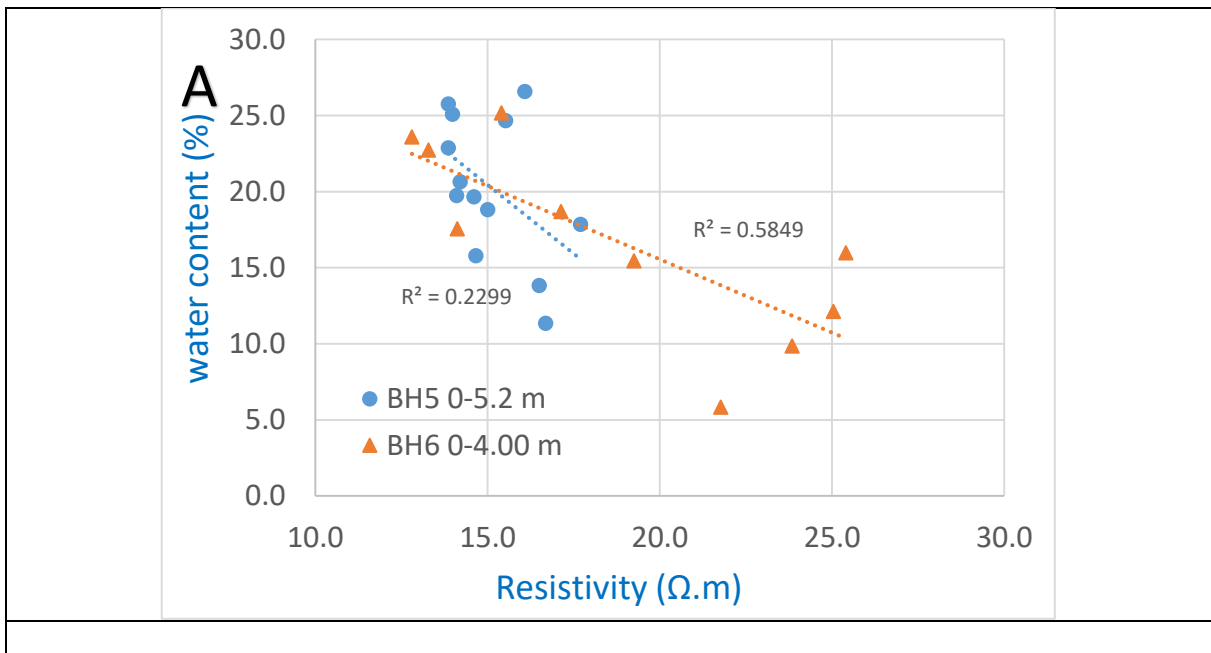


Figure 10 Relationship between A) specific resistivity and water content and B) specific resistivity and grain size in different structural units of the levee body for the boreholes drilled on the levee crown (BH-3) and the protected side (BH-4) at 18.00 lkm of Tisza levee.

In case of BH-5 and BH-6, an inverse proportional function was noticed between water content and resistivity with a coefficient of determination $R^2 = 0.22, 0.58$ for BH-5 and BH6 respectively. It means that the water content had an effect on the resistivity values measured on that levee section. also when the grainsize D50 values were plotted against the resistivity at the same boreholes, we could notice a direct proportional relationship with a coefficient of determination $R^2 = 0.14, 0.35$ which means that the resistivity values are affected by grainsize of the levee materials at this section **Fig 11**.



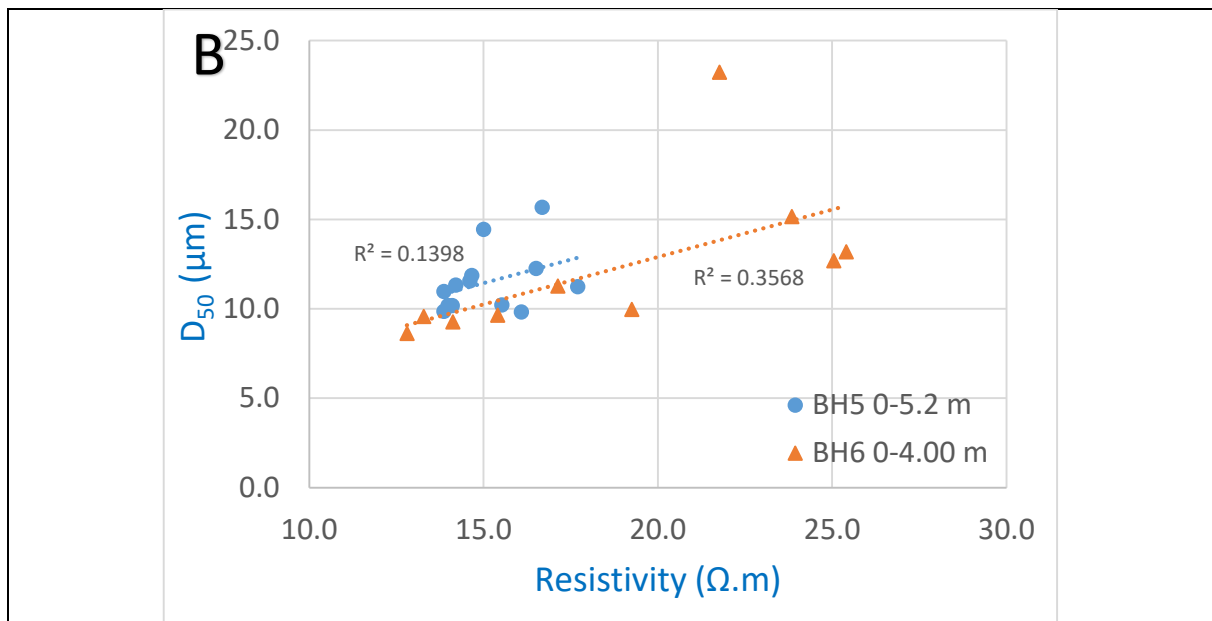


Figure 11 Relationship between A) specific resistivity and water content and B) specific resistivity and grain size in different structural units of the levee body for the boreholes drilled on the levee crown (BH-5) and the protected side (BH-6) at 31.4 lkm of Tisza levee.

Regarding BH-7 and BH-8, no relationships could be noticed when plotting all water content and D_{50} values against resistivity. But, it was realised that by handling the sedimentological units separately, then clear trends can be recognised in the upper half of BH-7 and in the lower half of BH-8 while the rest of the two boreholes could not give the expected relationship between the parameters. In more details, by plotting water content and grain size against resistivity for the upper half of BH-7 (from 0.4 m to 3.2 m), the former exhibited an inverse while the latter exerted a directly proportional function with a coefficient of determination $R^2 = 0.4$ and 0.18 respectively as it is expected. This means that both the mentioned parameters have an effect on the resistivity values and this because of the successive alterations of fine and medium silt at this depth range. The same behaviour of relationships was noticed for the lower half of BH-8 (from 2.8 m to 4 m) in which the coefficient of determination R^2 was 1 for the inverse proportional function of water content and resistivity and 0.83 for the directly proportional function of D_{50} and resistivity. At the same time, rather insignificant and unexpected relationships were seen in the lower half of borehole 7 (from 3.6 m to 6 m) and in the upper half of BH-8 (from 0 to 2.4 m), meaning resistivity stayed the same regardless of changes in water content and grain size (**Fig. 12**).

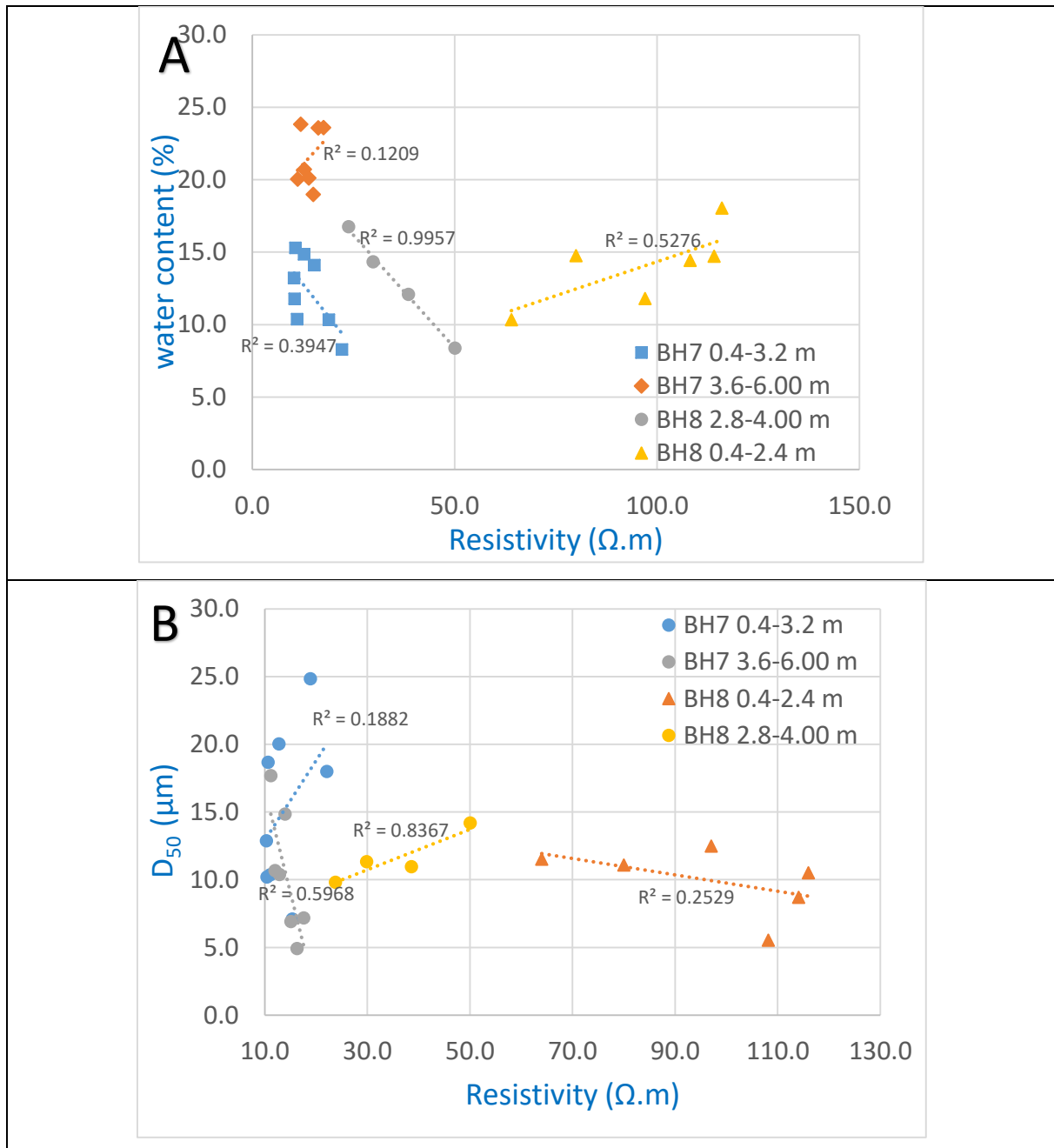
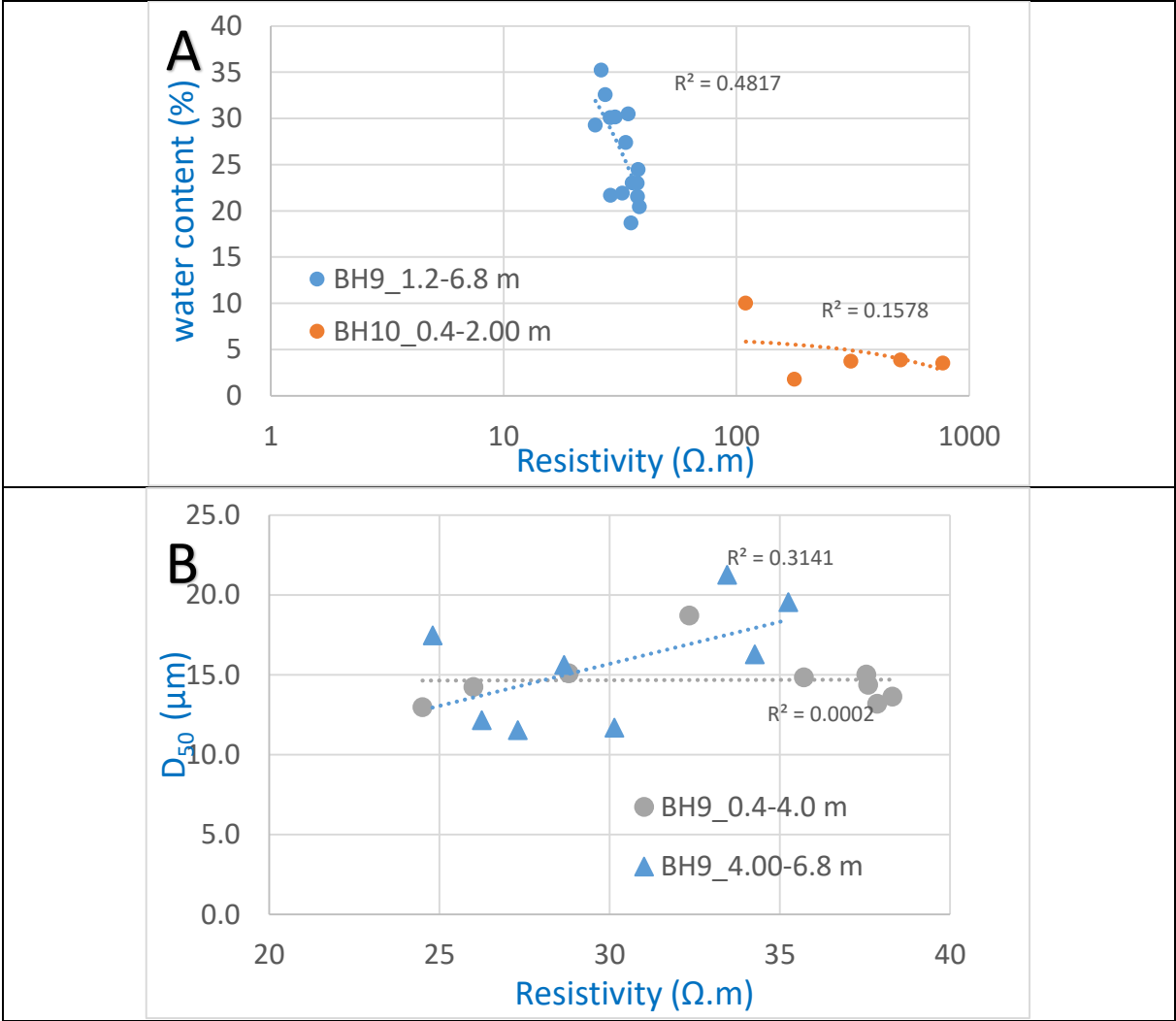


Figure 12 Relationship between A) specific resistivity and water content and B) specific resistivity and grain size in different structural units of the levee body for the boreholes drilled on the levee crown (BH-7) and the protected side (BH-8) at 37.00 lkm of Tisza levee.

Regarding BH-9, by plotting the whole water content and resistivity data a clear inverse proportional function could be recognized with a strong coefficient of determination $R^2 = 0.48$. The same relationship between the previous two parameters could be recognized but only for the upper half of BH-10 with a coefficient of determination $R^2 = 0.15$ while the second half of BH-10 did not show any relationship. This interprets the dependent of resistivity of the levee body and the upper part of the protected side on water content parameter while the resistivity of the protected side remained the same after 2 m. Regarding D_{50} values, no relationship could

be noticed when plotting all D_{50} values against resistivity. But, it was realised that by handling the sedimentological units into two parts (from 0.4 m to 4 m and from 4 m to 6.8 m for BH-9) and (from 0.4 to 2 m for BH-10), the relationship shows a clear trend. D_{50} values shows a directly proportional with the resistivity with a satisfied coefficient of determination $R^2 = 0.31$ and at the depth range from 0.4 m to 4 m for BH-9 and $R^2 = 0.41$ at the depth range from 0.4 m to 2 m for BH-10 and this reflects the dependency of resistivity values on grainsize of the levee materials at the mentioned depth range, while the depth range between 4 m and 6.8 m for BH-9 did not show any relationship which means that the resistivity stayed the same after 4 m at the levee core regardless of changes in grain size **Fig 13**.



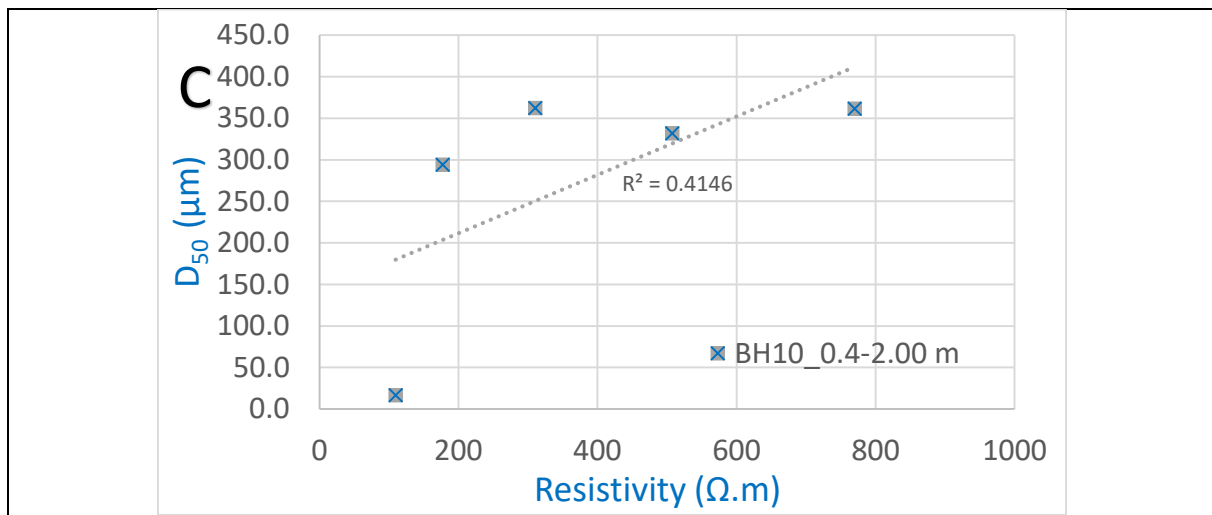
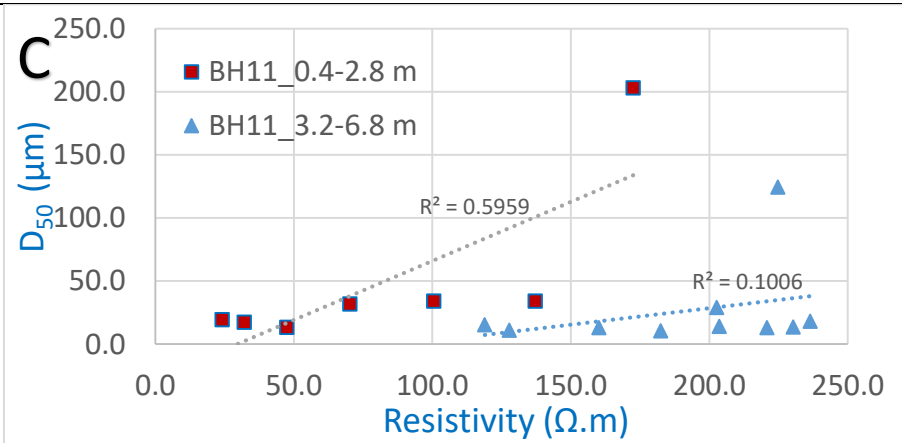
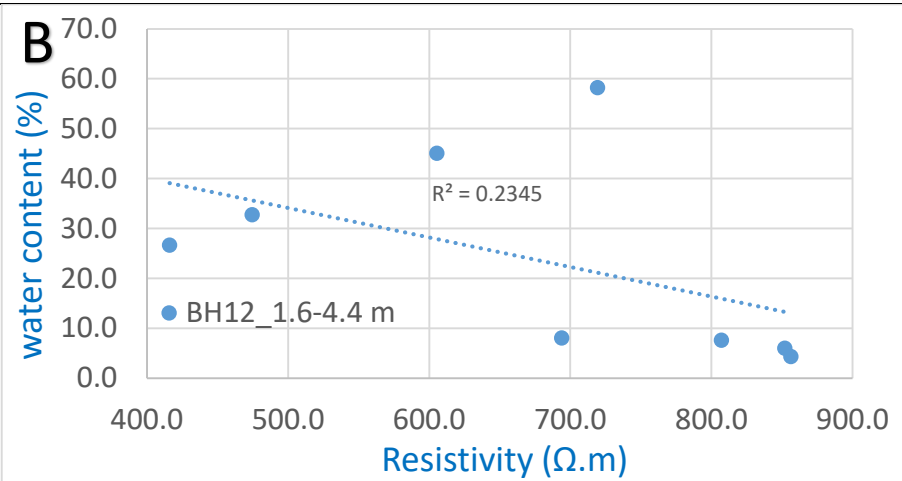
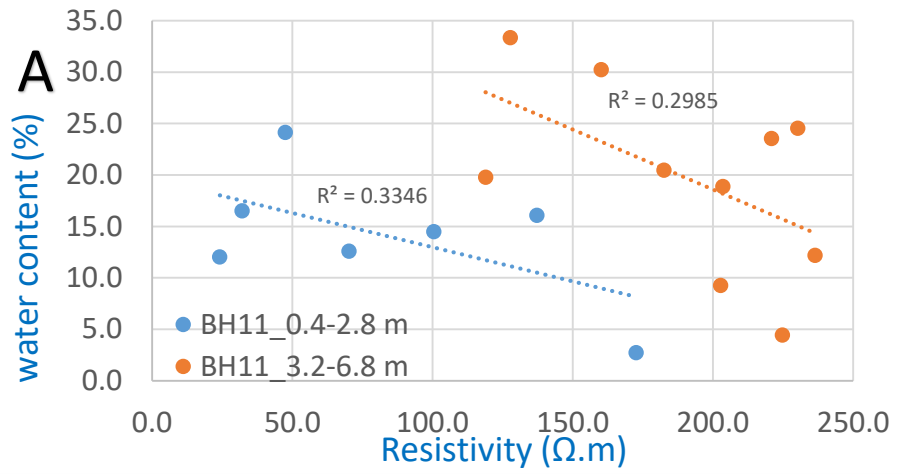


Figure 13 Relationship between A) specific resistivity and water content and B, C) specific resistivity and grain size in different structural units of the levee body for the boreholes drilled on the levee crown (BH-9) and the protected side (BH-10) at 03.00 lkm of Maros levee.

Regarding BH-11 and BH-12, no relationships could be noticed when plotting all water content and D_{50} values against resistivity. But, the sedimentological units were handled separately and clear trends can be recognised in the upper half of BH-11, lower half of BH-11 and in the lower half of BH-12. In more details, by plotting water content and grainsize against resistivity for the upper half of BH-11 (from 0.4 m to 2.8 m), the former exhibited an inverse while the latter exerted a directly proportional function with a coefficient of determination $R^2 = 0.33$ and 0.6 respectively as it is expected. This means that both the mentioned parameters have an effect on the resistivity values. The same behaviour of relationships was noticed for the lower half of BH-11 (from 3.2 m to 6.8 m) in which the water content and grainsize were plotted against resistivity. The former exhibited an inverse while the latter exerted a directly weak proportional relationship with a coefficient of determination $R^2 = 0.3$ and 0.1 respectively. Regarding the lower half of BH-12 (1.6 m to 4.4 m), the water content and grainsize were plotted against resistivity and the coefficient of determination R^2 was 0.23 for the inverse proportional function of water content and resistivity and 0.65 for the directly proportional function of D_{50} and resistivity. At the same time, insignificant relationship was realised in the upper half of BH-12 (from 0 m to 1.2 m) meaning resistivity stayed the same regardless of changes in water content and grain size (**Fig. 14**).



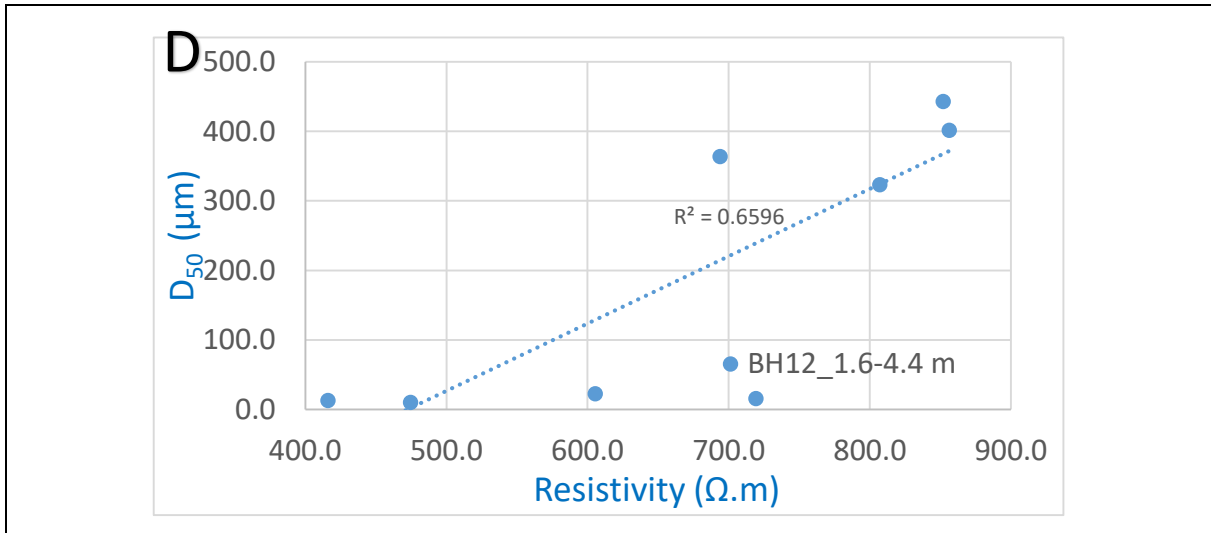
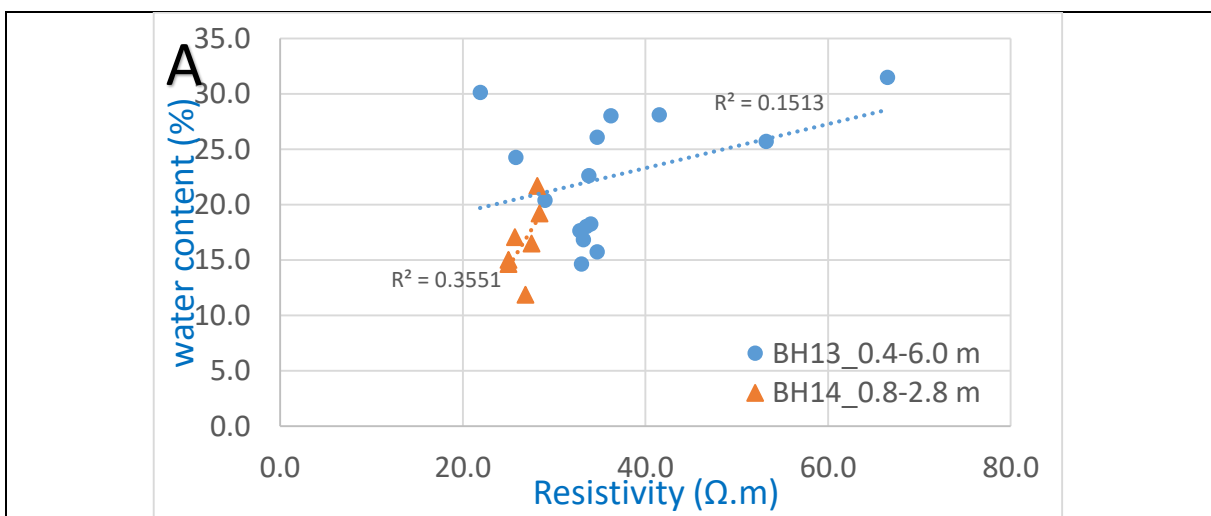


Figure 14 Relationship between A, B) specific resistivity and water content and C, D) specific resistivity and grain size in different structural units of the levee body for the boreholes drilled on the levee crown (BH-11) and the protected side (BH-12) at 08.00 lkm of Maros levee.

Regarding BH-13 and BH-14, water content and D50 were plotted against resistivity. In case of BH-13, unexpected direct proportional function between water content and resistivity with very weak coefficient of determination $R^2 = 0.15$ and also unexpected inverse proportional between D50 and resistivity with $R^2 = 0.007$ was noticed. In case of BH-14, Resistivity was plotted against water content at a depth ranges between 0.8 m to 2.8 m and unexpected direct proportional function was noticed between them with a coefficient of determination $R^2 = 0.3551$ and at the former depth range for BH-14, the resistivity was plotted against D50 values and exhibited the normal expected relationship with a coefficient of determination $R^2 = 0.36$

Fig 15.



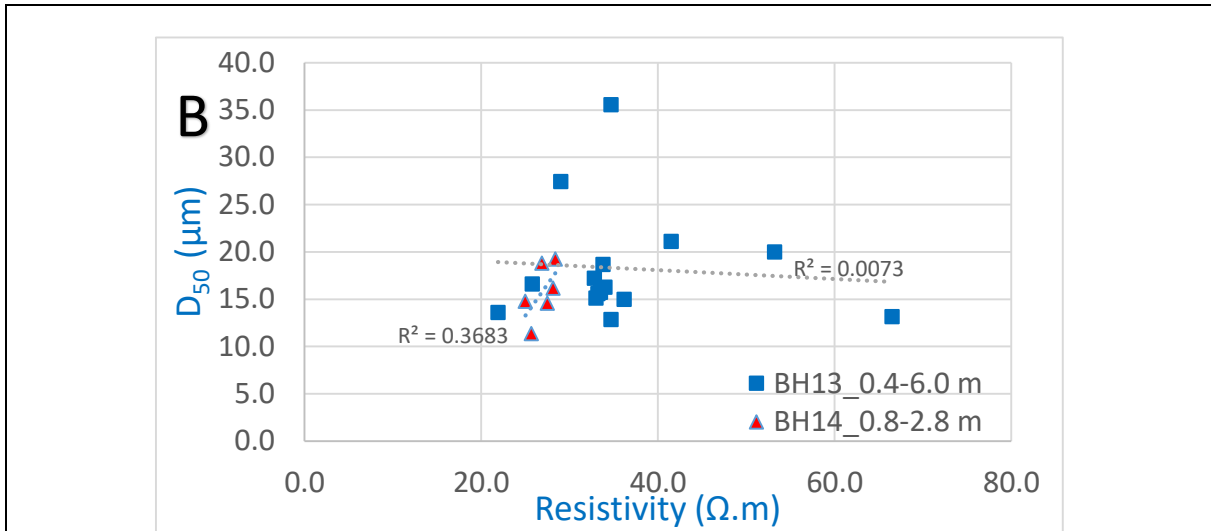
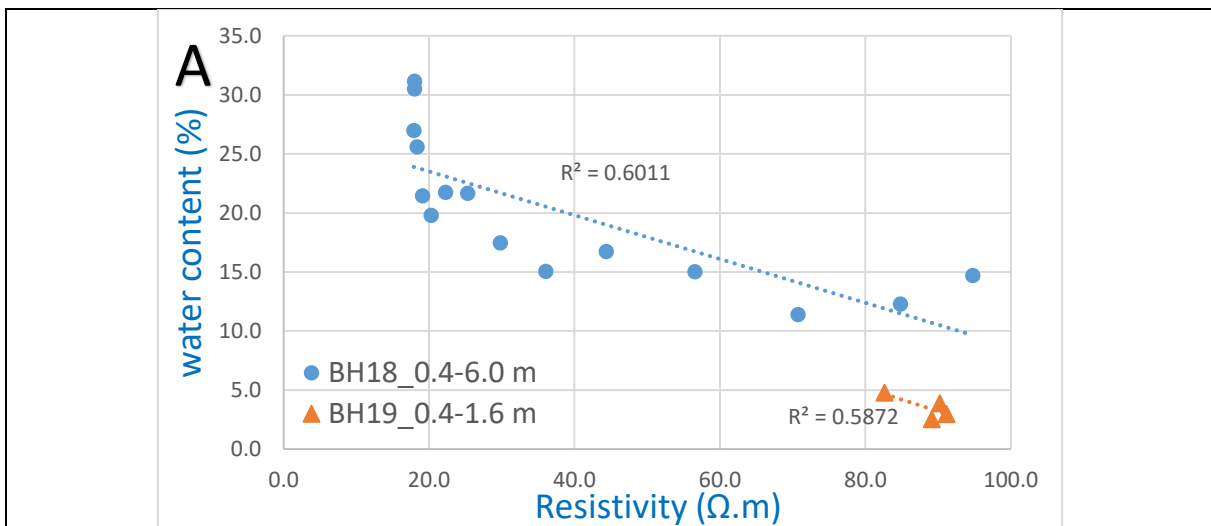


Figure 15 Relationship between A) specific resistivity and water content and B) specific resistivity and grain size in different structural units of the levee body for the boreholes drilled on the levee crown (BH-13) and the protected side (BH-14) at 10.00 lkm of Maros levee.

Regarding BH-18 drilled on the crown of Maros levee and BH-19 drilled on the protected side slope of Maros levee, water content and D50 were plotted against resistivity. Regarding BH-18 (depth range from 0.4 m to 6.00 m) and BH-19 (depth range between 0.4 m to 1.6 m), an expected inverse proportional function between resistivity and water content was obtained with a strong coefficient of determination $R^2 = 0.6$ for both drillings. In case of resistivity and D50 expected normal proportional function, a strong and medium normal coefficient of determination $R^2 = 0.64$ and 0.43 were obtained for BH-18 and BH-19 respectively **Fig 16**.



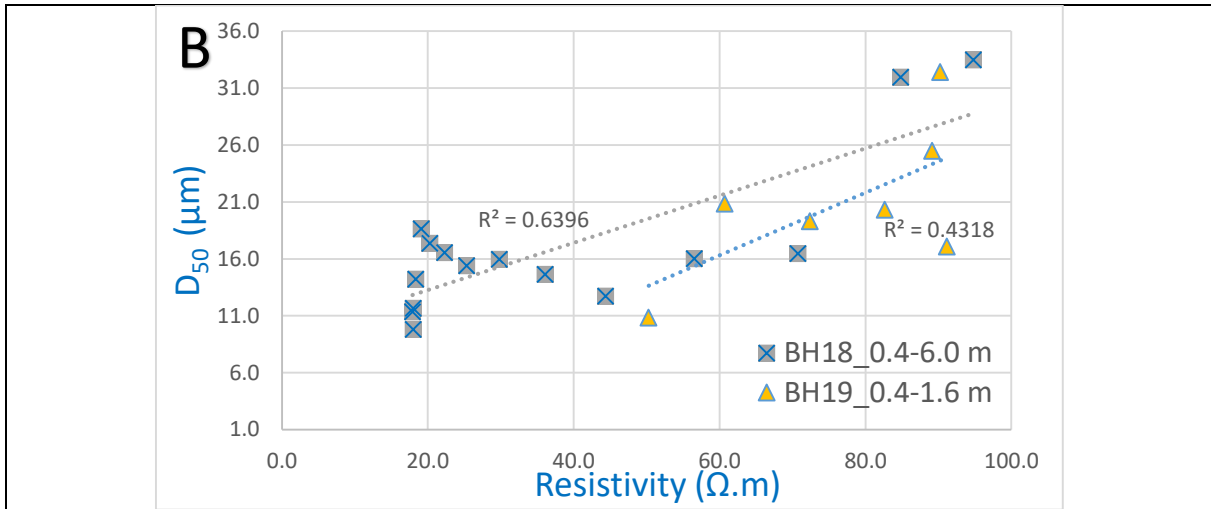


Figure 16 Relationship between A) specific resistivity and water content and B) specific resistivity and grain size in different structural units of the levee body for the boreholes drilled on the levee crown (BH-18) and the protected side (BH-19) at 20.00 lkm of Maros levee.